

Fall 2005

# Integration of micro nano and bio technologies with layer -by -layer self -assembly

Dinesh Shankar Kommireddy  
*Louisiana Tech University*

Follow this and additional works at: <https://digitalcommons.latech.edu/dissertations>



Part of the [Biomedical Engineering and Bioengineering Commons](#), and the [Materials Science and Engineering Commons](#)

---

## Recommended Citation

Kommireddy, Dinesh Shankar, "" (2005). *Dissertation*. 581.  
<https://digitalcommons.latech.edu/dissertations/581>

This Dissertation is brought to you for free and open access by the Graduate School at Louisiana Tech Digital Commons. It has been accepted for inclusion in Doctoral Dissertations by an authorized administrator of Louisiana Tech Digital Commons. For more information, please contact [digitalcommons@latech.edu](mailto:digitalcommons@latech.edu).

# NOTE TO USERS

This reproduction is the best copy available.

**UMI**<sup>®</sup>



**INTEGRATION OF MICRO NANO AND BIO TECHNOLOGIES**  
**WITH LAYER-BY-LAYER SELF-ASSEMBLY**

By

Dinesh Shankar Kommireddy, M.S.

A Dissertation Presented in Partial Fulfillment  
of the Requirements of the Degree  
Doctor of Philosophy

**COLLEGE OF ENGINEERING AND SCIENCE**  
**LOUISIANA TECH UNIVERSITY**

**August 2005**

UMI Number: 3191632

### INFORMATION TO USERS

The quality of this reproduction is dependent upon the quality of the copy submitted. Broken or indistinct print, colored or poor quality illustrations and photographs, print bleed-through, substandard margins, and improper alignment can adversely affect reproduction.

In the unlikely event that the author did not send a complete manuscript and there are missing pages, these will be noted. Also, if unauthorized copyright material had to be removed, a note will indicate the deletion.

**UMI**<sup>®</sup>

---

UMI Microform 3191632

Copyright 2006 by ProQuest Information and Learning Company.

All rights reserved. This microform edition is protected against unauthorized copying under Title 17, United States Code.

ProQuest Information and Learning Company  
300 North Zeeb Road  
P.O. Box 1346  
Ann Arbor, MI 48106-1346

LOUISIANA TECH UNIVERSITY  
THE GRADUATE SCHOOL

7/28/2005  
Date

We hereby recommend that the dissertation prepared under our supervision by **Dinesh Shankar Kommireddy** entitled "**Integration of Micro Nano and Bio Technologies with Layer-by-Layer Self-Assembly**" be accepted in partial fulfillment of the requirements for the Degree of Doctor of Philosophy.

Yusi Lvov

Supervisor of Dissertation Research

Ray T. Sturley

Head of Department

Engineering

Department

Recommendation concurred in:

Yusi Lvov

David M. Mills

Sabitha L. Lebb

[Signature]

Hi Si

Advisory Committee

Approved:

Bala Ramachandran

Director of Graduate Studies

Stan Neger

Dean of the College

Approved:

Terry M. McDonough

Dean of the Graduate School

## ABSTRACT

In the past decade, layer-by-layer (LbL) nanoassembly has been used as a tool for immobilization and surface modification of materials with applications in biology and physical sciences. Often, in such applications, LbL assembly is integrated with various techniques to form functional surface coatings and immobilized matrices. In this work, integration of LbL with microfabrication and microfluidics, and tissue engineering are explored. In an effort to integrate microfabrication with LbL nanoassembly, microchannels were fabricated using soft-lithography and the surface of these channels was used for the immobilization of materials using LbL and laminar flow patterning. Synthesis of poly(dimethyldiallyl ammonium chloride)/poly(styrene sulfonate) and poly(dimethyldiallyl ammonium chloride)/bovine serum albumin microstrips is demonstrated with the laminar flow microfluidic reactor. Resulting micropatterns are 8-10  $\mu\text{m}$  wide, separated with few micron gaps. The width of these microstrips as well as their position in the microchannel is controlled by varying the flow rate, time of interaction and concentration of the individual components, which is verified by numerical simulation. Spatially resolved pH sensitivity was observed by modifying the surface of the channel with a pH sensitive dye.

In order to investigate the integration of LbL assembly with tissue engineering, glass substrates were coated with nanoparticle/polyelectrolyte layers, and two different cell types were used to test the applicability of these coatings for the surface modification

of medical implants. Titanium dioxide ( $\text{TiO}_2$ ), silicon dioxide, halloysite and montmorillonite nanoparticles were assembled with oppositely charged polyelectrolytes. *In-vitro* cytotoxicity tests of the nanoparticle substrates on human dermal fibroblasts (HDFs) showed that the nanoparticle surfaces do not have toxic effects on the cells. HDFs retained their phenotype on the nanoparticle coatings, by synthesizing type-I collagen. These cells also showed active proliferation on the nanoparticle substrates. Cells attached on  $\text{TiO}_2$  substrates showed faster rate of spreading compared with the other types of nanoparticle coatings. Mesenchymal stem cells (MSCs) were used as a second cell type to support and elaborate on the results obtained with the HDFs. Increasing surface roughness was observed with increasing number of layers of  $\text{TiO}_2$ . Tests with a higher number of layers of  $\text{TiO}_2$ , showed an increased attachment, proliferation and faster spreading of the MSCs on a larger number of layers of  $\text{TiO}_2$ .

## APPROVAL FOR SCHOLARLY DISSEMINATION

The author grants to the Prescott Memorial Library of Louisiana Tech University the right to reproduce, by appropriate methods, upon request, any or all portions of this Dissertation. It is understood that "proper request" consists of the agreement, on the part of the requesting party, that said reproduction is for his personal use and that subsequent reproduction will not occur without written approval of the author of this Dissertation. Further, any portions of the Dissertation used in books, papers, and other works must be appropriately referenced to this Dissertation.

Finally, the author of this Dissertation reserves the right to publish freely, in the literature, at any time, any or all portions of this Dissertation.

Author K. Dinkesh Shankar

Date 10/24/2005

## TABLE OF CONTENTS

	Page
<b>List of Tables</b> .....	ix
<b>List of Figures</b> .....	x
<b>Acknowledgments</b> .....	xvii
<b>CHAPTER 1. INTRODUCTION</b> .....	<b>1</b>
1.1 Integration of LbL and Microfabrication.....	1
1.2 Integration of LbL and Tissue Engineering.....	4
1.2.1. Super-Hydrophilic Nanoparticle Coatings.....	4
1.2.2. Cell Culture on Nanoparticle Thin Films.....	5
1.3 Organization of the Dissertation.....	6
<b>CHAPTER 2. LITERATURE REVIEW</b> .....	<b>8</b>
2.1 Background of Laminar Flow Microfluidic Devices.....	8
2.1.1 Integration of Thin Film Sensors with LbL.....	14
2.2 Integration of LbL and Tissue Engineering.....	17
2.2.1 Super-Hydrophilic, Biocompatible Nanoparticle Thin Films.....	17
2.2.2 Nanophase Materials for Cell Culture.....	18
<b>CHAPTER 3. EXPERIMENTAL SECTION</b> .....	<b>25</b>
3.1 Microfabrication and Layer-by-Layer Assembly.....	26
3.1.1 Materials.....	26
3.1.2 Instrumentation.....	27
3.1.3 Fabrication of Microchannels.....	27
3.2 Experimental Setup.....	29
3.3 Numerical Simulation.....	30
3.3.1 Effect of Flow Rate.....	31
3.3.2 Effect of Diffusion Coefficient.....	35
3.4. Layer-by-Layer Assembly for Microfluidics.....	36
3.5. Layer-by-Layer Assembly for Superhydrophilic Nanoparticle Coatings.....	37
3.5.1. Materials.....	37
3.5.2. Instrumentation.....	38

3.6. Layer-by-layer Assembly for Tissue Engineering and Wettability Studies .....	39
3.7 Surface Roughness of LbL Assembled TiO <sub>2</sub> Thin Films .....	40
3.8 Cell Culture .....	40
3.8.1 Cytotoxicity .....	41
3.8.2 Cell Number .....	41
3.8.3 Cell Attachment .....	42
3.8.4 Scanning Electron Microscopy of Cells on Nanoparticle Substrates .....	42
3.8.5 Statistical Analysis .....	43
<b>CHAPTER 4. INTEGRATION OF MICROFLUIDICS AND LAYER-BY-LAYER ASSEMBLY .....</b>	<b>44</b>
4.1 Interpolyelectrolyte Complex Microfabrication .....	44
4.2 Polyelectrolyte/Ion Complex Microfabrication .....	50
4.3 Polyelectrolyte/Protein Complex Microfabrication .....	54
4.4 Effect of Electric Field on the Position of the Polyelectrolyte Complex .....	56
4.5 pH Sensitive Channels .....	58
4.6 Selective Modification of Microparticles inside the Channel .....	60
4.7 Conclusion .....	62
<b>CHAPTER 5. INTEGRATION OF MICROFABRICATION AND LAYER-BY-LAYER ASSEMBLY .....</b>	<b>64</b>
5.1 Interferometric Imaging of the Free Standing Thin Films .....	67
5.2. Point Load Experiments on Free Standing Films .....	70
<b>CHAPTER 6. LBL ASSEMBLED HYDROPHILIC COATINGS .....</b>	<b>74</b>
6.1 Thickness of Polyelectrolyte/TiO <sub>2</sub> films .....	74
6.2 Optical Properties of PSS/TiO <sub>2</sub> films .....	77
6.3 Wettability of PSS/TiO <sub>2</sub> Multilayer Coatings on Different Substrates .....	78
6.4 Effect of Different Types of Nanoparticles on Wettability of LbL Coating .....	83
6.5 Biocompatibility of TiO <sub>2</sub> Coated Substrates .....	84
6.6 Conclusion .....	86
<b>CHAPTER 7. INTEGRATION OF LAYER-BY-LAYER ASSEMBLY AND CELL CULTURE .....</b>	<b>89</b>
7.1 Thickness of the Nanoparticle Thin Films .....	89
7.2 Cytotoxicity of Nanoparticle Thin Films on Human Dermal Fibroblasts .....	90
7.3 Proliferation and Phenotype of Human Dermal Fibroblasts on Nanoparticle Thin Films .....	91
7.4 Cell Spreading on Nanoparticle Thin Films .....	93
7.5 Conclusion .....	99

<b>CHAPTER 8. LAYER BY LAYER ASSEMBLED TiO<sub>2</sub> THIN FILMS FOR ATTACHMENT AND SPREADING OF STEM CELLS</b> .....	<b>101</b>
8.1 Thickness of the Nanoparticle Thin Films .....	101
8.2 Cell Numbers by MTT Assay .....	102
8.3 Surface Roughness of TiO <sub>2</sub> Thin Films .....	104
8.4 Cytotoxicity of TiO <sub>2</sub> Coated Substrates .....	105
8.5 Cell Proliferation on TiO <sub>2</sub> Substrates .....	106
8.6 Cell Attachment on TiO <sub>2</sub> Substrates .....	107
8.7 Cell Spreading Visualized by Scanning Electron Microscopy .....	108
8.8 Conclusion .....	114
<b>CHAPTER 9. SUMMARY AND FUTURE WORK</b> .....	<b>117</b>
<b>REFERENCES</b> .....	<b>121</b>
<b>VITA</b> .....	<b>133</b>

## LIST OF TABLES

	Page
<b>Table 2.1.</b> The mean and standard deviation of the surface roughness parameters of three samples of ceramic abutments.....	19
<b>Table 5.1.</b> Elastic modulus and residual stress of 11G11 nanomembranes of different size.....	69
<b>Table 6.1.</b> Comparison of contact angles of different nanoparticles coated on glass substrates.....	84

## LIST OF FIGURES

	Page
<b>Figure 2.1.</b> (a) Fabrication of trenches, (b) polymeric complex, (c) chemiluminescence and (d) fabrication of calcite and apatite microcrystals inside a microchannel made of PDMS <sup>9</sup> .....	10
<b>Figure 2.2.</b> Etching of silver and gold and the fabrication of complex electrical circuitry contained inside a microchannel <sup>9</sup> .....	10
<b>Figure 2.3.</b> (a) Top view of a microfluidic channel, (b) patterning of different cell types inside a channel, (c) Selective staining of cells inside a channel filled with cells and (d) patterned detachment of cells inside the microfluidic channel by laminar flow patterning <sup>31</sup> .....	11
<b>Figure 2.4.</b> (a) Schematic of a diffusion immunoassay in a T-sensor and (b) a microfluidic device used for testing the immunoassay <sup>15</sup> .....	12
<b>Figure 2.5.</b> Schematic of microfluidic device for cell lysis and fractionation/ detection of intercellular components <sup>35</sup> .....	12
<b>Figure 2.6.</b> Attachment of human gingival fibroblast to the different ceramic surfaces. Each bar represents the mean of percentage of attachment in one of two identical experiments performed in triplicate. * Statistically significant differences compared with the polished surfaces $P < 0.05$ <sup>95</sup> .....	19
<b>Figure 2.7.</b> Human bone marrow cell attachment to Ti alloy disks with three surface roughness values and the control. Attachment is displayed as the percentage of cells attached after 0.5 and 2 h of incubation. 1200, 600 and 180 is the grit of the paper with which the surface of Ti was polished. Values are the mean $\pm$ SD of six cultures. *, ** indicate a significant difference with plastic at the corresponding time point (* $p < 0.05$ ; ** $p < 0.01$ ) <sup>96</sup> .....	20
<b>Figure 2.8.</b> Human bone marrow cell proliferation after 8, 11, 14 and 16 days of culture on Ti alloy for the three groups (Ti1200, Ti600 and Ti180) and the control (tissue culture plate). Values are the mean $\pm$ SD of six cultures. * indicates a significant difference with both plastic and Ti180 at the corresponding time point ( $p < 0.05$ ) <sup>96</sup> .....	21

<b>Figure 2.9.</b> Osteoblast proliferation on ceramics. (a) □ borosilicate glass (reference material), ▨ 167 nm grain size alumina (conventional), and ▩ 24 nm grain size alumina (nanophase); (b) □ borosilicate glass (reference material), ▨ 4520 nm grain size titania (conventional), and ▩ 39 nm grain size titania (nanophase); and (c) □ borosilicate glass (reference material), ▨ 179 nm grain size hydroxyapatite (conventional), and ▩ 67 nm grain size hydroxyapatite (nanophase). Osteoblast proliferation under standard cell culture conditions was determined after 1, 3, and 5 days. Values are mean ± SEM; n=3; * P<0.01 (compared to respective conventional grain size ceramic); + P<0.01 (compared to borosilicate glass) <sup>99</sup> .....	23
<b>Figure 3.1.</b> Microchannel formation through lithography, hot embossing and soft-lithography.....	28
<b>Figure 3.2.</b> Schematic representation of laminar flow patterning experiment.....	30
<b>Figure 3.3.</b> Schematic illustration of the laminar flow patterning experimental setup.....	30
<b>Figure 3.4.</b> Left, Simulation results for equal flow rates in the left and right inlet channels and right, line graph of the mass fraction in the middle of the outlet channel.....	33
<b>Figure 3.5.</b> Simulation of the condition where the flow rate in the left inlet is two times the flow rate of the inlet on the right.....	33
<b>Figure 3.6.</b> Simulation of the condition where the flow rate in the left inlet is three times the flow rate of the inlet on the right.....	34
<b>Figure 3.7.</b> Simulation of the condition where the flow rate in the left inlet is five times the flow rate of the inlet on the right.....	34
<b>Figure 3.8.</b> Simulation of the condition where the flow rate in the left inlet is ten times the flow rate of the inlet on the right.....	35
<b>Figure 3.9.</b> Simulation of the variation of diffusion coefficient in the reaction channel.....	36
<b>Figure 3.10.</b> Line graph of the reaction product in the reaction channel.....	36
<b>Figure 4.1.</b> Optical micrographs of the formation of the polyelectrolyte complex inside the channel by varying the flow rates, (a) equal and (b) different flow rates.....	46
<b>Figure 4.2.</b> Interpolyelectrolyte complex inside a 's' shaped channel.....	46

<b>Figure 4.3.</b> (a,b,c) Confocal fluorescence microscopy and atomic force microscopy images of the PDDA/PSS interpolyelectrolyte complex synthesized in the channel microreactor .....	48
<b>Figure 4.4.</b> Numerical simulation of PDDA - PSS interaction inside channel microreactor .....	49
<b>Figure 4.5.</b> Confocal fluorescent image of PDDA/PSS micropattern on glass support. PDDA was labelled with fluorescein isothiocyanate .....	50
<b>Figure 4.6.</b> Optical image of PAH/Citrate micropattern on glass support .....	51
<b>Figure 4.7.</b> Fluorescence microscopy images of PAH/citrate complex fabricated in Y-type micro reactor .....	52
<b>Figure 4.8.</b> Fluorescence microscopy images of PAH/citrate complex fabricated in S-type micro-reactor .....	53
<b>Figure 4.9.</b> Atomic force microscopy image of PAH/citrate micropattern deposited onto glass support .....	53
<b>Figure 4.10.</b> (a) Confocal fluorescence and (b) atomic force microscopy images of the PDDA/BSA micropattern. PDDA was labeled with FITC. Inlet flow rate was mL•min <sup>-1</sup> in both inlet channels; initial concentration of PDDA and BSA 0.1 mg•mL <sup>-1</sup> .....	55
<b>Figure 4.11.</b> Effect of electric field on the position of the interpolyelectrolyte complex formed in the channel .....	57
<b>Figure 4.12.</b> Confocal fluorescence image of the pH sensitive channel showing different fluorescent intensities in different regions of the same channel .....	59
<b>Figure 4.13.</b> The line scan as a function of distance across the channel .....	59
<b>Figure 4.14.</b> (a) Schematic view of anisotropic micropatterning of Rhodamine -labeled microparticles with fluorescein- labeled dextran macromolecules, (b) confocal fluorescent image and (c) overlaid fluorescent image of resulting anisotropic microparticles .....	61
<b>Figure 5.1.</b> Schematic of the multilayer nanomembrane covering openings in the array of microfabricated device .....	65
<b>Figure 5.2.</b> SEM image of a silicon substrate with gradient opening arrays, scale bar is 200 $\mu$ m .....	66
<b>Figure 5.3.</b> Optical image of the of 4×4 array covered with LbL film .....	66

<b>Figure 5.4.</b> The interference pattern of the nanomembrane array under the pressure differential of 1266 Pa .....	67
<b>Figure 5.5.</b> Deflection-pressure data for freely-suspended nanomembranes with different diameters .....	68
<b>Figure 5.6.</b> Four independent deflection-pressure sets of data (columns) obtained simultaneously for freely suspended nanomembranes with identical diameters along with the average behavior (solid line). The labels correspond to the membranes over different openings, as shown in figure 5.4 .....	69
<b>Figure 5.7.</b> Optical micrograph of point-load experiment with the AFM tip pointing at one of the membrane .....	71
<b>Figure 5.8.</b> The deflection of nanomembranes with different diameters tested with the colloidal AFM probe under the applied force of 70 nN as a function of the membrane diameter .....	71
<b>Figure 5.9.</b> The bending rigidity of the nanomembranes as a function of the membrane diameter and the theoretical prediction of elastic membrane deformation (solid line) .....	72
<b>Figure 6.1.</b> Film thickness as a function of deposited TiO <sub>2</sub> layers .....	76
<b>Figure 6.2.</b> Scanning electron micrograph of (PDDA/PSS) <sub>3</sub> +(TiO <sub>2</sub> /PSS) multilayer cross-section on a silver electrode. The particle diameter is ca 21 nm (Hitachi S-900 SEM operating at 25 kV; the sample is coated with 2 nm of Pt) .....	77
<b>Figure 6.3.</b> UV-vis absorbance with increasing number of layers of TiO <sub>2</sub> .....	78
<b>Figure 6.4.</b> Water contact angle measurements on glass with the deposition of different number of layers of TiO <sub>2</sub> .....	79
<b>Figure 6.5.</b> Water contact angle measurements on PMMA with the deposition of different number of layers of TiO <sub>2</sub> .....	80
<b>Figure 6.6.</b> Water contact angle measurements on PDMS with the deposition of different number of layers of TiO <sub>2</sub> .....	81
<b>Figure 6.7.</b> Water contact angle of glass, PMMA and PDMS substrates after coating with different number of PSS/TiO <sub>2</sub> bilayers without plasma treatment of the substrates .....	82

<b>Figure 6.8.</b> Water contact angle of PMMA and PDMS substrates after coating with different number of PSS/TiO <sub>2</sub> bilayers with plasma treatment of the substrates.....	82
<b>Figure 6.9.</b> Change in water contact angle for various coatings on PMMA during storage; treatment was performed on the first day.....	83
<b>Figure 6.10.</b> Cell culture of human dermal fibroblasts on glass .....	85
<b>Figure 6.11.</b> Cell culture of human dermal fibroblasts on PMMA .....	85
<b>Figure 6.12.</b> Cell culture of human dermal fibroblasts on PDMS .....	86
<b>Figure 7.1.</b> Thickness of the nanoparticle thin films measured using quartz Resonators.....	90
<b>Figure 7.2.</b> Live/dead assay performed on a glass substrate coated with 2 layers of Silica .....	91
<b>Figure 7.3.</b> BrdU cell proliferation on a substrate coated with 2 layers of TiO <sub>2</sub> .....	92
<b>Figure 7.4.</b> MTT based cell activity on LbL assembled nanoparticle thin films .....	92
<b>Figure 7.5.</b> Collagen expression by HDFs on a substrate coated with 3 layers of montmorillinoite .....	93
<b>Figure 7.6.</b> Cells attached on control substrate after 4 hours of seeding.....	94
<b>Figure 7.7.</b> Cells attached on a substrate coated with 3 layers of halloysite, after 4 hours of seeding.....	95
<b>Figure 7.8.</b> Cells attached on a substrate coated with 3 layers of silica, after 4 hours of seeding .....	95
<b>Figure 7.9.</b> Cells attached on a substrate coated with 3 layers of montmorillonite, after 4 hours of seeding.....	96
<b>Figure 7.10.</b> Cells attached on a substrate coated with 3 layers of TiO <sub>2</sub> , after 4 hours of seeding .....	96
<b>Figure 7.11.</b> Cells attached on control substrate after 24 hours of seeding .....	97
<b>Figure 7.12.</b> Cells attached on a substrate coated with 3 layers of halloysite, after 24 hours of seeding.....	97

<b>Figure 7.13.</b> Cells attached on a substrate coated with 3 layers of silica, after 24 hours of seeding	98
<b>Figure 7.14.</b> Cells attached on a substrate coated with 3 layers of ontmorillonite, after 24 hours of seeding	98
<b>Figure 7.15.</b> Cells attached on a substrate coated with 3 layers of TiO <sub>2</sub> , after 4 hours of seeding	99
<b>Figure 8.1.</b> Change in thickness of the deposited nanoparticle films, monitored using quartz crystal microbalance. Inset shows the linear increase in the thickness of the deposited layers	102
<b>Figure 8.2.</b> Cell numbers on 4 layers of nanoparticles deposited with respective polyelectrolyte layers. The cells were counted using MTT based assay on the third day after seeding the substrates	103
<b>Figure 8.3.</b> Change in surface roughness TiO <sub>2</sub> layers as a function of layer number	104
<b>Figure 8.4.</b> Representative data of surface roughness on a substrate coated with 2 layers of TiO <sub>2</sub>	105
<b>Figure 8.5.</b> Cytotoxicity assay performed on a glass substrate coated with 4 layers of TiO <sub>2</sub>	106
<b>Figure 8.6.</b> Cell numbers on various layers of TiO <sub>2</sub> coated on glass. (* p<0.01, + p<0.05 compared with the control)	107
<b>Figure 8.7.</b> Number of cells attached on the control and 1 layer and 4 layer substrates (* p<0.01, + p<0.05 compared with control)	108
<b>Figure 8.8.</b> Cells attached on control substrate, after 4 hours of seeding	109
<b>Figure 8.9.</b> Cells attached on a substrate coated with 1 layer of TiO <sub>2</sub> , after 4 hours of seeding	110
<b>Figure 8.10.</b> Cells attached on a substrate coated with 4 layers of TiO <sub>2</sub> , after 4 hours of seeding	110
<b>Figure 8.11.</b> Cells attached on control substrate, after 12 hours of seeding	111
<b>Figure 8.12.</b> Cells attached on a substrate coated with 1 layer of TiO <sub>2</sub> , after 12 hours of seeding	111
<b>Figure 8.13.</b> Cells attached on a substrate coated with 4 layer of TiO <sub>2</sub> , after 12 hours of seeding	112

<b>Figure 8.14.</b> Cells attached on control substrate after 24 hours of seeding .....	112
<b>Figure 8.15.</b> Cells attached on a substrate coated with 1 layer of TiO <sub>2</sub> , after 24 hours of seeding .....	113
<b>Figure 8.16.</b> Cells attached on a substrate coated with 4 layers of TiO <sub>2</sub> , after 24 hours of seeding .....	113

## ACKNOWLEDGMENTS

I would like to thank, Dr. Yuri Lvov, my dissertation advisor, for his continued encouragement through out the period of my Ph.D and for giving me an opportunity to work in his lab. I would also like to thank Dr. Tatsiana Shutava for her help and suggestions. I thank the group of students in Dr. Lvov's lab that worked with me for their help. Our collaborators, Dr. David Mills, Dr. Vladimir Tsukruk and Dr. Chaoyang Jiang are also thanked for their help and suggestions. Other people that I would like to thank are the IfM staff, especially Mr. Scott Williams, Dr. Dimtry Shchukin, Dr. Albena Ivanisevic, Mr. Shashikanth Sriram for their help and collaborations.

Finally I would like to thank the most important people in my life, my mother Dr. N. Krishnaveni, my father Dr. K. Sivasankara Reddy, my wife Swetha Chinnayelka and my brother, Avinash Kommireddy for helping me realize this dream. I dedicate this work to my family.

# CHAPTER 1

## INTRODUCTION

The objective of this work is the combination of two integration techniques: i) Layer-by-Layer (LbL)<sup>1,2</sup> assembly and microfabrication through the formation of microchannels and immobilization of various components in the channel and ii) integration of LbL assembly and tissue engineering through cell culture on nanoparticle thin films assembled using LbL assembly methods. This dissertation focuses on the formation of thin films and patterns using LbL electrostatic nano-assembly.

### **1.1 Integration of LbL and Microfabrication**

The study of interpolyelectrolyte complex formation at the interfaces is one of the important areas of interfacial and polymer chemistry. Linear polyelectrolyte<sup>3</sup>, DNA/polyelectrolyte<sup>4</sup>, and protein/polyelectrolyte<sup>5</sup> systems were studied in bulk solution demonstrating the protective, synergetic, catalytic, and hydrophilic (hydrophobic) effects of polyelectrolyte/biomacromolecule combinations. Such composite polyelectrolyte structures are of practical importance for medical purposes, as elements of biosensors, protective coatings, and biocompatible tools for targeted DNA or enzyme delivery in cells. A number of approaches have been developed, including LBL assembly<sup>1,2</sup>, mixing of the polyelectrolytes in stoichiometric and non-

stoichiometric ratio,<sup>3</sup> and *in-situ* interpolymerization<sup>6</sup> to provide polyelectrolyte structures with desired composition, properties, and biofunctionality. Ordered functional polyelectrolyte microstructures allow the production of nanoengineered systems for cell treatment and complex interpolyelectrolyte sensor elements<sup>7</sup>. Conventional photolithography technologies were used to fabricate such microstructures<sup>8</sup>, however, photolithography is not applicable to biological materials due to highly energetic physical or aggressive chemical treatment. Therefore, lithographic methods have significant limitations with respect to the type of materials that can be used and the resulting microstructures.

One of the most facile and versatile approaches for microfabrication in mild, ambient conditions is laminar flow synthesis inside microchannels as proposed by Whitesides *et al*.<sup>9</sup> This method employs a laminar stream of two or more miscible solutions in one capillary or microchannel. Laminar streams of multiple solutions in the same channel flow individually and the only method of interaction between dissolved reagents is transverse molecular diffusion. A multiphase laminar flow approach has been used for microfabrication of engineered inorganic structures<sup>10,11</sup>, patterned delivery of cells<sup>12</sup>, manipulation with lipid bilayers<sup>13</sup>, separation and detection<sup>14,15</sup> and adsorption of protein microstrips<sup>16</sup>. This approach is especially useful in handling proteins, cells, and other delicate biological structures and allows control of the spatial delivery of reagents inside microchannels.

The formation of patterns of oppositely charged polyelectrolytes, polyelectrolyte-proteins and polyelectrolyte-ions in a microfluidic channel made using soft lithography<sup>17</sup> is discussed as the first part of this dissertation work. As a sub section of the first part, the

integration of microfabrication techniques and LbL nano-assembly, the formation of arrays of sensors by combining microfabrication techniques and nano-assembly by LbL is also discussed. The micron-resolved synthesis, at ambient conditions, of interpolyelectrolyte, polyelectrolyte/ion, and polyelectrolyte/protein complexes inside a laminar flow microreactor<sup>18</sup> was demonstrated on examples of poly(dimethyldiallylammonium chloride)/poly(styrene sulfonate), poly(allylamine hydrochloride)/citrate ions, and poly(dimethyldiallylammonium chloride)/bovine serum albumin complexes. Resulting micropatterns are elongated structures 8-30  $\mu\text{m}$  wide. The width of the polyelectrolyte complex and its position in a channel microreactor can be adjusted by the concentration, diffusion coefficient, and flow rate of individual components. Numerical simulation was performed to analyze the influence of individual laminar flow rates on the position of the liquid/liquid interface (and, as a result, the polyelectrolyte complex) inside the channel microreactor. The position of the interpolyelectrolyte complex was steered within the channel by changing the flow rate in the inlet channels. The surface of the channels was made sensitive to pH by coating the surface of the channel with pH sensitive 1-hydroxypyrene-3, 6, 8- trisulfonic acid (HPTS). This pH sensitive channel was used for creating selective fluorescent intensity changes inside the microchannel based on the pH of the inlet fluid. Selective modification of micron sized spheres inside the microchannel is also discussed.

As part of the sub-section of the first part of the integration of microfabrication with LbL assembly, the first approach to the fabrication of quasi-2D nano-membrane arrays on silicon substrates with controlled composition, thickness, shape and size, suitable for study as a sensor prototype is discussed. Free standing LbL films were made

using a cellulose acetate layer as a sacrificial coating. LbL films were deposited on this coating by a modification to the usual LbL process known as the spin assisted LbL process (SA-LbL)<sup>19</sup> where thin films are made by spinning the materials of interest on flat substrates. A gold nanoparticle layer inside the thin film was added to strengthen the thin films. Micromechanical properties were measured on these arrays by uniform load (bulging) tests. The combination of nano-scale LbL assembly and micro-pattern fabrication (*via* microfabrication techniques) to form freely suspended quasi 2-D nano-membrane micro-arrays with stable and extremely sensitive properties, suitable as sensing elements for a new generation of nano-sensors, is discussed.

## **1.2 Integration of LbL and Tissue Engineering**

### **1.2.1 Super-Hydrophilic Nanoparticle Coatings**

In the second section, the adsorption of nanoparticles on various substrates to form hydrophilic, biocompatible coatings is discussed. In the first subsection of this section, the formation of super-hydrophilic coatings of titanium dioxide (TiO<sub>2</sub>) nanoparticles is discussed. Previously, many researchers have shown hydrophilic surfaces produced from the formation of LbL assembled thin films of polyelectrolytes<sup>20</sup>. These thin films retain their hydrophilic nature for a very short time which is a major impediment for many applications where a long lasting hydrophilic coating is necessary, such as antifogging coatings, self cleaning coatings etc. Here, for the first time, we show the hydrophilic nature of titanium dioxide (TiO<sub>2</sub>) nanoparticle thin films coated on glass, poly(methyl methacrylate) (PMMA) and polydimethylsiloxane (PDMS) and these coatings exhibit a long lasting hydrophilic nature. The super-hydrophilic characteristics

of TiO<sub>2</sub> films were previously observed only when the films were irradiated with UV light<sup>21</sup>. We demonstrate here that a stable super-hydrophilic coating, which does not require UV irradiation<sup>22</sup>, can be developed based on TiO<sub>2</sub> nanoparticles and polymer nanocomposites via LbL assembly. The wettability of any surface, such as glass, PMMA and PDMS, can be controlled by coating the substrates with alternate layers of TiO<sub>2</sub> nanoparticles and polyelectrolytes, such that stable, long lasting hydrophilic coatings can be obtained. TiO<sub>2</sub> is among the most frequently used biocompatible materials for implants where good attachment of cells to these materials is essential. In this work, human dermal fibroblasts (HDFs) have been shown to thrive on TiO<sub>2</sub> nanoparticle LbL films, thus demonstrating the biocompatibility of these surfaces.

### **1.2.2 Cell Culture on Nanoparticle Thin Films**

In the second sub section, the formation of thin films of various nanoparticles to test the attachment, proliferation and spreading of cells is discussed<sup>23</sup>. Polymeric coatings for the formation of cell adhesive coatings on different substrates have been reported by many researchers<sup>24</sup>. These coatings, however, that have been shown to promote cell adhesion, are limited by their ability to provide nanometer scale surface topography for the cells to adhere to and spread out over the surface. It has been shown by Webster et. al. that the attachment of cells increases in the presence of nanometer scale surface features<sup>25</sup>. Here, we have applied the theory that nanoparticles can be assembled with polyelectrolytes and the fact that the cells show a preferentially increased attachment to nanostructured surfaces to form thin films of nanoparticles with the desired surface topography. The objective of the formation of nanoparticle thin films is to have a surface roughness favorable for the cells to attach and spread on the surface. Through

nanoparticle thin films assembled via LbL, one can have a multilayer structure consisting of nanoparticles and polymers and have a controlled surface roughness produced on the substrate surface without compromising the integrity of the assembled thin films. Here, various nanoparticles were assembled on glass substrates as thin films ranging in thickness from 6 nm to 300 nm. The attachment of human dermal fibroblasts (HDFs)<sup>23</sup> and mouse mesenchymal stem cells (MSC)<sup>26</sup> was tested on these nanoparticle thin films. It will be shown in the following chapters that the nanoparticle thin films, with controlled roughness, are important for inducing the proper attachment, proliferation and spreading of cells. TiO<sub>2</sub> thin films provided the best surfaces for these two cell types in terms of attachment, proliferation and spreading. In general, more cells attached to rougher surfaces than on smoother surfaces. The attachment of cells was observed to be faster on rougher surfaces (larger number of layers of nanoparticles) than on smoother surfaces.

### **1.3 Organization of the Dissertation**

This dissertation is divided into 9 chapters. In the second chapter, the literature review and background information on the integration of LbL with microfabrication techniques and the integration of LbL and tissue engineering is discussed. In the next chapter, the experimental details, including the materials, methods, fabrication techniques, instrumentation and numerical simulation are discussed. In Chapter 4, the integration of LbL and microfabrication through microfluidic channels are discussed. Chapter 5 focuses on the integration of LbL with microfabrication for the formation of freestanding thin film sensors. Chapter 6 focuses on the formation of nanoparticle thin films for super-hydrophilic biocompatible coatings using TiO<sub>2</sub> nanoparticles. In Chapter 7, the cell culture techniques on nanoparticle thin films is discussed. Two types of cells

are studied in this chapter. In Chapter 8, the assembly of polyelectrolytes on glass substrates for the adsorption of hormones is discussed. The conclusions for each work are drawn at the end of the chapter discussing the work. Finally, in the ninth chapter, summary of the entire work and future work is discussed.

## CHAPTER 2

### LITERATURE REVIEW

The literature review is divided into two sections, 1) covers the background of the microfluidic devices and our integration attempts of microfabrication with LbL assembly and 2) the background of nanophase materials for the formation of cell adhesive layers and our efforts to integrate tissue engineering (cell culture) and LbL.

#### **2.1 Background of Laminar Flow Microfluidic Devices**

Conventional photolithography and other relevant technologies (multilayer photolithography, electron beam lithography, inductively coupled plasma etching, etc.)<sup>27,8</sup> are widely used in industry to fabricate ordered 2D and 3D microstructures, mostly based on silicon. This technology is rather complex and contains several series of planar pattern-transfer steps. Harsh chemical or energetic treatment accompanies each transfer step. To reduce possible defects and destruction of delicate constituents, a number of alternative methods for microfabrication were developed<sup>28,29</sup> which include electrochemical fiber growths, electroless deposition, light tweezer assisted deposition and micromolding in capillaries. Most of these methods are acceptable for working with bioorganic materials, however, they are complicated and do not have the desirable level of diversity.

Integration of softlithography and microfluidics has produced many fluidic devices which are used in the fields of chemistry and biology<sup>30</sup>. Laminar flow of multiple fluids inside a single channel allows them to flow separately. The only method of interaction between the fluids is molecular diffusion across the interface<sup>9,10</sup> between the fluids. Usually, laminar flow synthesis is carried out inside microchannels or microcapillaries prepared by softlithographic techniques. Multiphase laminar flow has been used for microfabrication of lipid bilayers inside capillaries<sup>13</sup>, patterned delivery of cells and proteins<sup>31</sup>, selective deposition of material inside microfluidic channels<sup>9,32</sup>, separation<sup>14</sup>, detection<sup>15</sup> and membraneless fuel cells<sup>11</sup>. The microfluidic approach was shown to be especially valuable for working with bioactive compounds<sup>33</sup>.

Whitesides et. al., reported microfabrication using multiphase laminar flow patterning inside microchannels made of PDMS<sup>9</sup>. In the first paper, demonstrating the phenomena of multiphase liquid flow parallel to each other with minor diffusion across the liquid-liquid interphase, they demonstrated the fabrication of trenches, polymeric complex, chemiluminescence, fabrication of calcite and apatite microcrystals, etching of silver and gold and the fabrication of complex electrical circuitry contained inside a microchannel (Figure 2.1 and Figure 2.2).

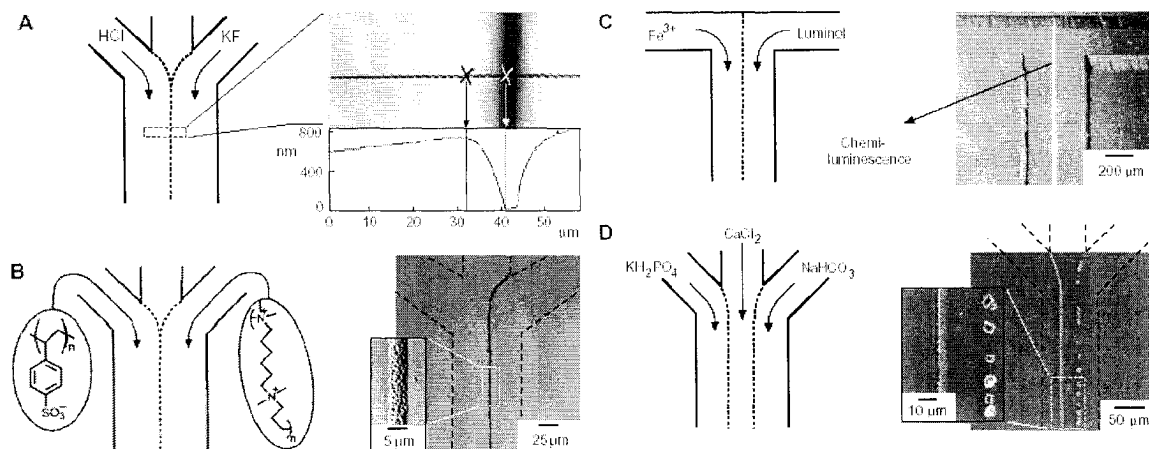


Figure 2.1. (a) Fabrication of trenches, (b) polymeric complex, (c) chemiluminescence and (d) fabrication of calcite and apatite microcrystals inside a microchannel made of PDMS<sup>9</sup>.

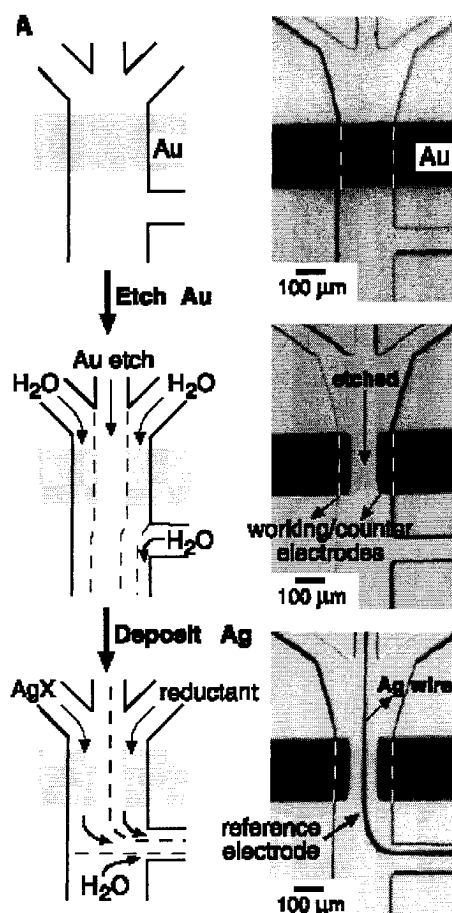


Figure 2.2. Etching of silver and gold and the fabrication of complex electrical circuitry contained inside a microchannel<sup>9</sup>.

The work done in the integration of microfluidics and biology by the group headed by Whitesides is the patterning of proteins inside the microchannels, the selective detachment of cells and patterning of cells inside the channels (Figure 2.3)<sup>31</sup>.

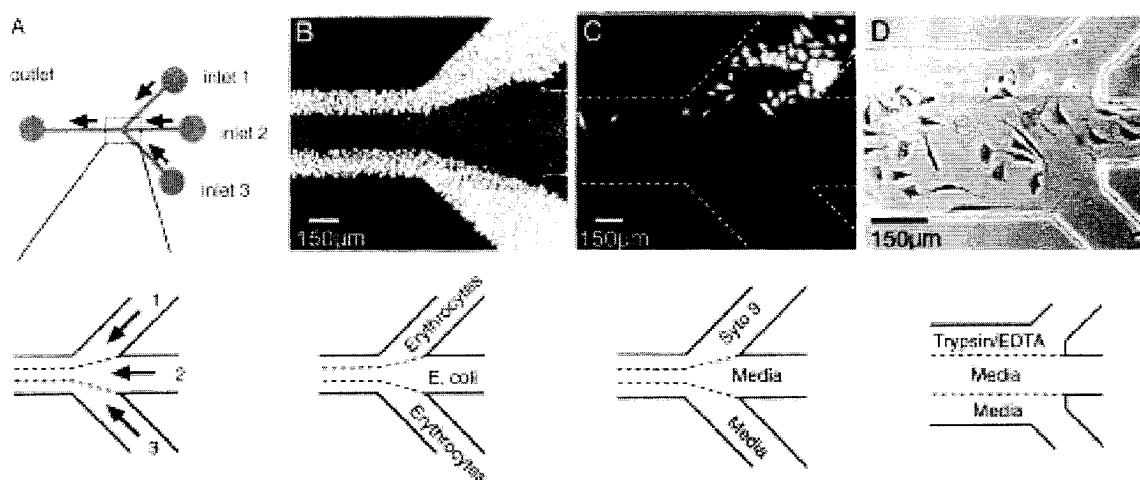


Figure 2.3. (a) Top view of a microfluidic channel, (b) patterning of different cell types inside a channel, (c) Selective staining of cells inside a channel filled with cells and (d) patterned detachment of cells inside the microfluidic channel by laminar flow patterning<sup>31</sup>.

Yager et. al. developed a similar microfluidic device, ‘T-sensor’ for applications in biochemical, chemical and cellular analysis inside confined volumes. The generation of pH gradients inside a microchannel<sup>34</sup>, cell lysis and protein extraction<sup>35</sup>, diffusion immunoassay and separation<sup>15</sup> of proteins inside microfluidic channels was achieved (Figure 2.4 and Figure 2.5).

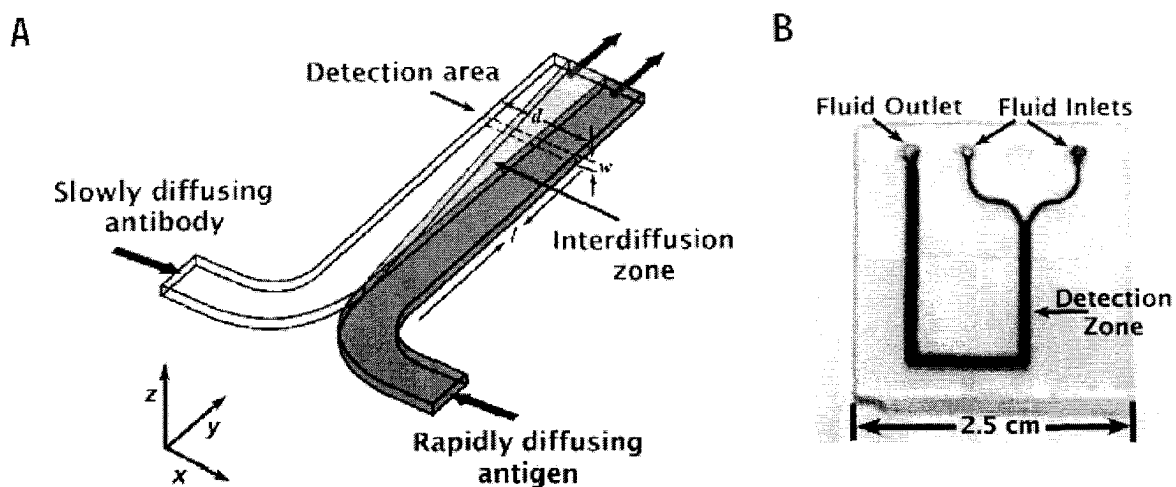


Figure 2.4. (a) Schematic of a diffusion immunoassay in a T-sensor and (b) a microfluidic device used for testing the immunoassay<sup>15</sup>.

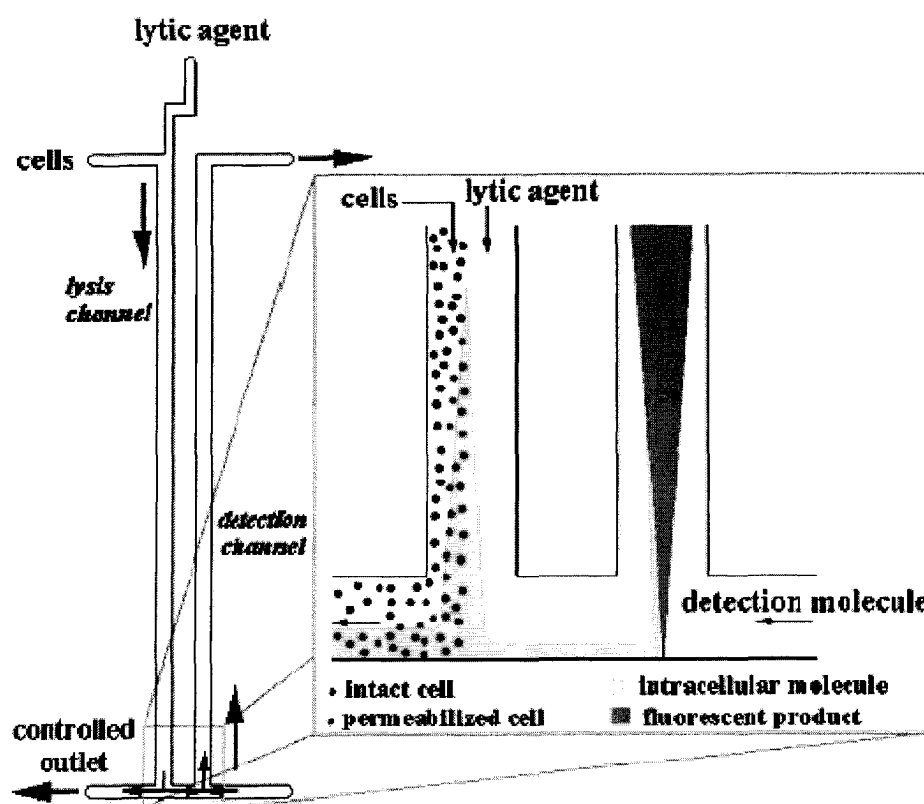


Figure 2.5. Schematic of microfluidic device for cell lysis and fractionation/detection of intercellular components<sup>35</sup>.

The groups headed by Whitesides and Yager are the principle researchers in this field of laminar flow synthesis/fabrication inside microchannels. The other notable works in this field are selective chemical treatment of cellular microdomains using multiple laminar streams<sup>36</sup>, detection and sorting of cells and particles<sup>37</sup>, fluorescence activated cell sorting<sup>38</sup>, lipid manipulation inside a channel<sup>13</sup>, design and characterization of immobilized enzymes in microfluidic systems<sup>39</sup> and assay for bacterial chemotaxis<sup>40</sup>. These works have been accomplished by application of the basic principle of diffusion across the liquid-liquid barrier in multi-phase laminar flow microfluidic channels.

Synthesis of polyelectrolyte complexes is one of the well studied areas in polymer chemistry. Previously, many methods and methodological approaches for fine, nanoengineered and simple, fabrication were developed<sup>41,42,43</sup> for the formation of polyelectrolyte complexes. Among them is the reaction between stoichiometric and non-stoichiometric quantities of oppositely charged polyelectrolytes<sup>3</sup> LbL assembly<sup>1,2</sup> *in-situ* polymerization and electroinduced polymerization. Interpolyelectrolyte complexes are of practical interest for water treatment and purification, paper making, as solid electrolytes in batteries, corrosion-protective agents, coagulants, etc. Furthermore, introducing bioactive materials (DNA, proteins, cells, enzymes, drug formulations) as constituents of the polyelectrolyte complex considerably extends its application to the fields of biotechnology, pharmacy, and medicine<sup>44,45</sup>. Different polyelectrolyte combinations with bioactive material demonstrate the synergetic and protective properties of polyelectrolyte components.

In spite of the large number of methods worked out so far to synthesize polyelectrolyte complexes in bulk or planar structures, there is an absense of simple and

comprehensive technologies to fabricate nanoengineered polyelectrolyte complexes on the microlevel. Such a lack of new approaches is especially significant for bioconjugated polyelectrolyte combinations. When introducing bioactive material in polyelectrolyte complex, it is important to retain the initial activity and structure<sup>46</sup> of the complex. For this purpose, micropatterning of biostructures should be conducted in mild, ambient conditions. Bioactive polyelectrolyte micro-nano structures can be used as elements of biosensors (polymeric circuits involving bioactive sensor element, transmission wires, signal detectors, etc.), protective coatings, and biocompatible tools for targeted DNA or enzyme delivery.

In this work, we have successfully integrated the laminar flow fabrication method to produce micropatterns of interpolyelectrolyte, polyelectrolyte/protein and polyelectrolyte/ion complexes inside the channels. We also show that the width of the polyelectrolyte complex and its position in the channel microreactor can be adjusted by the concentration, diffusion coefficient, and flow rate of individual components. We also show the selective treatment of microparticles inside the channel and the selective deposition and treatment of the channel surface with a pH sensitive dye.

### **2.1.1 Integration of Thin Film Sensors with LbL**

Sensor arrays in the millimeter down to the micrometer range are of great importance to applications involving sensing and imaging. In such applications, flexible membranes with submicron thickness are required. These flexible membranes and microcantilevers with submicron dimensions are emerging as key elements in biological, chemical, pressure and thermal sensors<sup>47</sup>. In order to have a significant amount of deflection under low stimuli, rigid membranes which are typically manufactured from

silicon, must have large lateral dimensions and micro/nanoscale thickness<sup>48,49,50</sup>. The current silicon based technologies are subject to severe limitations when considerable miniaturization is required for device fabrication for applications that use these types of sensors. Reducing the lateral dimensions of these flexible membranes from millimeter size range down to the microscopic range significantly increases their rigidity, which is a condition that cannot be compensated for by reducing the membrane's thickness. Efforts to fabricate membranes from polymers and lipids have not been very successful. These materials have produced films that are too fragile to withstand significant mechanical stress<sup>51,52,53</sup>. These factors combined with the ever growing need for the miniaturization of sensors from microscale to nanoscale dimensions face significant challenges using the technologies that are available today.

Conventional LbL assembly is a well known technology for the fabrication of engineered, multilayered, nanocomposite devices and thin films<sup>54</sup>. LbL self-assembly is exploited for the fabrication of multilayered structures with various applications in drug delivery<sup>55</sup>, electrochromic surfaces<sup>56</sup>, nanoreactors<sup>57</sup>, fuel cells<sup>58</sup> and nano structured mechanical thin films<sup>59</sup>. In the last decade, a variety of materials have been used for LbL assembly which include nanoparticles<sup>60,22</sup>, carbon nanotubes<sup>61</sup>, inorganic materials<sup>62</sup>, quantum dots<sup>63</sup> and biomaterials<sup>64</sup>. Although conventional LbL assembly is widely applied, recently described spin-assisted LbL (SA-LbL) assembly<sup>65</sup> makes the assembly process more efficient. It seems that, due to the polymer chain orientation, the SA-LbL leads to increasing stability of ultrathin multilayered films<sup>66</sup>. Therefore, robust freely suspended LbL films with nanoscale thickness (below 100 nm) with record micromechanical properties have been recently fabricated and offered as prospective

sensing elements for membrane-based thermal and acoustic microsensors<sup>67</sup>. These nanomembranes demonstrated low flexural rigidity combined with extraordinary high toughness (ultimate strength up to 100 MPa and elastic modulus of 1-10 GPa)<sup>68,69,70</sup>. Freely standing quasi-2D polymer films with well-defined shapes that have been synthesized recently, can be exploited for these purposes<sup>71</sup>. Integration of these compliant nanomembranes into prospective microsensors and microscopic arrays requires their assembly onto micropatterned silicon substrates with organized columns and rows of optical cavities. Examples of patterned freely standing LbL films have been recently demonstrated for magnetic sensors<sup>72</sup>.

In our work for the integration of LbL with microfabrication techniques, we use two approaches, a) integration of LbL with microchannels (prepared using soft lithographic techniques) for the formation of polyelectrolyte complexes and study the effects of flow rates and diffusion coefficients on these complexes, selective surface modification of microparticles and for the formation of pH sensitive microchannels and b) formation of sensor arrays of free standing thin films by the integration of LbL and lithography based microfabrication techniques (to form arrays of holes to be covered by the free standing thin films) to accelerate the optimization of flexible sensors applicable in biological, thermal and chemical fields.

## **2.2 Integration of LbL and Tissue Engineering**

### **2.2.1 Super-Hydrophilic, Biocompatible Nanoparticle Thin Films**

Understanding the properties of surfaces with superhydrophilicity (contact angle =  $0^\circ$ ) or superhydrophobicity (contact angle  $> 90^\circ$ ) are of great interest for research and practical applications. These kinds of surfaces are used to create self cleaning surfaces, which could potentially be used as surface protective coatings on various surfaces. Titanium dioxide ( $\text{TiO}_2$ ) has been studied as a material for formation of hydrophilic coatings<sup>73,21</sup>. Apart from its use as a photocatalyst for phenol degradation<sup>74,75</sup>,  $\text{TiO}_2$  films under ultraviolet (UV) light become super-hydrophilic, i.e., provide zero degree contact angles. This property has been exploited by industry to create antifogging and selfcleaning coatings<sup>76</sup>.

There are a number of techniques for the formation of  $\text{TiO}_2$  layers including coatings using self assembled monolayers (SAMs)<sup>21</sup>, spin coating<sup>77</sup>, chemical vapor deposition (CVD)<sup>78</sup>, sputter deposition<sup>79</sup> etc. Layer-by-Layer (LbL) electrostatic assembly is an innovative nanofabrication technique for producing multilayer structures with nanometer precision through alternate deposition of oppositely charged components (polymers, proteins and nanoparticles) via electrostatic interaction<sup>1,2</sup>. Simplicity of the LbL assembly technique makes it an attractive and cost-effective method for the formation of ultra-thin films with desirable properties for corrosion control<sup>80</sup>, biocompatibility<sup>81</sup>, hydrophilic and hydrophobic polymeric coatings<sup>82,83</sup>, sensors<sup>84</sup>, etc. Following the successful demonstration of the formation of  $\text{TiO}_2$  nanoparticle thin films using LbL technique<sup>85</sup>, LbL assembled  $\text{TiO}_2$  nanoparticles have been applied in solar cells<sup>86</sup> and rectifying junctions on metal nanowires<sup>87</sup>. The super-hydrophilic

characteristics of TiO<sub>2</sub> films were previously observed only when the films were irradiated with UV light<sup>86,87</sup>. We demonstrate here that a stable super-hydrophilic coating, which does not require UV irradiation, can be based on TiO<sub>2</sub> nanoparticles and polymer nanocomposites via LbL assembly. The wettability of any surface, such as glass, poly(methyl methacrylate) (PMMA) and polydimethylsiloxane (PDMS), can be controlled by coating the substrates with alternate layers of TiO<sub>2</sub> nanoparticles and polyelectrolytes, such that stable, long lasting hydrophilic coatings can be obtained. TiO<sub>2</sub> is among the most frequently used biocompatible material for implants<sup>88</sup> where good attachment of cells to these materials is essential.

### **2.2.2 Nanophase Materials for Cell Culture**

One of the main factors influencing the attachment and subsequent survival of cells on materials is the surface roughness. There are many physical factors influencing the attachment of cells on surfaces which include surface wettability, surface free energy, roughness, composition and method of preparation. Here we will concentrate on surface roughness effects on the attachment of cells. Titanium and aluminium surfaces are widely used in the implants industry to replace the defective or damaged bones. Many researchers have studied the effects of the surface roughness of these surfaces for the attachment and proliferation of various kinds of cells. Table 2.1 shows the effects on the roughness of surfaces with different treatments<sup>89</sup>. A subsequent study on these surfaces showed that the percentage of cells attached to the rougher surfaces was more than the surface with a smoother finish (Figure 2.6). The initial attachment was good on smooth surfaces, but as the number of hours advances, the rough surfaces show more cells than the smooth ones. One of the reasons cited here is the effect of surface area. The rougher

surfaces have a higher surface area than the smoother ones. So the rough surfaces had more surface for the cells to attach to and proliferate than the polished surfaces.

Table 2.1. The mean and standard deviation of the surface roughness parameters of three samples of ceramic abutments<sup>93</sup>.

Sample	$S_a$ (SD) $\mu\text{m}$	$S_{cv}$ (SD) $\mu\text{m}$	$S_{dr}$
Milled	0.34 (0.02)	10.21 (0.25)	1.14 (0.01)
Sintered	0.22 (0.02)	10.22 (0.42)	1.08 (0.01)
Polished	0.06 (0.01)	16.99 (2.75)	1.01 (0)

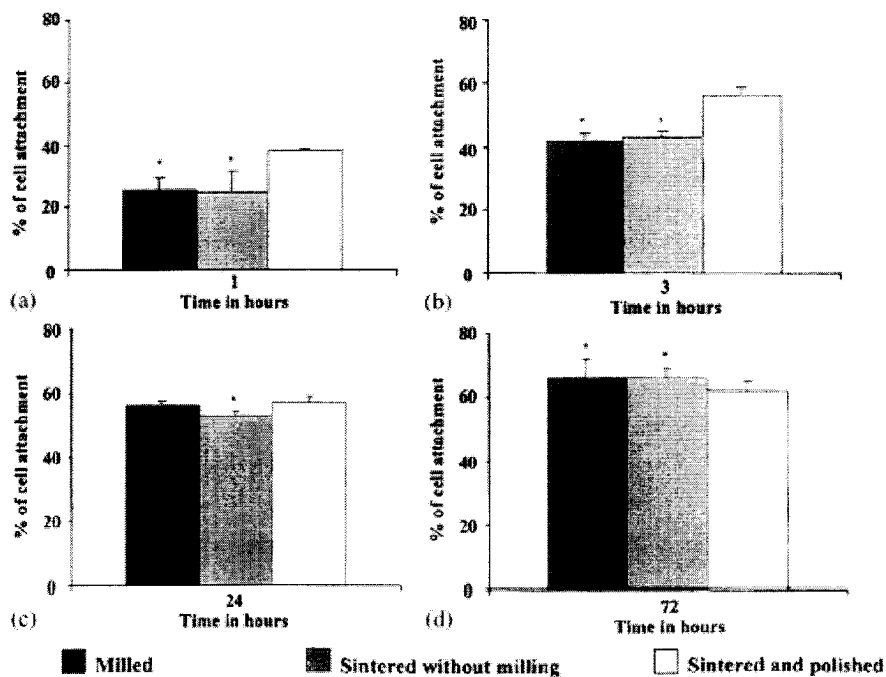


Figure 2.6. Attachment of human gingival fibroblast to the different ceramic surfaces. Each bar represents the mean of percentage of attachment in one of two identical experiments performed in triplicate. \* Statistically significant differences compared with the polished surfaces  $P < 0.05$ <sup>93</sup>.

Another study on the attachment of cells also found that the surface with rougher texture offers a better surface for the attachment and proliferation of cells (Figure 2.7 and Figure 2.8)<sup>90</sup>. The findings from this study show that human bone marrow cells can detect changes in roughness of the order of 600 nm and bovine serum albumin is adsorbed preferentially onto the smoother Ti alloy. The rough substrate binds a higher amount of total serum protein and fibronectin than does the smooth surface. The increased cellular attachment on rough Ti alloy could be explained by the preferential adsorption of fibronectin onto this substrate. Other studies on the attachment of cells on surfaces of varying roughness also found that the cells attached and proliferated better on rougher surfaces than on the same material with a smoother surface finish<sup>91</sup>.

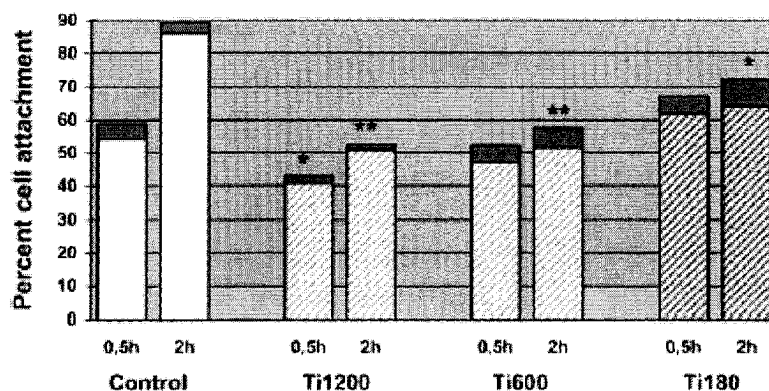


Figure 2.7. Human bone marrow cell attachment to Ti alloy disks with three surface roughness values and the control. Attachment is displayed as the percentage of cells attached after 0.5 and 2 h of incubation. 1200, 600 and 180 is the grit of the paper with which the surface of Ti was polished. Values are the mean  $\pm$  SD of six cultures. \*, \*\* indicate a significant difference with plastic at the corresponding time point (\*  $p < 0.05$ ; \*\*  $p < 0.01$ )<sup>94</sup>.

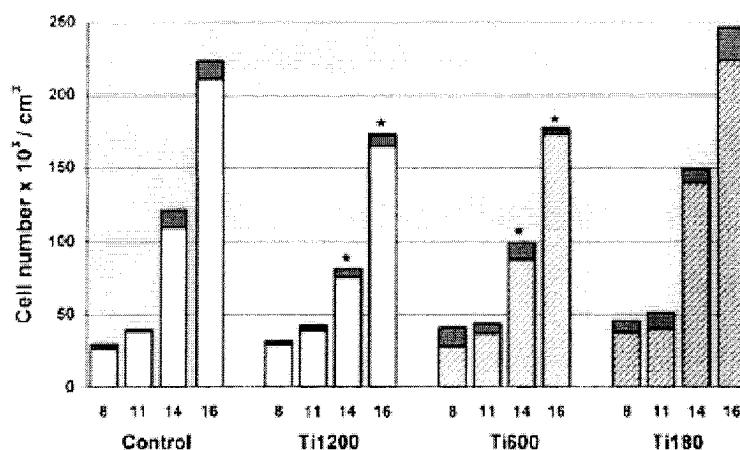


Figure 2.8. Human bone marrow cell proliferation after 8, 11, 14 and 16 days of culture on Ti alloy for the three groups (Ti1200, Ti600 and Ti180) and the control (tissue culture plate). Values are the mean  $\pm$  SD of six cultures. \* indicates a significant difference with both plastic and Ti180 at the corresponding time point ( $p < 0.05$ )<sup>94</sup>.

Recently, nanostructured surfaces are being investigated extensively to study the effects of nanophase surface roughness on the attachment of cells. Thomas Webster's group at Purdue University is the main research group working on the attachment of cells to nanostructured materials<sup>92,93</sup>. They have shown the increased attachment of cells on different kinds of nanostructured surfaces including fibers nanophase ceramics and metals. A comparison of borosilicate glass with surfaces with various grain sizes (roughness) was performed to evaluate the attachment of osteoblasts to these surfaces and is depicted in Figure 2.9.

Cell-surface interactions are of great importance and is an area of intense research for orthopedic, dental and other types of implants<sup>94</sup>. The initial interaction of cells with these surfaces has been shown to affect the long term viability of the implants<sup>95</sup>. Nanophase materials have recently been shown to have greater advantages over conventional materials for increased cell attachment<sup>96,97</sup>. Nano-structured materials offer many

possibilities for the modification of various materials for optimal attachment, proliferation and spreading of different kinds of cells. The attachment of cells was shown to increase in the presence of or when coated with nano-phase materials<sup>98</sup>. The increased surface area of nano-phase materials as compared to unmodified surfaces, for the cells to attach to and spread was attributed to the increased attachment of cells on these surfaces<sup>93,99</sup>. Different aspects, such as surface wettability and free energy<sup>100</sup>, surface roughness and material composition<sup>101</sup>, method of preparation<sup>102</sup>, etc. of nano-structured materials have been studied for attachment and were determined to be major factors influencing the behavior of cells, *in-vitro*. A variety of nanostructured materials such as, ceramics<sup>103</sup>, nanoparticles<sup>104</sup>, polymers<sup>105</sup> and extracellular matrix proteins<sup>106</sup>, when coated or present<sup>107</sup>, have been shown to be effective in increasing the proliferation of different kinds of cells. A range of different techniques have been employed for the modification of implantable materials including self assembled monolayers, chemical modification, spin coating, etc.

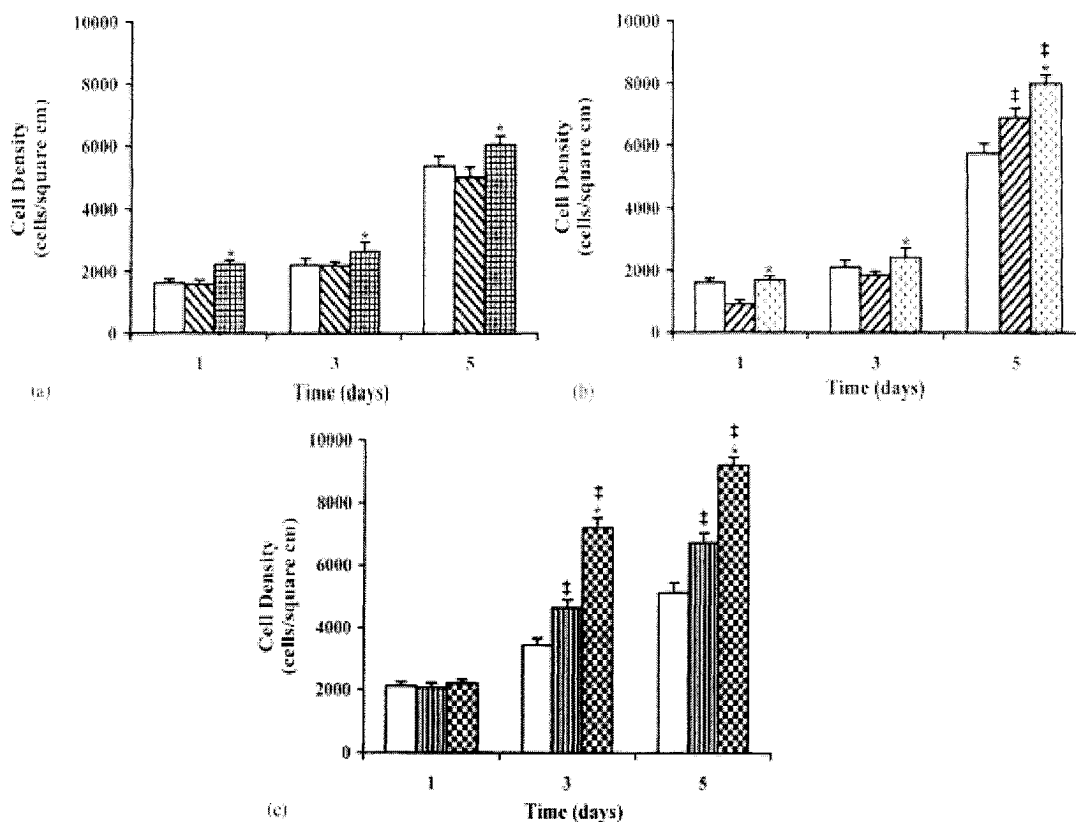


Figure 2.9. Osteoblast proliferation on ceramics. (a) □ borosilicate glass (reference material), ▨ 167 nm grain size alumina (conventional), and ▩ 24 nm grain size alumina (nanophase); (b) □ borosilicate glass (reference material), ▨ 4520 nm grain size titania (conventional), and ▩ 39 nm grain size titania (nanophase); and (c) □ borosilicate glass (reference material), ▨ 179 nm grain size hydroxyapatite (conventional), and ▩ 67 nm grain size hydroxyapatite (nanophase). Osteoblast proliferation under standard cell culture conditions was determined after 1, 3, and 5 days. Values are mean  $\pm$  SEM;  $n=3$ ; \*  $P<0.01$  (compared to respective conventional grain size ceramic); +  $P<0.01$  (compared to borosilicate glass)<sup>99</sup>.

A new technique used for surface modification is the LbL nanoassembly, which works on the principle of electrostatic attraction between oppositely charged species, such as polymers, nanoparticles, enzymes/proteins and so on. The LbL technique has been employed in various applications in biological and materials fields. LbL assembly offers a greater advantage over other methods of surface modification, in that the

adsorption of material can be controlled with nanometer precision and the architecture of the assembled films can be tuned to include multiple components (internal multilayered organization) with specific purposes for each component without compromising the integrity of the assembled multilayer film or the material being coated.

In this work, we will discuss the formation of surfaces with nanophase roughness using the assembly of nanoparticle thin films on glass substrates and the attachment of cells to these surfaces. Recently, for the first time, we have shown the LbL assembly of nanoparticles for the modification of various surfaces for improved attachment of cells<sup>22</sup>. Attachment of cells on an otherwise cell repellent surface was observed after coating those surfaces with TiO<sub>2</sub> nanoparticles. In a related study, TiO<sub>2</sub> thin films were shown to be the best surfaces for the faster attachment and spreading of cells compared with other kinds of nanoparticle thin films<sup>26</sup>. Based on these initial studies, TiO<sub>2</sub> nanoparticles were chosen for studying the effects of surface roughness of LbL assembled thin films on the attachment, proliferation and spreading of mouse mesenchymal stem cells (MSC).

## CHAPTER 3

### EXPERIMENTAL SECTION

The experimental section is divided into the two parts which describe the different sections of this dissertation. In the first part, the experimental details about the integration of microfabrication and LbL assembly will be discussed. In the second part, the biological aspects of the thin films formed using LbL assembly will be discussed. Materials, methods and instrumentation will be discussed in detail in this section.

Some of the characterization tools available for the thin films formed using LbL are the quartz crystal microbalance (QCM), UV-visible spectroscopy, atomic force microscopy (AFM), scanning electron microscopy (SEM), contact angle measurement devices, confocal and fluorescent microscopy, surface profiler, small-angle X-ray and neutron reflectivity, Fourier transform infrared spectroscopy, X-ray photoelectron spectroscopy, ellipsometry and surface plasmon resonance. The above listed characterization tools can be used for determining the thickness, composition and to determine the adsorption of material on the substrates of interest. The tools mentioned above are some of the more frequently used tools for characterization purposes. However there are many other tools (not mentioned) that can be used for characterization. All of the tools mentioned above have their own advantages and limitations. Depending on the kind of substrate used and the environment in which the assembly takes place, the tools

of interest are chosen, that will give optimal results. The tools used to characterize the LbL thin films, in this dissertation are: Quartz crystal microbalance (QCM) (USI systems, Japan) which was used to determine the thickness of the thin films deposited using LbL, UV-vis spectroscopy (Agilent 8453 UV-vis) was used to determine the deposition of the thin films using the absorbance of the material deposited, confocal microscope (Leica) was used to image the fluorescent molecules deposited using LbL and to visualize cells for the viability tests, surface profiler (Wyko) was used to measure the surface roughness of the nanoparticles assembled. Scanning electron microscope (AMRAY) was used to image the cells for the spreading tests, atomic force microscope (Quesant) was used to acquire the images of the polyelectrolyte complexes.

### **3.1 Microfabrication and Layer-by-Layer Assembly**

#### **3.1.1 Materials**

Positive photoresist (AZ 9260) was purchased from MicroChemicals. Silicon wafers were purchased from Montco Silicon Technologies, Inc. Poly(dimethyldiallylammonium chloride) (PDDA, MW ~ 200,000, Aldrich), poly(allylamine hydrochloride) (PAH, MW 10,000, Aldrich), which are positive polyelectrolytes at pH<11.5 and pH<8.5, respectively, and poly(styrene sulfonate) (PSS, MW 70,000, Aldrich), which is a negative polyelectrolyte at pH> 1.5, were used for the formation of polyelectrolyte complexes. 8-Hydroxypyrene-1,3,6-trisulfonic acid Trisodium salt (HPTS, SIGMA-H1529) and PDDA solutions were premixed in the ratio of 1:4 according to the procedure described earlier<sup>108</sup>. For confocal fluorescence microscopy investigations, PDDA and PAH were labeled with fluorescein isothiocyanate

(FITC) and PSS was labeled with tetramethyl rhodamine isothiocyanate (TRITC) according to the procedure for amine labeling<sup>109</sup>. Bovine serum albumin (BSA) and sodium citrate were purchased from Sigma. All chemicals were used as received. The water in all experiments was prepared in a three-stage Millipore Milli-Q Plus purification system and had a resistivity higher than 18 M $\Omega$ ·cm.

### **3.1.2 Instrumentation**

A mask aligner was used to transfer the pattern of the channels for the mask to the photoresist on the silicon wafer. Inductively coupled plasma etching (Alcatel) was used to etch the silicon wafers after exposure. Hot embossing ((JENOPTIK Mikrotechnik) was used to transfer the pattern from the silicon wafer on to poly(methyl methacrylate) (PMMA). Oxygen plasma was used to bond the channels (PDMS) to glass slides. A syringe pump (Kd scientific) was used to pump solutions into the channels. The formed complexes were visualized using the confocal microscope, AFM and optical microscope.

### **3.1.3 Fabrication of Microchannels**

Lithography on silicon was performed using a thick layer of positive photoresist. Then, the wafer was etched using inductively coupled plasma etching (Alcatel, 601E, USA) to prepare channels of 200-400  $\mu$ m wide. The resulting wafer pattern was used as a mold for the subsequent hot-embossing of a PMMA sheet. This hot-embossing step transfers the channels onto the PMMA sheet as raised lines. The PMMA replica was used as the final mold to form microchannels in a polydimethyl siloxane (PDMS) membrane. To obtain final PDMS microchannels, PDMS (Sylgard 184 silicone elastomer) and the curing agent (Sylgard 184 curing agent) were mixed in 10:1 ratio, poured onto the PMMA replica, and heated at 80<sup>0</sup>C for 30 minutes. The channels formed in the PDMS

and a glass slide were then exposed to oxygen plasma for 30 seconds and were brought into contact immediately, which attached the PDMS channel to the glass surface irreversibly<sup>9</sup>. The schematic representation of the formation of the channels is depicted in Figure 3.1.

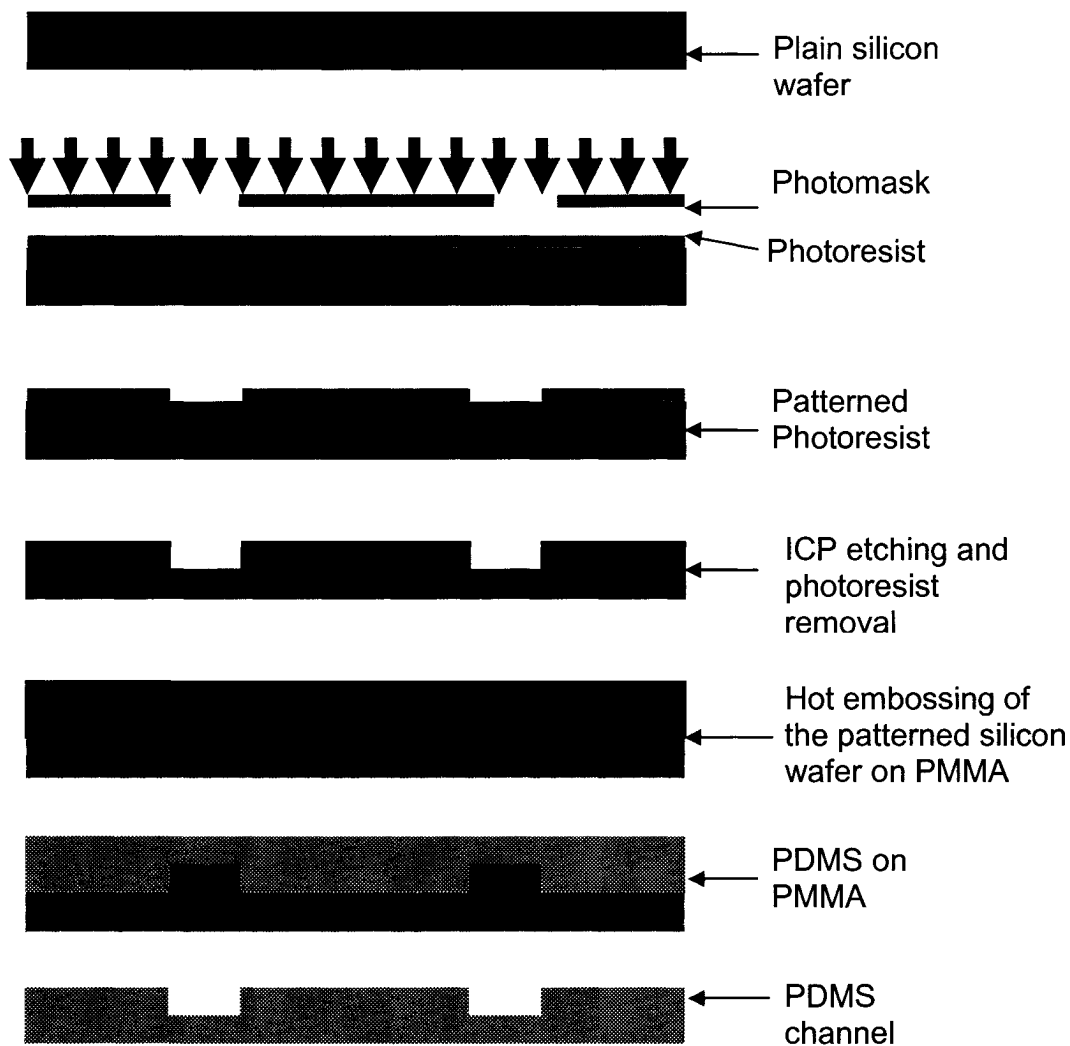


Figure 3.1. Microchannel formation through lithography, hot embossing and soft-lithography.

### **3.2 Experimental Setup**

The procedure is schematically illustrated in Figure 3.2. Y- and S-type reactor microchannels were employed to demonstrate the formation of interpolyelectrolyte, polyelectrolyte/protein or polyelectrolyte/ion micropatterns. To fabricate polyelectrolyte microarrays on the glass support, a PDMS membrane with the channel pattern molded into its surface was brought into a contact with the flat surface of the glass slide, after oxygen plasma treatment. Each reactor channel was provided with two inlets and one outlet. Reagents from the inlet channels converge into a single laminar stream in the reactor microchannel. Each reagent solution was gently pumped into its inlet by a syringe pump. An experimental setup is schematically represented in Figure 3.2:(a, b) polyelectrolyte complex formation inside Y and S-type channel microreactors; (c) side view perpendicular to the reactor microchannel PDMS sheet, with microchannels molded in its surface was placed on the flat surface of glass support to form polyelectrolyte micropatterns with PDDA, PSS and bovine serum albumin (BSA). (d) microphotographs of the channel microreactors. The microfluidic reactor system as shown in Figure 3.3, is composed of two inlet channels (1, 2), reactor microchannel (3), and one outlet channel (4). Each reagent solution was gently pumped into its inlet using a syringe pump equipped with two syringes (5). Solutions flowing in the inlet channels converge into a single laminar stream in the reactor microchannel. Detailed explanation about the experiments conducted using these channels and the materials used will be discussed in the results section.

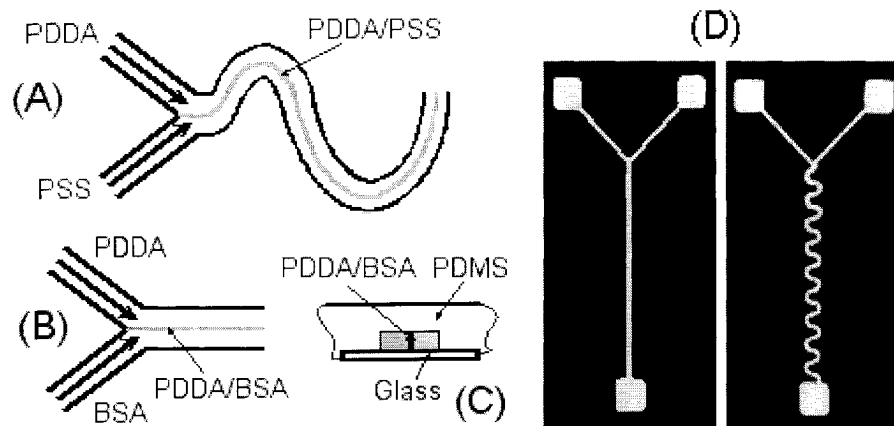


Figure 3.2. Schematic representation of laminar flow patterning experiment.

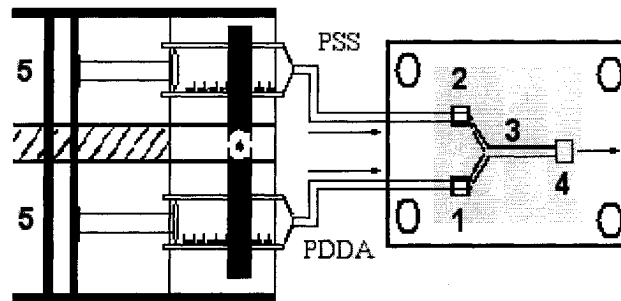


Figure 3.3. Schematic illustration of the laminar flow patterning experimental setup.

### 3.3 Numerical Simulation

The reaction of species in microchannels of various geometries and conditions has been studied for a long time. Two or more species flowing under laminar conditions in microchannels interact only by molecular diffusion. If adjacent layers of fluid flow smoothly over or next to each other, the flow is called laminar flow. At higher flow rates (velocity) the flow changes from laminar flow conditions to turbulent flow conditions. The velocity where the transition from laminar to turbulent takes place depends on the geometry of the channel (tube) and the viscosity of the fluid(s). The onset of turbulence

was determined experimentally and is defined by a dimensionless parameter known as the Reynolds number (Re) which is defined by:

$$\text{Re} = \frac{\rho v d}{\mu}$$

where  $\rho$  is the fluid density,  $v$  is the velocity of flow,  $d$  is the diameter of the channel and  $\mu$  is the viscosity of the fluid<sup>110</sup>. It has been shown experimentally that the onset of turbulence occurs at Reynolds number over 3000. The condition of flow at  $\text{Re} < 2100$  is known as the laminar flow condition. The condition of flow at the intermediate range  $2100 > \text{Re} > 3000$  is known as the transition region where the transition from laminar to turbulence occurs.

### **3.3.1 Effect of Flow Rate**

Theoretical modeling for “Y”-shaped channels was done using CoventorWare software version 2001.3 (<http://coventor.com>), a fully integrated microelectromechanical systems (MEMS) design environment, to analyze the effect of solution flow rates on the position of the polyelectrolyte complex in the microchannel. The reaction between PDDA and PSS, PDDA and BSA was assumed to be a first order nonreversible diffusion-controlled reaction. The diffusion coefficient of the polyelectrolytes (PDDA, PSS and PAH) in aqueous solutions was taken as  $10^{-7} \text{ cm}^2 \cdot \text{s}^{-1}$ , that of the BSA was taken as  $5 \cdot 10^{-6} \text{ cm}^2 \cdot \text{s}^{-1}$ <sup>111,112</sup>. For citrate ions the diffusion coefficient was assumed to be  $10^{-5} \text{ cm}^2 \cdot \text{s}^{-1}$ . Since the reaction between the oppositely charged polyelectrolytes is fast and irreversible, the reaction rate constant was taken as very high and was set to the maximum allowable in the software.

The individual flow rates of the inlet solutions were varied and the position of the complex inside the channel was simulated using the software. Increasing the flow rate in

one of the inlet channels increases the amount of solution flowing in that channel and this shifts the formation of the complex towards the side with the lower flow rate. This shifting of the complex using the flow rate variation is a powerful tool to position the complex at a predetermined location inside the channel. This can also be done during the reaction. The simulation results for the variation in flow rate are illustrated as follows. below. Figure 3.4 shows the condition simulated where the flow rates in the inlet channels is equal. It can be seen that the reaction product is formed in the middle of the channel. The simulation of the variation in flow rates is shown in Figures 3.5-3.8. The flow rate in the left inlet channel is increased by a factor of 2, 3, 5 and 10 times. One can see the shift in the product formation from the middle of the channel for equal flow rate towards the side having a lower flow rate. This is due to the volume of the liquid (reactants) flowing in the channels. The higher the flow rate, the higher is the volume of the liquid flowing in that channel and this pushes the product formed from the middle of the channel to the side with lower flow rate (lower volume of liquid flow). Figure 3.5 shows the condition of flow where the flow rate in the inlet channel in the left is twice the flow rate of the fluid on the inlet channel in the right. Figure 3.6 shows the condition where the flow rate in the left channel is three times the flow rate in the channel on the right. Figure 3.7 and Figure 3.8 show the flow conditions where the flow rates in the left channel are 5 and 10 times the flow rate in the right inlet channel. It can be seen from the line graphs (plot on the right side of each figure) and the channels images that the reaction product shifts from the left side to the right side by increasing the flow rates.

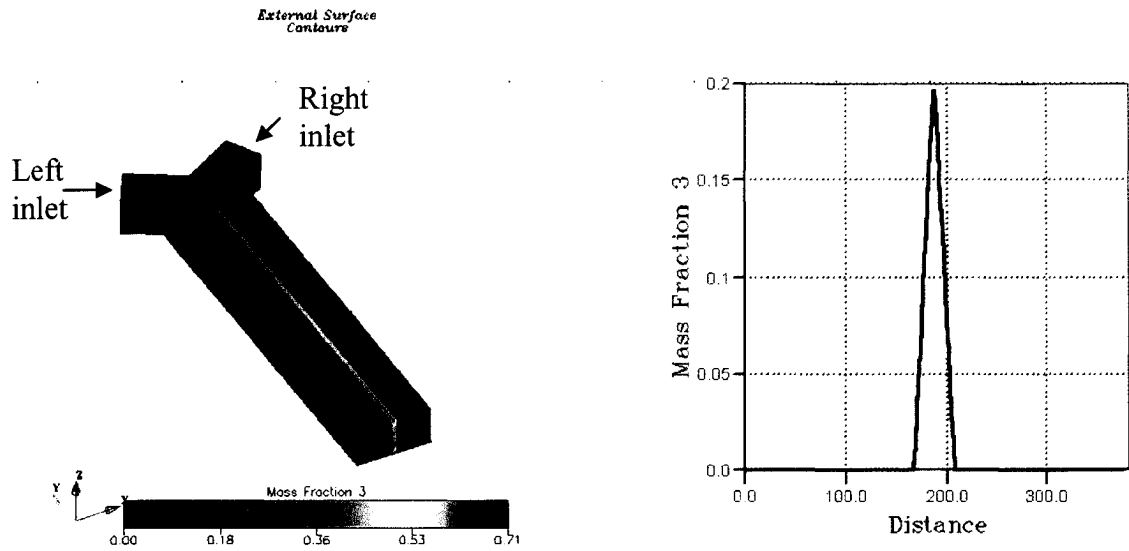


Figure 3.4. Left, Simulation results for equal flow rates in the left and right inlet channels and right, line graph of the mass fraction in the middle of the outlet channel.

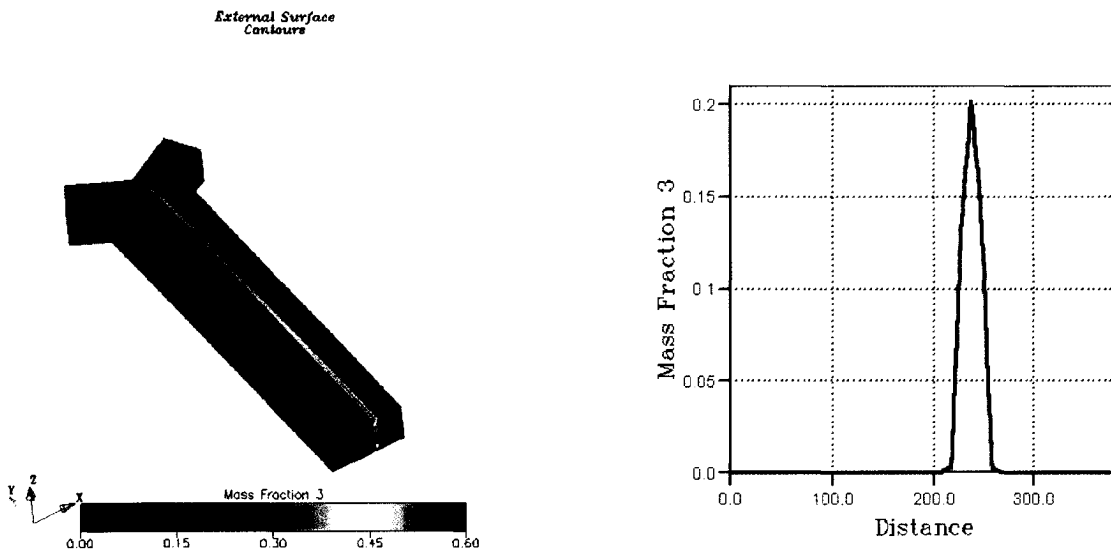


Figure 3.5. Simulation of the condition where the flow rate in the left inlet is 2 times the flow rate of the inlet on the right.

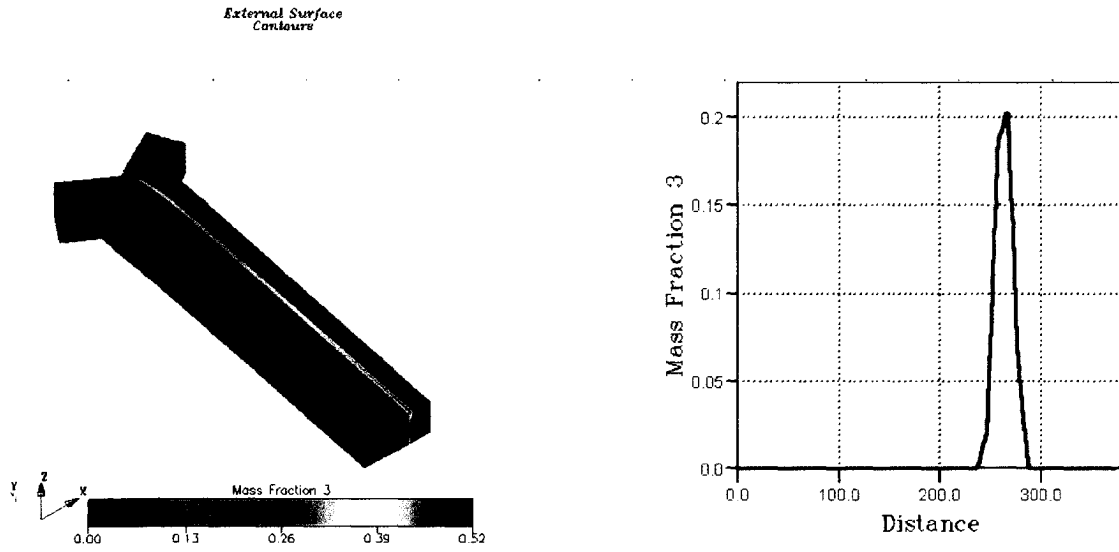


Figure 3.6. Simulation of the condition where the flow rate in the left inlet is three times the flow rate of the inlet on the right.

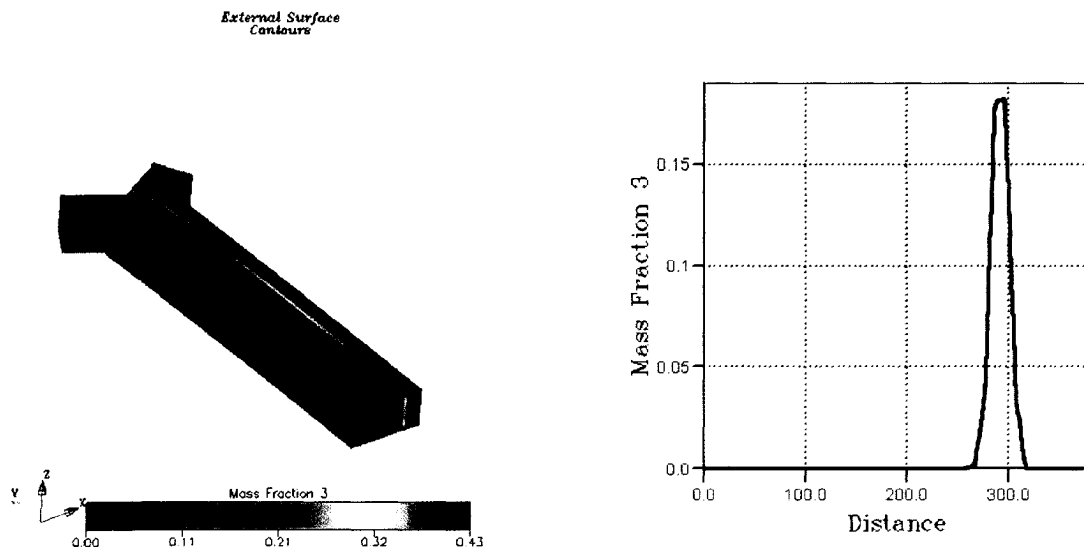


Figure 3.7. Simulation of the condition where the flow rate in the left inlet is five times the flow rate of the inlet on the right.

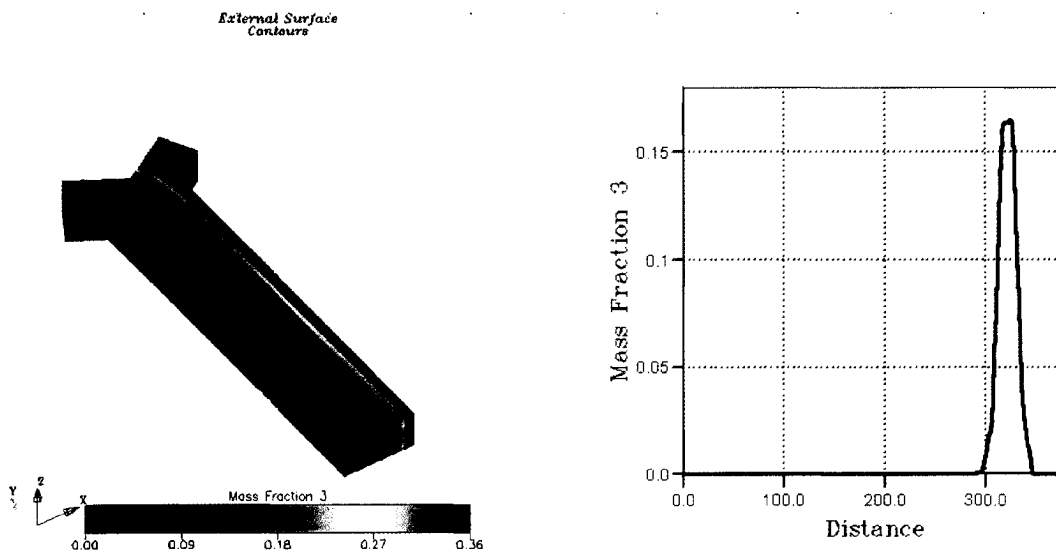


Figure 3.8. Simulation of the condition where the flow rate in the left inlet is ten times the flow rate of the inlet on the right.

### **3.3.2 Effect of Diffusion Coefficient**

The simulation of the condition where the diffusion coefficient is higher on one side of the inlet channels is shown in Figure 3.9. In this simulation, the diffusion coefficient of the species in the left inlet channel is 100 times more than the diffusion coefficient of the species in the right inlet channel, which is the simulation of the polyelectrolytes in the right inlet and the ions in the left inlet. Since the ions have a higher diffusion coefficient than the polyelectrolytes, the diffusion of ions into the polyelectrolyte side of the reaction channel can be clearly seen. The line graph of this simulation is shown in Figure 3.10.

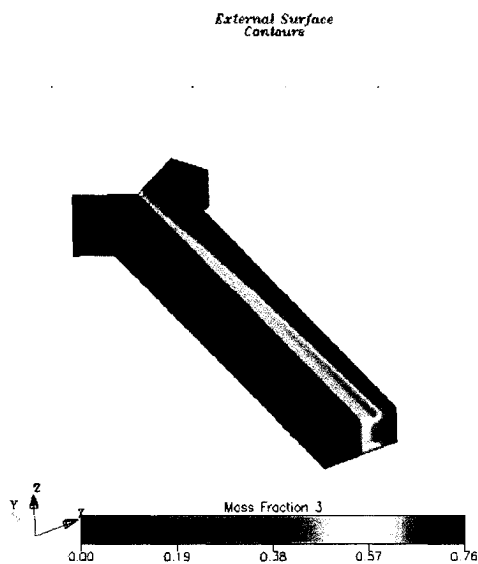


Figure 3.9. Simulation of the variation of diffusion coefficient in the reaction channel.

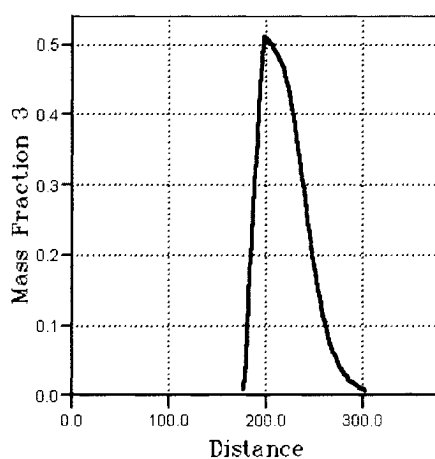


Figure 3.10. Line graph of the reaction product in the reaction channel.

### **3.4. Layer-by-Layer Assembly for Microfluidics**

LbL was used for the formation of pH sensitive thin films inside the microchannel surface. First, the channel surface was coated with a positively charged pH sensitive polyelectrolyte (PDDA-HPTS) by flowing it into one of the inlet channels for 10 min at

0.1 mL/min. Then the channels were rinsed by injecting DI water into the channels at a rate of 0.1 mL/min for 5 min. Then the channel was coated with a negatively charged polyelectrolyte(PSS) by flowing it through the channel for 10 min at 0.1 mL/min. By repeating this process, the channel surface was coated with 7 bilayers of PDDA-HPTS/PSS. The channels were then used to pump solutions of different pH to obtain the spatial resolution in the sensitivity to pH, in-situ.

### **3.5 Layer-by-Layer Assembly for Superhydrophilic Nanoparticle Coatings**

#### **3.5.1 Materials**

Poly(styrene sulfonate) sodium salt (PSS, 70KDa, Sigma), poly(dimethyldiallyl ammonium chloride) (PDDA, 200KDa, Sigma), poly(allylamine hydrochloride) (PAH, 70 KDa, Sigma) were used as received without further purification. TiO<sub>2</sub> (diameter 21nm, Aeroxide TiO<sub>2</sub>, P25 Degussa AG, Germany), montmorillonite (Aldrich, USA), Halloysite G clay ( diameter 50 nm x 500 nm cylinder, New Zealand China Clays Ltd, New Zealand) and silica nanoparticles (diameter 7-9 nm, Nissan Chemical Industries Ltd., Japan) were dispersed in DI water and used for LbL assembly. Glass microscope slides were purchased from VWR scientific. Polydimethylsiloxane (PDMS) was obtained from Dow Corning and the preparation of the PDMS substrates were explained in detail previously. Poly(methyl methacrylate) (PMMA) was obtained as sheets from AIN Plastics, USA. Human dermal fibroblasts (HDF) were purchased as cryopreserved stocks from Cascade Biologics, Inc. Microscope glass slides were used as substrates for LbL assembly and were purchased from VWR scientific. Mesenchymal stem cells (MSCs) were purchased as cryopreserved stocks from ATTC. Cell viability was performed using

the cytotoxicity test kit obtained from Molecular Probes. Cell proliferation was tested with the incorporation of bromodeoxyuridine (BrdU, Oncogene) in the cell culture media. Cell phenotype was determined using polyclonal antibodies (Rockland Immunochemicals) raised against human type I collagen.

### **3.5.2 Instrumentation**

A dipping machine (Riegler & Kirstein GmbH, Germany) was used for the formation of thin films of nanoparticles on the substrates. Confocal (Leica) and fluorescent microscopes were used for the cell viability and attachment studies. Surface roughness step tester (Wyko surface profiler, Veeco instruments, USA) was used for measuring the surface roughness of the substrates. For thickness measurements, nanoparticles/polyelectrolytes were coated on 9 MHz quartz crystal resonators. The change in frequency of the resonators, monitored using a USI-system, Japan, was correlated with an increase in film thickness by  $\delta d = -0.016\delta F$ , where  $\delta d$  is the change in the thickness and  $\delta F$  is the change in frequency. The UV-visible absorbance measurements of the TiO<sub>2</sub> nanoparticles on quartz slides were monitored using an *Agilent 8453* UV-vis spectrometer. The water contact angle (WCA) was measured by the sessile drop method using a Data Physics *OCA* contact angle measurement device. Scanning electron microscopy (AMRAY) was used to visualize the manner of cell attachment and the degree of cell spreading on the substrates. The surface potential of the nanoparticles was measured using a Brookhaven Zeta Plus micro-electrophoretic instrument.

### **3.6. Layer-by-Layer Assembly for Tissue Engineering and Wettability Studies**

All solid substrates (glass, PDMS and PMMA) were washed in DI water, dried in a stream of nitrogen and used for LbL assembly. Three precursor bilayers of PDDA/PSS were deposited by sequential dipping of substrates in polyelectrolyte solutions. All polyelectrolytes were used at a concentration of 3 mg/mL and pH 6.0. Nanoparticles were dispersed in DI water, ultrasonicated for 30 minutes and used for LbL assembly. Polyelectrolytes were used at a concentration of 3 mg/mL in DI water and nanoparticles were used at a concentration of 6 mg/mL in DI water. The deposition of the precursor layers was followed by the alternate adsorption of the required number of PSS/TiO<sub>2</sub> bilayers with the final layer being TiO<sub>2</sub> in all cases. The entire LbL process on all the substrates was accomplished using a dipping machine. For thickness measurements, nanoparticles were coated on 9 MHz quartz crystal resonators according to the procedure described above and the frequency measured after the deposition of each layer. For WCA measurements, the bare substrates (glass, PMMA and PDMS) were rinsed in DI water and dried in a stream of nitrogen. Then 0.5  $\mu$ L of DI water was placed on the substrates and the change in the WCA measured over time. After deposition of the required number of TiO<sub>2</sub> layers, WCA was measured for each substrate as described above.

Before plasma treatment, all substrates were rinsed in DI water and dried in a stream of nitrogen. They were treated with oxygen plasma for 1min (300W, 6 cm<sup>3</sup>/min oxygen) using a Techniques MicroRIE and immediately dipped in a solution of PDDA. The same sequence of layers, as was used for the bare substrates (non plasma treated), was deposited. The effect of other nanoparticle layers on the substrate wettability was

demonstrated by the deposition of montmorillonite, halloysite and silica nanoparticles, alternated with PDDA (three precursor bilayers of PSS/PDDA) on glass. PSS/PAH and PSS/PDDA thin films were deposited on bare PMMA to investigate the stability of these coatings under storage. The dried polyelectrolyte and nanoparticle/polyelectrolyte films were maintained under dark conditions at room temperature for several days. The WCA was the measured for the as-kept films.

### **3.7 Surface Roughness of LbL Assembled TiO<sub>2</sub> Thin Films**

A non-contact optical profiler operating in the VSI mode was used for the measurement of the average surface roughness ( $R_a$ ) of the substrates coated with TiO<sub>2</sub>. Six  $R_a$  measurements per sample were taken and 3 samples per layer number were measured and were plotted as averages against the number of layers of TiO<sub>2</sub> deposited in alternation with PSS. Each substrate had TiO<sub>2</sub> as the top most layer. The quantity  $R_a$  is

given by: 
$$R_a = \frac{1}{M * N} \sum_{i=1}^M \sum_{j=1}^N |Z_{ij}|$$

where  $M$  and  $N$  are the number of data points in the  $X$  and  $Y$  direction of the array and  $Z$  is the surface height relative to the reference plane.

### **3.8 Cell Culture**

MSC and HDFs were maintained in Dulbecco's Modified Eagles Medium (DMEM) containing 10% fetal bovine serum and 1% antibiotic-antimycotic (complete DMEM). Culture media was replaced with fresh complete DMEM every other day and cells were allowed to grow until sufficient cell density was reached, cells were then

trypsinized, collected by centrifugation at 1000 rpm for 5 minutes, and resuspended in complete DMEM prior to plating on the nanoparticle coated substrates. Substrates coated with the nanoparticles were immersed in a 75% ethanol solution and rinsed in Hank's balanced salt solution (HBSS). The substrates were removed from HBSS and placed in 60 mm dishes and HDFs and MSCs were seeded onto the nanoparticle coated substrates. The dishes containing the nanoparticle coated substrates were then incubated at 37°C and 5% CO<sub>2</sub> and 95% air within a humidified environment.

### **3.8.1 Cytotoxicity**

A qualitative two color cytotoxicity assay was performed to determine the cytotoxicity of the substrates coated with nanoparticles. The substrates were incubated with the cells for 48 hours and rinsed with sterile PBS twice and were incubated with viability/cytotoxicity reagents (LIVE/DEAD assay, Molecular Probes, USA) for 30 minutes. The cells were then visualized using a confocal fluorescence microscope.

### **3.8.2 Cell Number**

MTT assay was performed on the cells attached on the nanoparticle thin films to determine cell numbers. A calibration curve correlating the absorbance with the number of cells was obtained first. Briefly, the cells were seeded on the substrates at a density of 6000 cells/cm<sup>2</sup> and were incubated for 72 hours with media changes every other day. At the end of 72 hours, the media in the culture dishes was drained and the substrates were removed from the culture dishes and put in fresh dishes. The cells were then incubated with 10% MTT solution in the media for 4 hours. The culture dishes were drained of the MTT solution in the media and the formazan crystals that formed due to the interaction of the MTT solution with the cells was dissolved in acidified isopropyl alcohol. The

absorbance of the resulting solution was read spectrophotometrically, using an *Agilent 8453* UV-vis spectrometer, and correlated with the calibration curve.

### **3.8.3 Cell Attachment**

For the cell attachment studies, the substrates (3 samples for every time period for every layer) were seeded with equal densities and the cells were allowed to attach to the substrate for 4, 12 and 24 hours. The substrates were then taken out, rinsed twice in PBS and then incubated with the cytotoxicity reagents for 30 minutes. Images of the cells on the substrates were then taken using a Nikon digital camera mounted on a Nikon Eclipse inverted fluorescence microscope and the cells in each image was counted to determine the number of cells present.

### **3.8.4 Scanning Electron Microscopy of Cells on Nanoparticle Substrates**

Scanning electron microscopy was used to visualize the manner of cell attachment and the degree of cell spreading on the substrates. Briefly, the cells were incubated on the substrates for 1, 4, 12 and 24 hours. The substrates were then taken out of the petridishes and were rinsed three times with sterile PBS. The cells on the substrates were then fixed with 2.5% glutaraldehyde in PBS for 1 hour, washed three times in PBS and incubated with osmium tetroxide for 1 hour. The cells on the substrates were then rinsed three times with PBS. The cells were then dehydrated by sequential dipping in increasing concentrations of alcohol. The cells on the substrates were finally critical point dried, 6 nm of gold/palladium alloy sputter coated on the substrates and the cells were visualized using an Amray scanning electron microscope.

### **3.8.5 Statistical Analysis**

Mean and standard deviations (SD) were calculated for descriptive statistical documentation. The unpaired students t-test was applied for analytical statistics.

## CHAPTER 4

### INTEGRATION OF MICROFLUIDICS AND LAYER-BY-LAYER ASSEMBLY

#### 4.1 Interpolyelectrolyte Complex Microfabrication

The microfluidic reactor system is composed of two inlet channels (1, 2), reactor microchannel (3), and one outlet channel (4). Before the experiment, the microfluidic system was filled with DI water. Then, each reagent solution was gently pumped into its inlet by a KdScientific pump equipped with two syringes (5). Solutions flowing in inlet channels converge into a single laminar stream in the reactor microchannel. S- and Y-types of the reactor microchannels were employed to demonstrate the fabrication of polyelectrolyte micro-stripes of different shape by means of the microfluidic laminar approach.

When two or more liquids flow in parallel at low values of Reynolds number, there is no turbulence at the interface between them; thus, any blurring of the interface between fluid streams occurs primarily due to diffusion of particles in a transverse direction. Laminar flow controls the spatial delivery of two oppositely charged polyelectrolytes within the microchannel and allows the reaction to be exclusively conducted at the liquid/liquid interface. The width of the resulting interpolyelectrolyte complex is determined by the diffusion of the reagents across the interface and flow rates

of the inlet streams. Reagents with high diffusion coefficient (ions, small molecules) form broad micropatterns inside the microchannel while the reaction between high molecular weight polyelectrolytes, proteins, DNA, etc. results in thin (about several microns) micropatterns.

PDDA and PSS inlet solutions of different concentration were used to obtain interpolyelectrolyte micropatterns inside the reactor microchannel. The Reynolds number of the inlet laminar streams was  $<1$ , which is far below the critical Reynolds number (2100) at which the turbulence starts.  $1 \text{ mg}\cdot\text{mL}^{-1}$  PDDA and  $1 \text{ mg}\cdot\text{mL}^{-1}$  PSS solutions, flowing at the same flow rate ( $0.01 \text{ mL}\cdot\text{min}^{-1}$ ), react at the liquid/liquid interface resulting in a PDDA/PSS interpolyelectrolyte complex positioned precisely in the middle of the reactor microchannel Figure 4.1(a). Variation in the flow rates shifts the complex from the side with the higher flow rate to the side with the lower flow rate. The experimental results supporting the simulation of this shift is shown in Figure 4.1 (a) and (b). A similar phenomenon can be observed by taking the more geometrically complicated S-type microchannel instead of simple Y-type example. The interpolyelectrolyte complex entirely mimics the shape of the microchannel (Figure 4.2). The only limitation of the channel geometry is to keep the flow of the two streams parallel and laminar. The width of the interpolyelectrolyte complex is mostly affected by PDDA and PSS concentrations in the inlet solutions and can be varied from  $10\text{-}20 \text{ }\mu\text{m}$  (for  $2 \text{ mg}\cdot\text{mL}^{-1}$  solutions or more) to  $6\text{-}8 \text{ }\mu\text{m}$  (for  $0.1 \text{ mg}\cdot\text{mL}^{-1}$  solutions). The ratio between the concentrations of the reagents in the inlet channels does not influence the width of the resulting microstripe while the total flow rate (within the range  $0.01 - 2 \text{ mL}\cdot\text{min}^{-1}$ ) has a minor control over it.

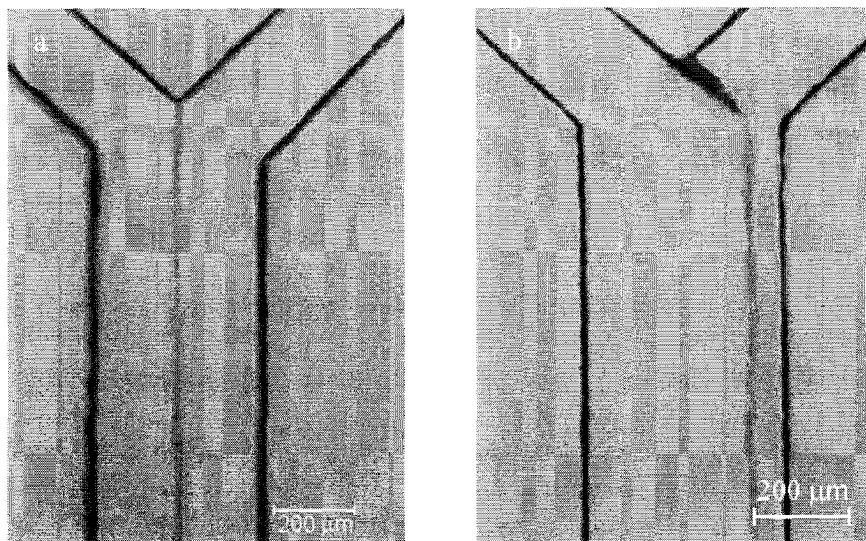


Figure 4.1. Optical micrographs of the formation of the polyelectrolyte complex inside the channel by varying the flow rates, (a) equal and (b) different flow rates.

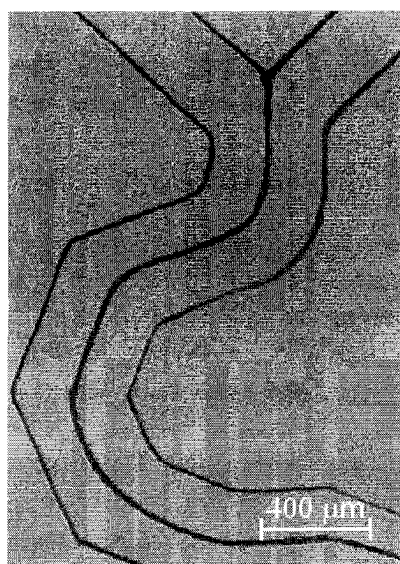


Figure 4.2. Interpolyelectrolyte complex inside a 's' shaped channel.

Numerical simulation of the interpolyelectrolyte interaction inside Y-type reactor microchannel was carried out using the CoventorWare MEMS design environment to

determine the effect of different flow rates of both PDDA and PSS laminar streams on the position of PDDA/PSS complex. The reaction between PDDA and PSS polyelectrolytes was assumed to be a first order irreversible reaction with a high reaction constant. The results of the simulation with the same flow rate in both inlet channels showed the formation of the interpolyelectrolyte complex in the center of the reactor microchannel, while differing flow rates shift the complex towards the side with the lower flow rate stream (as explained in the experimental section). This can be attributed to the volume of the fluid flowing in the channel. As the flow rate of one stream increases, the volume of the channel occupied by this fluid also increases resulting in the pushing of the diffusion zone towards the lower flow rate side. PDDA/PSS complex formation at different inlet flow rates ( $0.05 \text{ mL}\cdot\text{min}^{-1}$  PDDA,  $0.01 \text{ mL}\cdot\text{min}^{-1}$  PSS) confirms the simulation results. Increasing the flow rate in one channel by five times moves the liquid/liquid interface in the direction of the low flow rate stream. Thus, the flow rate ratio between inlet streams is an easy and powerful parameter for adjusting the position of interpolyelectrolyte micropattern in the reactor microchannel.

Confocal fluorescence microscopy and atomic force microscopy (AFM) were utilized to analyze the inner structure of the PDDA/PSS polyelectrolyte complex. Figure 4.3 (a-c) represents a typical confocal fluorescent image of the PDDA/PSS complex formed from  $1 \text{ mg}\cdot\text{mL}^{-1}$  initial inlet solutions of two polyelectrolytes. PDDA was labeled with fluorescein isothiocyanate and PSS with tetramethyl rhodamine isothiocyanate. The interpolyelectrolyte pattern has fibrous, dendrimeric structure with lots of agglomerates and regions of different width. The distribution of both polyelectrolytes inside the interpolyelectrolyte complex is homogeneous, as seen from the true color overlay image

of two labeled polyelectrolytes (Figure 4.3(c)). AFM analysis (Figure 4.3(d)) of dried PDDA/PSS micropattern indicates that the interpolyelectrolyte complex is composed of *c.a.* 100-400 nm agglomerates. At lower magnification, large micron-sized agglomerates are also seen.

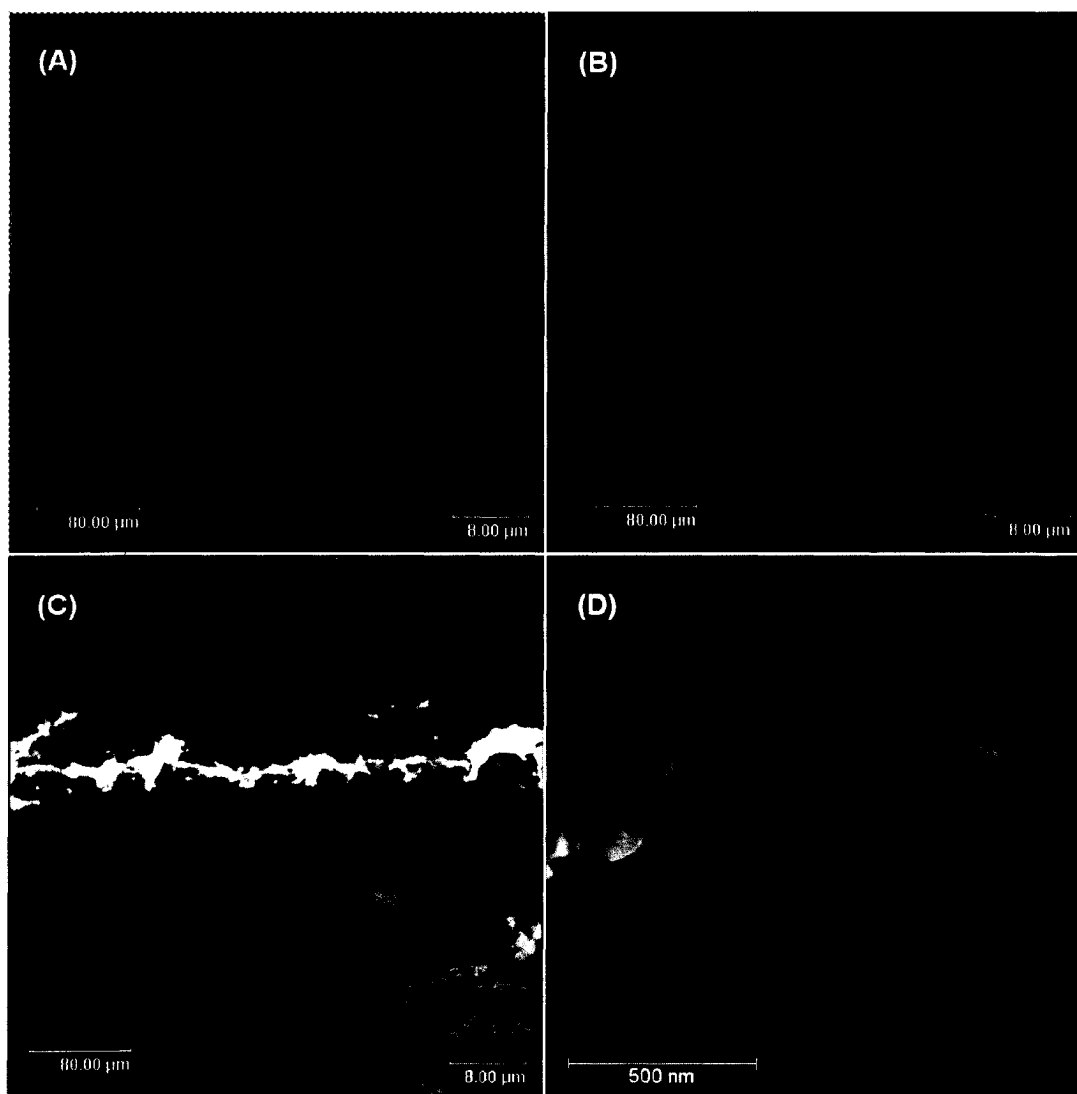


Figure 4.3. (a,b,c) Confocal fluorescence microscopy and (d) atomic force microscopy images of the PDDA/PSS interpolyelectrolyte complex synthesized in the channel microreactor.

A flow rate variation can be performed during the reaction to control the position of the interpolyelectrolyte microarrays on the glass support with 5  $\mu\text{m}$  resolution. The results of the interplay at different flow rates in the two inlets show that the interface of the interpolyelectrolyte complex shifts towards the side with the lower flow rate (Figure 4.4). Fluorescence microscopy visualized the resulting PDDA/PSS micropattern on the glass slide (Figure 4.5), where 20  $\mu\text{m}$  labeled PDDA/PSS stripes are separated by 20  $\mu\text{m}$  gaps. A wide central microstripe was obtained at 1:1 flow ratio and 2 min of reaction time. Then, the flow ratio was changed *in-situ* to 1:1.8 and 1.8:1 (lower and upper microstripes, 40 sec reaction time for each microstripe). The width and geometry of the interpolyelectrolyte micropatterns are governed by the microchannel geometry, total flow rate (which determines reaction time), and concentration of the reagents in the inlet channels. By introducing more than two polyelectrolytes in the reactor microchannel (adding more inlet channels), one can form complex interpolyelectrolyte micropatterns with diverse polymer compositions.

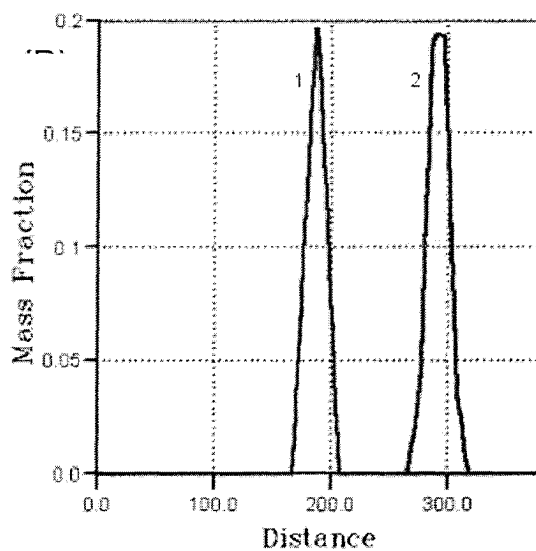


Figure 4.4. Numerical simulation of PDDA - PSS interaction inside channel microreactor.

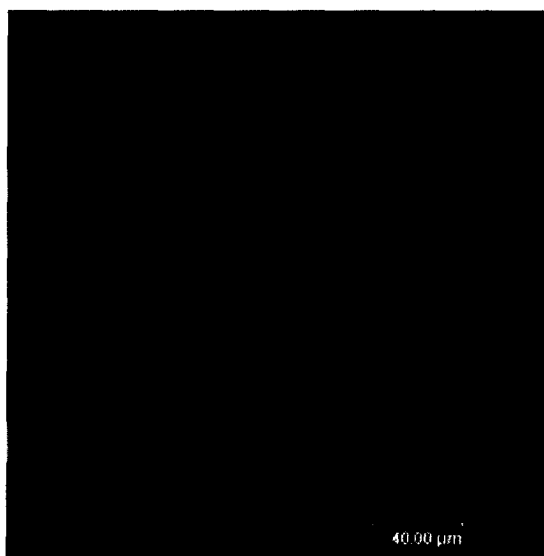


Figure 4.5. Confocal fluorescent image of PDDA/PSS micropattern on glass support. PDDA was labelled with fluorescein isothiocyanate.

#### **4.2 Polyelectrolyte/Ion Complex Microfabrication**

Contrary to the PDDA/PSS complex, the reaction between polyelectrolyte (PAH,  $1 \text{ mg}\cdot\text{mL}^{-1}$  solution) and ions (citrate ions,  $1 \text{ mg}\cdot\text{mL}^{-1}$  solution) leads to the diffusive broadening of the polyelectrolyte complex inside the reactor microchannel and formation of a wide,  $50 \text{ }\mu\text{m}$  pattern (Figure 4.6). Presumably, this is caused by the considerable difference in diffusion coefficients of citrate ions ( $\sim 10^{-5} \text{ cm}^2\cdot\text{s}^{-1}$ ) and poly(allylamine hydrochloride) molecules ( $\sim 10^{-7} \text{ cm}^2\cdot\text{s}^{-1}$ ). The more mobile citrate ions deeply penetrate into the PAH solution, thus increasing the reaction area. This explanation of the anomalously broad PAH/citrate micropattern is also confirmed by numerical modeling using the CoventorWare simulation environment. The simulation revealed that the diffusion of the reagents, if their diffusion coefficients are significantly different from the each other, results in the formation of a skewed “conical” complex (Figure 4.6). Hence,

the more mobile component of the polyelectrolyte structure significantly increases the width of the microstrips and, as a consequence, decreases their spatial resolution.

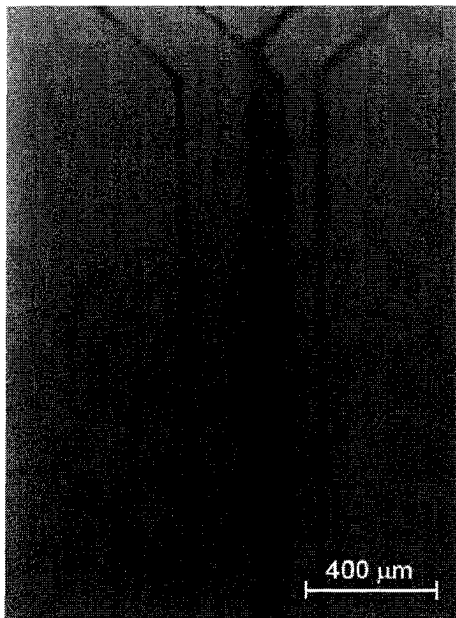


Figure 4.6. Optical image of PAH/Citrate micropattern on glass support.

Confocal fluorescence microscopy analysis of PAH/citrate micropatterns (Figure 4.7) shows a different inner structure of PAH/citrate complex as compared to PDDA/PSS. The PAH/citrate microstripe is homogeneous and uniform without any distinct features like the blobs and fibers observed for the PDDA/PSS complex. Similar homogeneity was observed for the PAH/citrate complex fabricated in the S-type reactor microchannel (Figure 4.8). AFM images of dried PAH/citrate micropattern also verified the even distribution of polyelectrolyte molecules throughout. Dried PAH/citrate complex has a smooth morphology with a small number of 500-800 nm agglomerates which most likely formed while preparing the micropattern for AFM analysis (Figure 4.9). The regular structure of PAH/citrate micropattern can be explained by the high mobility of

.

citrate ions. Being formed at the first contact of two laminar streams, the initial polyelectrolyte complex is highly permeable for citrate ions, which can deeply penetrate inside the PAH stream and reacting with polyelectrolyte molecules. This caused the broadening and homogeneity of the PAH/citrate micropattern whereas PSS or PDDA molecules hardly penetrate the PDDA/PSS layer and form a fibrous and more irregular structured complex.

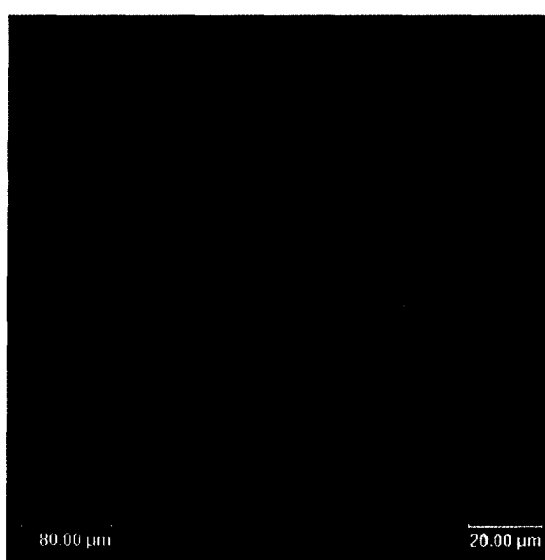


Figure 4.7. Fluorescence microscopy images of PAH/citrate complex fabricated in Y-type micro-reactor.

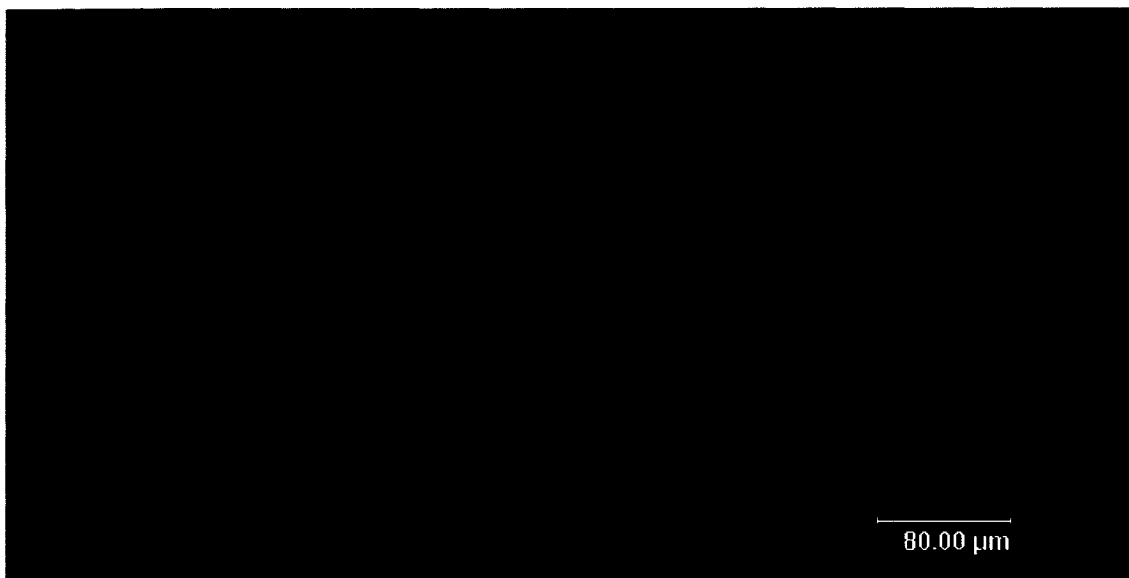


Figure 4.8. Fluorescence microscopy images of PAH/citrate complex fabricated in S-type micro-reactor.

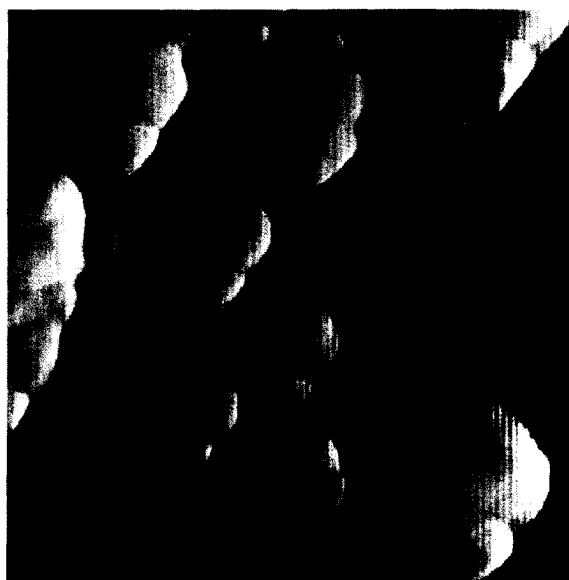


Figure 4.9. Atomic force microscopy image of PAH/citrate micropattern deposited onto glass support.

### **4.3 Polyelectrolyte/Protein Complex Microfabrication**

Formation of a polyelectrolyte/protein micropattern in the fluidic microreactor was accomplished on a sample of PDDA/BSA complex. Polyelectrolyte/protein microarrays are of interest as components of biosensors, cell microenvironment, blood purification systems, etc. The use of BSA as the inlet reagent ( $1 \text{ mg}\cdot\text{mL}^{-1}$  solution) instead of PSS, results in the formation of PDDA/BSA complex in the channel microreactor. The width of this polyelectrolyte/protein pattern, as illustrated in the fluorescent image in Figure 4.10 (a), is about  $15 \text{ }\mu\text{m}$ . The polyelectrolyte/protein microstructure is globular and agglomerated. Similar effects of flow rate ratio and initial inlet concentration, previously observed for the interpolyelectrolyte complex, were also found for the PDDA/BSA protein complex. The width of the micropattern can be adjusted by the initial concentration of the reagents while the position of the micropattern can be varied by changing the flow rate ratio.

AFM studies of the PDDA/BSA complex confirmed its inner globular structure, (Figure 4.10 (b)). Large  $300 \text{ nm}$  globules and smaller  $50\text{-}100 \text{ nm}$  globules can be identified. Large globules, previously observed for both PDDA/PSS and, (but less pronounced), PAH/citrate micropatterns, appeared during sample preparation for AFM analysis while small  $50 \text{ nm}$  globules represent the globular structure of BSA aggregates<sup>113</sup>. Protein globules could be incorporated into the polyelectrolyte matrix forming the so-called host-guest structure. Hence, by the laminar flow microfabrication approach, it is possible to obtain microengineered globular polyelectrolyte/protein microarrays of predetermined position and width.

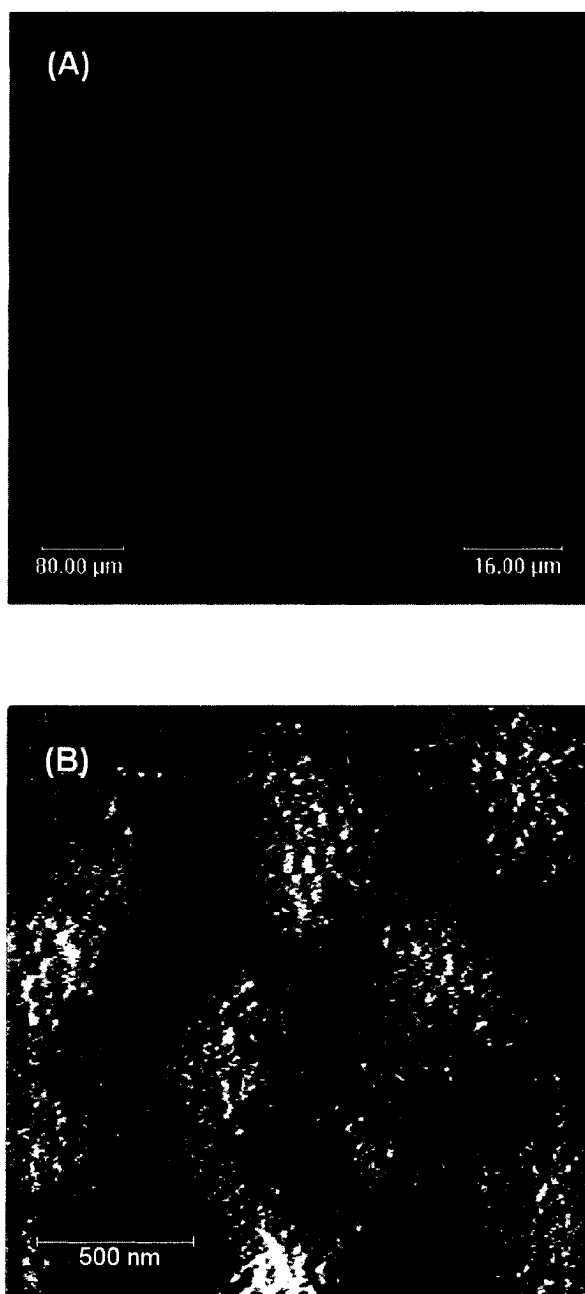


Figure 4.10. Confocal fluorescence (a) and atomic force microscopy (b) images of the PDDA/BSA micropattern. PDDA was labeled with FITC. Inlet flow rate was  $0.01 \text{ mL}\cdot\text{min}^{-1}$  in both inlet channels; initial concentration of PDDA and BSA  $0.1 \text{ mg}\cdot\text{mL}^{-1}$ .

#### **4.4 Effect of Electric Field on the Position of the Polyelectrolyte Complex**

As described previously, the main parameter controlling the position of the polyelectrolyte complex in the channel microreactor is the flow rate ratio between two reagent streams. At the same time, the place of the polyelectrolyte complex inside the channel microreactor can be regulated by applying an electric field to facilitate electrophoretic movement of oppositely charged polyions in the transverse direction. A microfluidic reactor, specially modified to perform experiments in an electric field, is represented in Figure 4.11(a). Gold electrode micropatterns were brought to each side of the microchannel and exposed to the solution to assure electrolyte contact. Electrode potential was set with a conventional power supply (Topward Electric Instruments Co., USA). Maximum potential value was +0.8 V or -0.4 V vs. SCE to prevent undesirable redox processes: H<sub>2</sub> and O<sub>2</sub> evolving as well as electrode corrosion. Applying either a positive potential to the electrode pattern placed in the polycation stream (PAH, 1 mg/ml solution) or negative potential to the electrode in polyanion stream (PSS, 1 mg/ml solution) results in the shifting of the interpolyelectrolyte complex from the center of the channel towards the side with the applied potential (Figure 4.11(b)). The interpolyelectrolyte microstripe has an inclined geometry in the channel microreactor. The slope depends on the value of the applied potential and flow rate of the reagents. It can be increased at higher potential or lower flow rate. Switching the polarity of the electrodes during the complex formation leads to its gradual movement to the other side of the reactor and formation of a smeared cone with the apex at the converge point (Figure 4.11(c)). Microstripes of more complicated geometry can be obtained by applying an electric potential of alternated value at different parts of the channel

microreactor. Employing a positive (+0.8 V) - zero - positive (+0.8 V) potential order along the channel microreactor leads to bending the interpolyelectrolyte microstripe (Figure 4.11 (d)). At first, the microstripe forms at one side of the microreactor, then, while reagent streams enter another, reversed potential region, it goes to the center of the channel.

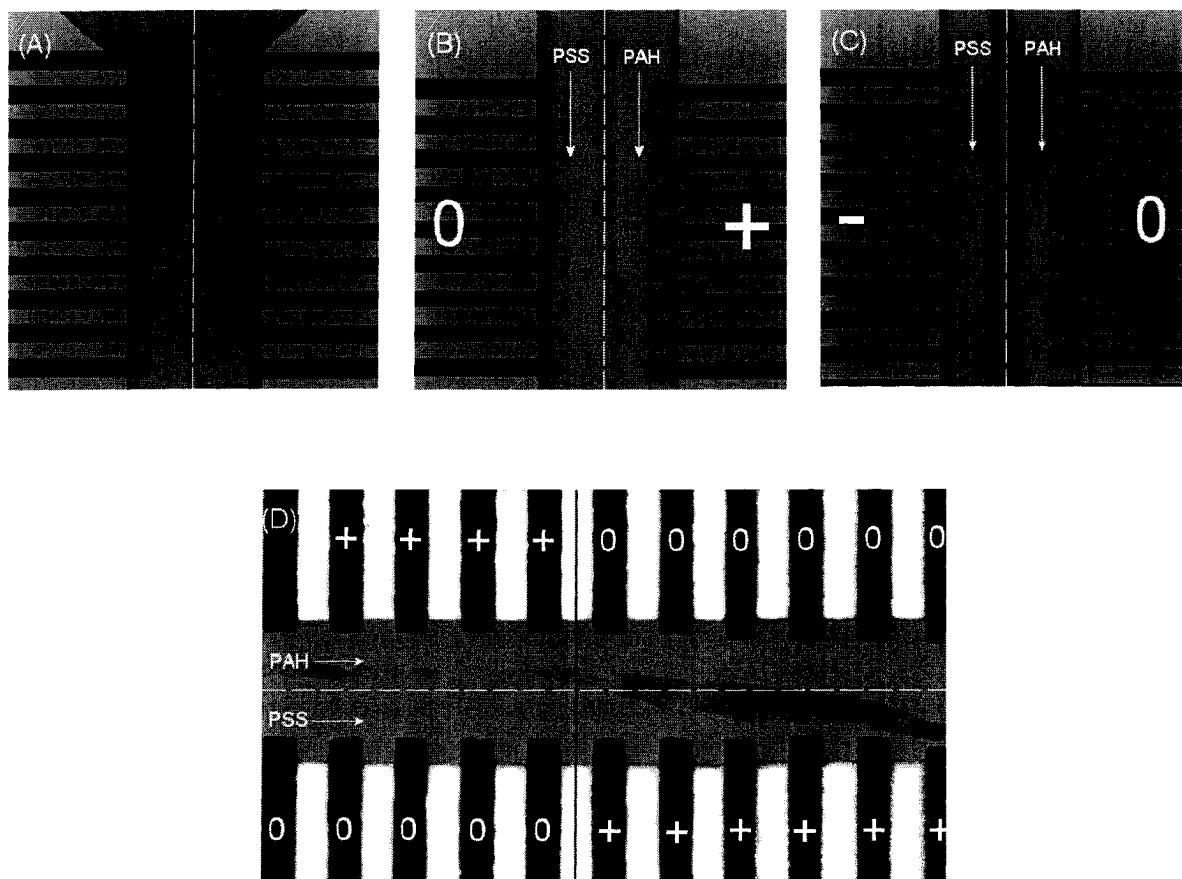


Figure 4.11. Effect of electric field on the position of the interpolyelectrolyte complex formed in the channel.

Confocal fluorescence microscopy analysis of the interpolyelectrolyte microstrips revealed homogeneous distribution of both polyelectrolytes throughout the whole volume of the microstripe, as was observed for interpolyelectrolyte complex

formed without applying electric field. Observed shift of microstripe position in the microreactor can be due to the attraction of polyions from their laminar stream to the oppositely charged electrode, which, as a consequence, leads to a sliding reaction interface in transverse direction and adding a migration component to the diffusion of the polyelectrolytes across the interface. A continuous slope rather than the sharp shift of the microstripe position, is caused by the superposition of the parallel laminar stream and perpendicular electric field migration of polyions.

#### **4.5 pH Sensitive Channels**

The microchannels were made sensitive to pH by layering the pH sensitive material (HPTS). PDDA-HPTS and PSS solutions were made in sodium acetate buffer at pH 5. Seven bi-layers of PDDA-HPTS and PSS were coated inside the channel. With a final layer of PDDA-HPTS. This was achieved by electrostatic layer-by-layer assembly. HPTS is a fluorescent pH indicator. By covering the inside of the channel with such material, biological/chemical reactions can be carried out inside the channel and the pH in different points can be estimated by monitoring the fluorescent intensity change of the pH sensitive material (HPTS). In Figure 4.12, a channel prepared by layer-by-layer assembly is shown, and shows a higher fluorescent intensity at pH 10 and lower intensity at pH 4. The solution with pH 10 was pumped from the lower inlet channel and the solution with pH 4 was pumped from the upper channel. The inlet channel in the middle was sealed. The line scan of the variation in intensity is shown in Figure 4.13.

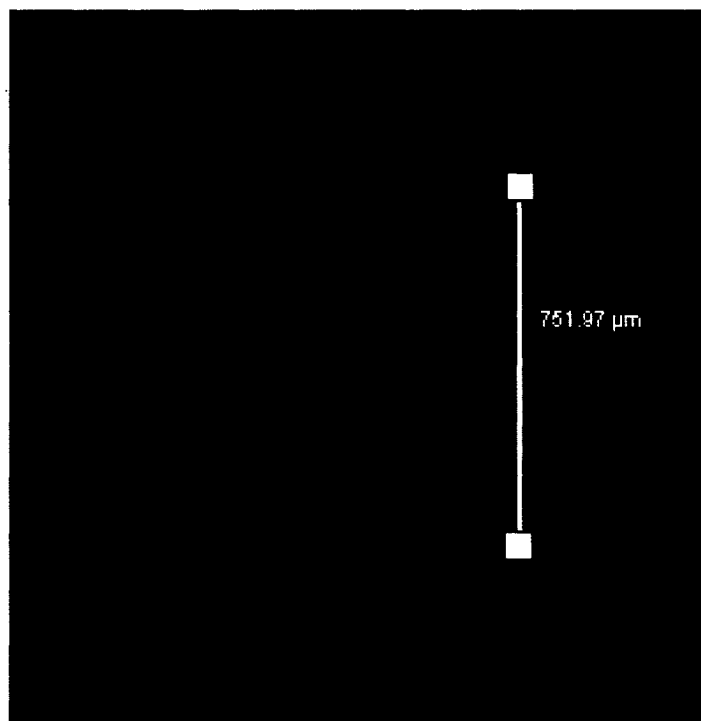


Figure 4.12. Confocal fluorescence image of the pH sensitive channel showing different fluorescent intensities in different regions of the same channel.

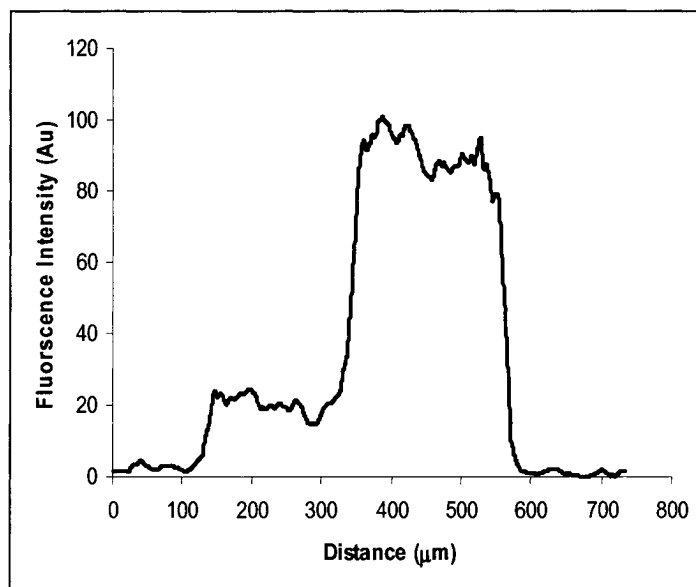


Figure 4.13. The line scan as a function of distance across the channel.

#### **4.6 Selective Modification of Microparticles inside the Channel**

Observed micron scale resolution in the patterns offers the possibility to employ a microfluidic approach for anisotropic modification of polyelectrolyte microcapsules and imparting them with advanced release and protection abilities<sup>114</sup>. Hollow polyelectrolyte capsules have semipermeable properties and, depending on the pH or ionic strength of the solution, can release or retain encapsulated material. Modifying part of the capsule wall can result in the fabrication of a unique microcapsule with anisotropic shell permeability.

To validate the microfluidic method for selected shell modification, initial Rhodamine-labeled melamine formaldehyde template microparticles were adsorbed inside the reactor microchannel prior to passing polyelectrolyte solution. Then, in one inlet channel FITC-labeled dextran ( $M_w \sim 10000$ ,  $1 \text{ mg} \cdot \text{mL}^{-1}$  solution) was introduced while the other inlet channel was filled with distilled water. Selected deposition of labeled dextran macromolecules on one half of the template microparticles fixed in the center of the channel microreactor was elaborated (Figure 4.14). Microparticles placed inside laminar streams were either completely covered with dextran or remained unmodified. Therefore, the microfluidic approach allows formation of micropatterns not only on the flat substrates, but also on the spherical shell of the microcapsules thereby changing its properties with spatial resolution.

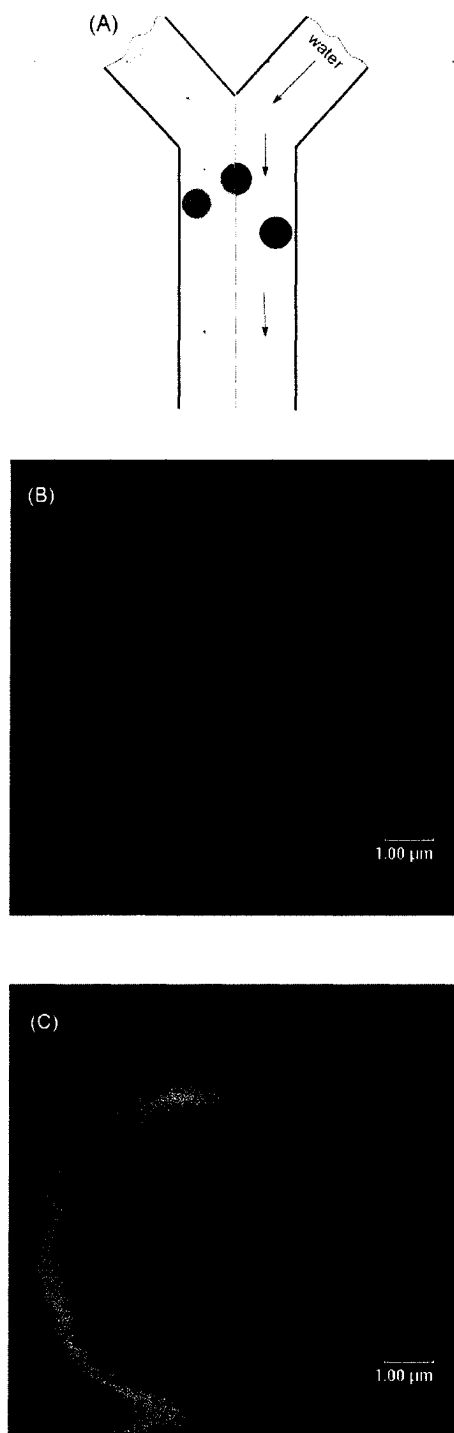


Figure 4.14. (a) Schematic view of anisotropic micropatterning of Rhodamine-labeled microparticles with fluorescein-labeled dextran macromolecules, (b) confocal fluorescent image and (c) overlaid fluorescent image of resulting anisotropic microparticles.

#### **4.7 Conclusion**

The laminar flow microfabrication approach was employed to synthesize different polyelectrolyte complexes at ambient conditions. Filament like 15  $\mu\text{m}$  interpolyelectrolyte poly(dimethyldiallylammonium chloride)/poly(styrene sulfonate), homogeneous and uniform 50  $\mu\text{m}$  poly(allylamine hydrochloride)/citrate, and 20  $\mu\text{m}$  globular poly(dimethyldiallylammonium chloride)/bovine serum albumin micropatterns were formed. Multiphase laminar flow microfabrication offers a large flexibility for producing 5-10  $\mu\text{m}$  micropatterns containing unstable and sensitive biological objects on the surface of any appropriate substrate (*i.e.* glass, polyimide, silicon). Theoretical simulation of the polyelectrolyte complex formation, which was confirmed experimentally, revealed that the flow rate and the diffusion coefficient of the reagents are the main parameters controlling the width of the micropatterns and their position in the channel microreactor. This simple deposition procedure makes it possible to obtain 5-10  $\mu\text{m}$  wide strips of proteins in complex with linear polyions on a flat surface. By varying the microchannel structure and flow rate of the reagents, it is possible to fabricate microarrays of different geometry, resolution, thickness, and composition. An electric field applied in transverse direction to the laminar flow can also be used to adjust the position of the polyelectrolyte complex and form more geometrically complicated polyelectrolyte micropatterns. Micropatterned polyelectrolyte structures, obtained by the microfluidic approach, can be utilized as selective bio- (enzymatic) microreactors, components of sensor circuits, and conductive bioimplants. pH sensitive microchannels are important when working with biological fluids like a cell suspension. The pH at a certain point in the channel may be connected with cell behavior. The demonstrated

microfabrication procedure can be especially useful in handling delicate and sensitive formulations and fabrication of bioactive microarrays. Selected deposition of labelled dextran macromolecules on one half of the microparticles fixed in the microreactor channel was also elaborated. The resulting micropatterned bioconjugated structures can be utilized as sensoric layers, selective bio- (enzymatic-) microreactors, components of micron scale bioimplants, and polyelectrolyte arrays. The application of cells, microcapsules, and blood platelets in assembling both micron-resolved microarrays and anisotropic modification by microfluidic approach is currently under investigation.

## CHAPTER 5

### INTEGRATION OF MICROFABRICATION AND LAYER-BY-LAYER ASSEMBLY

The goal of this study is twofold. First, we focused on assembly of ultrathin (thickness about 70 nm) SA-LbL films on an array of microfabricated openings arranged in a 4×4 square pattern on a silicon substrate. We demonstrated that, in fact, robust freely suspended 2-D nanomembrane microarrays can be assembled and an interference optical read-out scheme can be applied for concurrent monitoring of the collective deflection behavior of 16 different circular nanomembranes under external hydrostatic pressure. Towards this end, we found that at any given pressure one can collect multiple independent data sets for deflecting membranes of the same diameter and therefore, significantly improving experimental statistics. Second, within this array we design columns having openings with variable diameters to implement a simple but efficient version of the combinatorial approach<sup>115,116</sup> for reliable and fast screening of nanomembrane properties under a range of conditions. Moreover, it provides a means for the concurrent study of the collective deformational behavior of membranes with four different diameters, thus addressing their scale-dependent properties.

A detailed description of similar SA-LbL film formation, internal microstructure, and transfer routines has been already reported<sup>79</sup>. The overall thickness of 11G11 membrane was 68 nm and the surface microroughness within a 1×1m<sup>2</sup> area was

below 10 nm, which are typical values for similar SA LbL films. A layer of gold nanoparticles was encapsulated into the nanomembrane to enhance their micromechanical properties (Figure 5.1). The 4×4 array of circular openings contains four rows of openings with a constant diameter combined with four columns of openings with variable diameters (200, 100, 75, and 50  $\mu\text{m}$ ) (Figure 5.2). The LbL membrane transferred onto the 4×4 array covered all openings uniformly resulting in a light green color caused by light reflection from the gold nanoparticles with strong surface plasmon resonance (Figure 5.3).

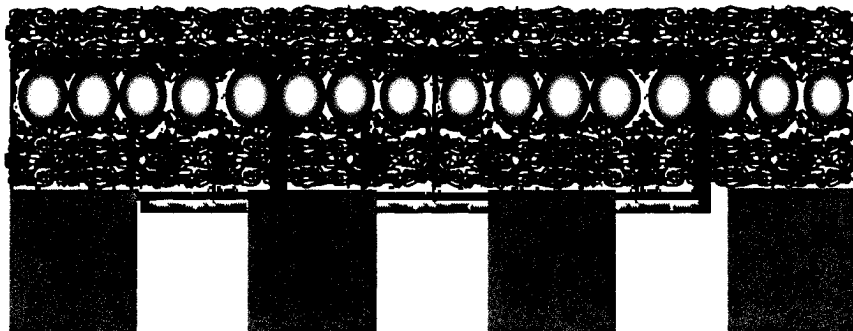


Figure 5.1. Schematic of the multilayer nanomembrane covering openings in the array of microfabricated device.

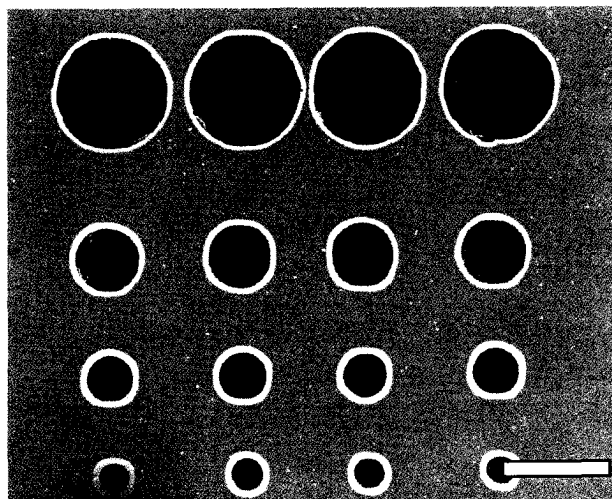


Figure 5.2. SEM image of a silicon substrate with gradient opening arrays, scale bar is 200  $\mu\text{m}$ .

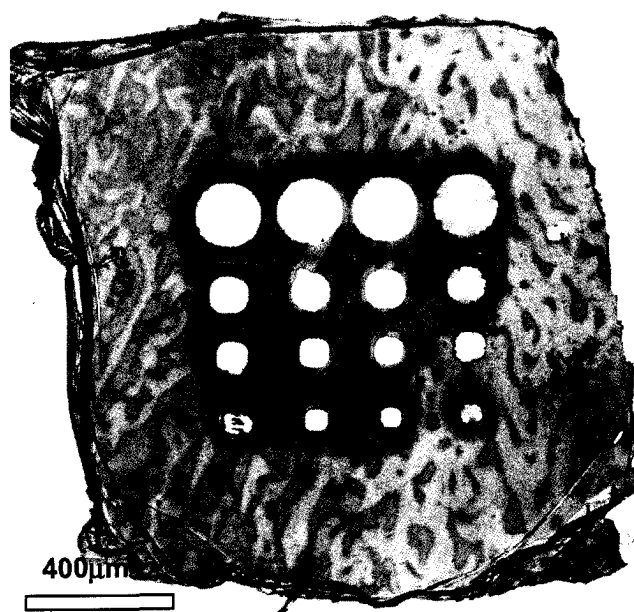


Figure 5.3. Optical image of the of 4 $\times$ 4 array covered with LbL film.

### 5.1 Interferometric Imaging of the Free Standing Thin Films

Figure 5.4 shows the interferometry pattern of a deflected LbL nanomembrane array under an external pressure differential of 1266 Pa (both positive and negative pressures applied produced similar results as demonstrated earlier). Uniform concentric Newton's rings observed for each opening were similar for all membranes with the same diameter which indicated consistent membrane deflections but different for vertical rows<sup>117</sup>.

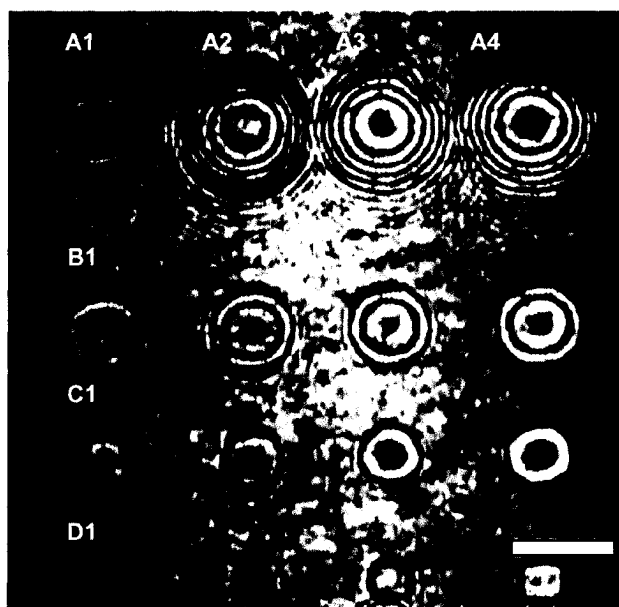


Figure 5.4. The interference pattern of the nanomembrane array under the pressure differential of 1266 Pa.

Further quantitative analysis was done by converting these interference patterns obtained under different pressures to pressure-deflection plots and deriving the elastic modulus and residual stress, as described in detail earlier (Figure 5.5). The elastic modulus of 11G11 nanomembranes deposited across 200  $\mu\text{m}$  was  $5.3 \pm 0.4$  GPa and the

residual stress was  $16.5 \pm 1.5$  MPa (Table 5.1). The elastic modulus for this membrane was slightly lower than that of 9G9 membranes studied before due to a lower volume fraction of gold nanoparticles providing film toughening. However, unlike previous measurements on a single opening, the application of the micropatterned array allows the generation of four independent pressure-deflection plots in one run (Figure 5.6). This approach significantly improves the quality of measurements and provides a reliable determination of the elastic modulus by avoiding uncertainties related to film transfer and testing under slightly different conditions. In fact, the standard deviation of current measurements was within  $\pm 10\%$  which is much lower than the typical value of  $\pm 30\%$  reported earlier for consequential measurements.

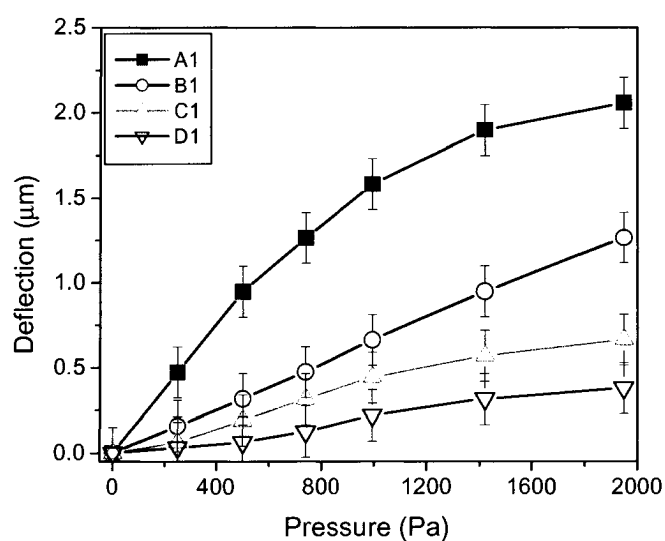


Figure 5.5. Deflection-pressure data for freely-suspended nanomembranes with different diameters.

Table 5.1. Elastic modulus and residual stress of 11G11 Nanomembranes of different size.

Membrane Diameter ( $\mu\text{m}$ )	Elastic modulus (GPa)	Residual stress (MPa)
200	$5.3 \pm 0.4$	$16.5 \pm 1.5$
100	$5.6 \pm 0.2$	$11.7 \pm 0.8$
75	$6.3 \pm 1.0$	$12.5 \pm 1.3$
50	$6.8 \pm 1.2$	$9.3 \pm 1.1$

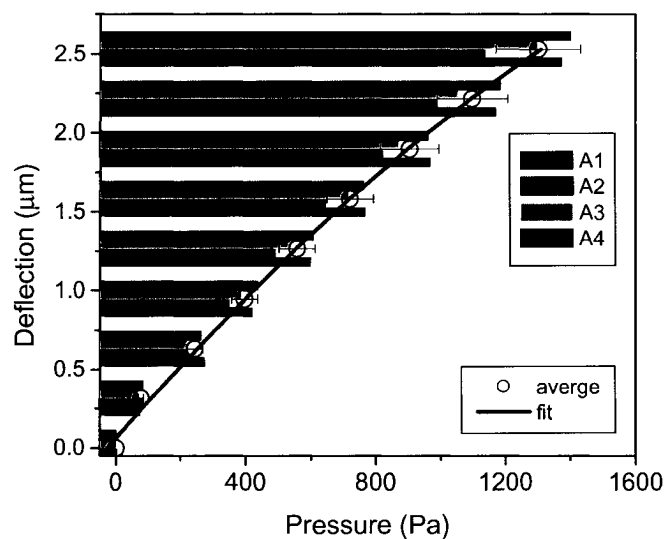


Figure 5.6. Four independent deflection-pressure sets of data (columns) obtained simultaneously for freely suspended nanomembranes with identical diameters along with the average behavior (solid line). The labels correspond to the membranes over different openings, as shown in Figure 5.4.

On the other hand, the systematically changed opening diameters in the columns allows us to address the question of the scale-dependency of the micromechanical

properties of compliant freely-suspended membranes which is critical for prospective sensor arrays with variable micropatterned dimensions. Indeed, deflection-pressure data for the membranes with smaller diameters showed an unexpected but consistent increase in the stiffness well beyond the statistical deviation. The largest elastic modulus reached 6.8 GPa for the smallest membranes, almost 30% increase (Table 5.1). This increase which, was not observed before in separated measurements, can be related to the reduced chance of having “weak” points within membranes which compromise the elastic properties.

### **5.2. Point Load Experiments on Free Standing Films**

As an alternative way to determine the effective bending rigidity of the membranes as a function of the membrane diameter, we applied a point-load experiment with a colloidal-probe AFM (Figure 5.7). Unlike deflection-pressure experiments which exploited the membrane regime with predominant tensile stresses, the point-load approach is limited to very small deformations (tens of nanometers instead of microns) allows for studying the bending regime and directly deriving the bending rigidity, as discussed in detail previously. By repeating this probing for membranes with different diameters, one can address the question of the scale dependency of the membrane flexibility. In fact, we observed a significant decrease of the membrane deflection achievable under fixed normal load for membranes with smaller diameters. The normal load of 70 nN resulted in elastic deflection of 50 nm for the largest membrane which decreased to 37 nm for the smallest membrane (Figure 5.8). Correspondingly, the bending rigidity,  $B$ , increased from 1.4 N/m to 1.9 N/m (Figure 5.9).



Figure 5.7. Optical micrograph of point-load experiment with the AFM tip pointing at one of the membrane.

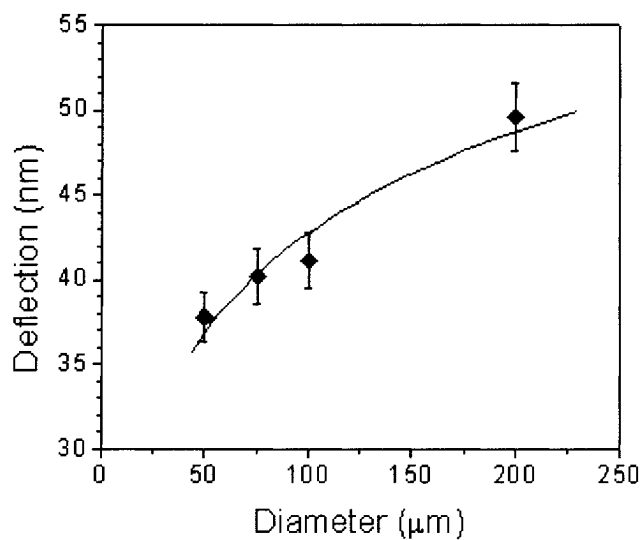


Figure 5.8. The deflection of nanomembranes with different diameters tested with the colloidal AFM probe under the applied force of 70 nN as a function of the membrane diameter.

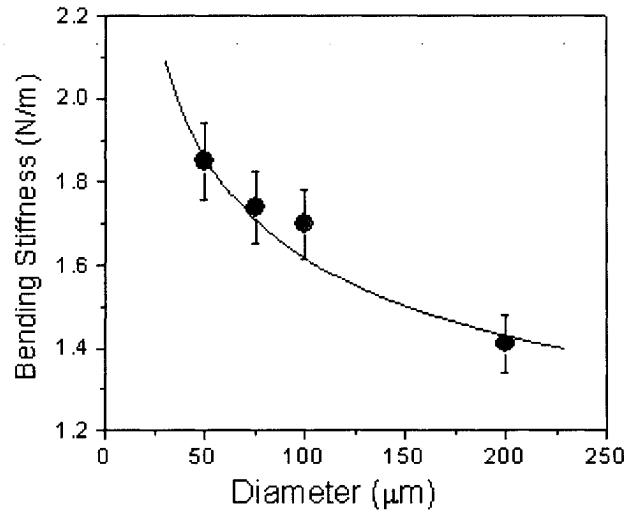


Figure 5.9. The bending rigidity of the nanomembranes as a function of the membrane diameter and the theoretical prediction of elastic membrane deformation (solid line).

Although an increasing bending rigidity for free-suspended membranes with decreasing diameter,  $D$ , is expected, the observed variation is very different from that predicted for a uniform load:  $B \sim D^4$ . Therefore, we consider the scale-dependent variation prediction by an alternative model with a normal load applied to a small surface area<sup>118</sup>. This model predicts the membrane deflection under a central point-load for circular shapes and is given by:

$$d(r) = \frac{P_0}{2\pi\sigma_0 h} \ln\left(\frac{R}{r}\right) \quad (1)$$

where  $d(r)$  is the membrane deflection at the location with distance from the center  $r$ ,  $P_0$  is the applied load,  $h$  is the film thickness, and  $\sigma_0$  is the residual stress.

Since the nanomembranes were extremely thin (less than 100 nm) as compared to their diameter, the bending stiffness of the membrane, which is defined as  $Eh^3/12(1-\nu^2)$ , was relatively small. By fitting experimental data from deflection under fixed normal

load (Figure 5.8), a residual stress of 20 MPa was obtained for all membranes, which is close to that measured independently at large deflections (Table 5.1). More over, from this fit the value  $r$ , which is characteristic of the radius of the point load was determined as 0.25  $\mu\text{m}$ , which is close to the radius of the contact area below 0.1  $\mu\text{m}$  estimated with the Hertzian model<sup>119</sup>. Finally, by applying eq. (1) to experimental data  $d(P)$  and applying the uniform residual stress of 20 MPa, the scale-dependent bending rigidity was calculated and compared with the experimental data (Figure 5.9). It is clear from this comparison, that the point load model with realistic loading parameters describes the scale-dependent behavior of compliant membranes with diameters as small as 50  $\mu\text{m}$ . This model predicts the increasing bending rigidity  $B \sim [\ln(D)]^{-1}$  which is in fact observed in our experiments and is much less dramatic than that for the uniform pressure load.

In conclusion, we assembled the 4×4 gradient array of freely-suspended ultrathin LbL nanomembranes and demonstrated its applicability for *concurrent monitoring* of collective deflection behavior of 16 circular nanomembranes under external hydrostatic pressure with microscopic interferometry. The gradient array designed with a variable diameter of openings in one direction provided a means for efficient and fast screening of scale-dependent membrane properties as well. By using this approach, we significantly improved experimental statistics and found a modest increase in the elastic modulus with decreasing membrane diameter. And, finally, we observed scale-dependent behavior of the bending rigidity with a slow, logarithmic increase with decreasing membrane diameter. This behavior is described by the model for bending elastic membranes under point-load with realistic loading characteristics close to the experimental conditions of colloidal probe AFM testing.

## CHAPTER 6

### LBL ASSEMBLED HYDROPHILIC COATINGS

One of the interesting applications of LbL in the past has been the formation of hydrophilic/hydrophobic coating using multilayer polymeric coating described by Rubner et al<sup>89,90</sup>. They detailed the fabrication of various polymeric layers for the formation of the hydrophilic coating and showed that the outermost layer determines the contact angle of water with the surface. In another study, the formation of hydrophobic coatings using polymers was detailed<sup>90</sup>. The effect of acid treatment on the contact angle of the polymeric coatings was discussed and they showed that superhydrophobic coatings were achieved. Many researchers in the past have shown the formation of superhydrophilic films by coating a thin layer of TiO<sub>2</sub> (various techniques have been used) and subsequent treatment with UV light<sup>79,80,83</sup>. Here, we will show the formation of thin films of TiO<sub>2</sub> nanoparticles (using LbL) and their effect on the wettability of three substrates with different initial water contact angles.

#### **6.1 Thickness of Polyelectrolyte/TiO<sub>2</sub> films**

The surface charge of the TiO<sub>2</sub> nanoparticles dispersed in water at pH ~ 4.5 was determined to be positive. Therefore, PSS, a strong anionic polyelectrolyte, was used for alternation with these nanoparticles. Figure 6.1 shows the change in film thickness with

respect to the number of layers deposited on a QCM resonator. The thickness of three PDDA/PSS precursor bilayers was approximately 5 nm. A linear increase in the film thickness with the adsorption of TiO<sub>2</sub>/PSS bilayers was observed. The average growth step for a TiO<sub>2</sub>/PSS bilayer was  $11 \pm 1$  nm which is an efficient thickness corresponding to the mean border of the layer. This thickness is approximately two times less than the diameter of the TiO<sub>2</sub> spheres ( $21 \pm 4$  nm) which gives a dense packing coefficient of  $11/21 \sim 0.52$ . A theoretical value for packing coefficient of solid spheres is 0.52 for cubic and 0.63 for hexagonal packing. The nanoparticles form a well packed layer and the next layer of nanoparticles is deposited mostly on top of the previously deposited layer. We may design such a nano-coating on any solid surface with a thickness proportional to the 11 nm growth step, and we will work mostly with a five bilayer coating (PDDA/PSS)\*3 + (TiO<sub>2</sub>/PSS)\*5 composition and 60 nm thickness.

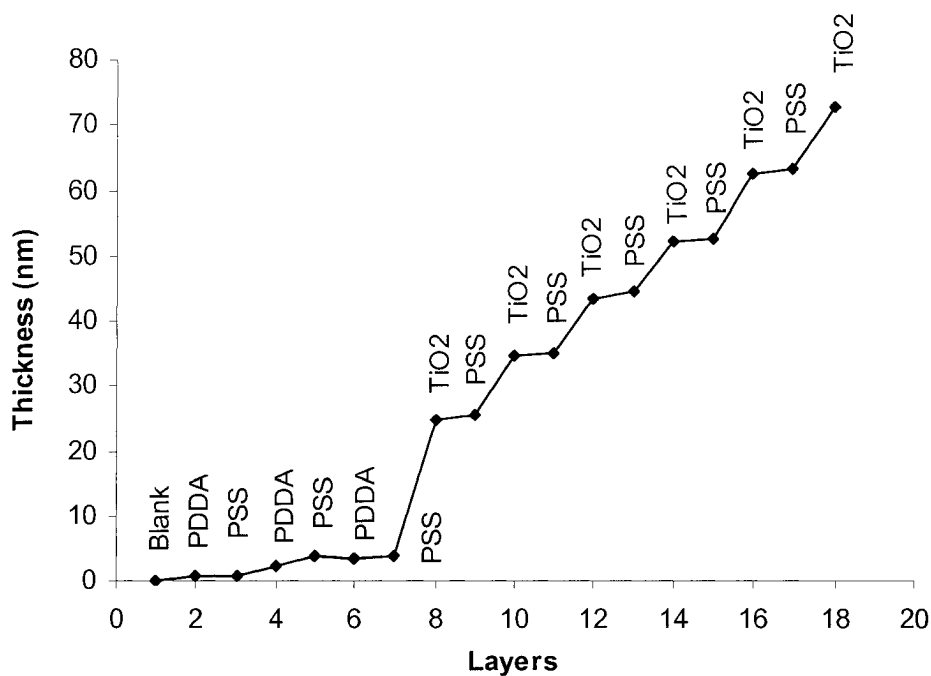


Figure 6.1. Film thickness as a function of deposited TiO<sub>2</sub> layers.

In Figure 6.2 one can see a scanning electron microscopy image of the PSS/TiO<sub>2</sub> multilayer cross-section. It is a dense packed film of  $21 \pm 4$  nm nanoparticles with surface roughness 3-4 times more than the diameter of the nanoparticles, and the characteristic dimension of the nanoparticle aggregates on the surface is of 50-60 nm. We did not optimize the surface roughness of the TiO<sub>2</sub> particle coatings, which may be an additional parameter for the optimization of such a coating.



Figure 6.2. Scanning electron micrograph of  $(\text{PDDA/PSS})_3 + (\text{TiO}_2/\text{PSS})$  multilayer cross-section on a silver electrode. The particle diameter is ca 21 nm (Hitachi S-900 SEM operating at 25 kV; the sample is coated with 2 nm of Pt).

### **6.2 Optical Properties of PSS/TiO<sub>2</sub> Films**

The optical density of precursor,  $(\text{PDDA/PSS})_3$ , films at wavelengths higher than 250 nm is very low with a small maximum at 230 nm due to the phenol ring of PSS (Figure 6.3). The deposition of a TiO<sub>2</sub> layer strongly increases the absorbance of the films with a broad maximum at  $\lambda = 280 - 350$  nm, while introducing a long tail of absorption in the visible range. The PSS layer gives small 230 nm peak in the film spectrum. Therefore, we can assume that the spectrum observed in the near UV and visible ranges can be attributed to the multilayer of TiO<sub>2</sub> nanoparticles assembled with PSS.

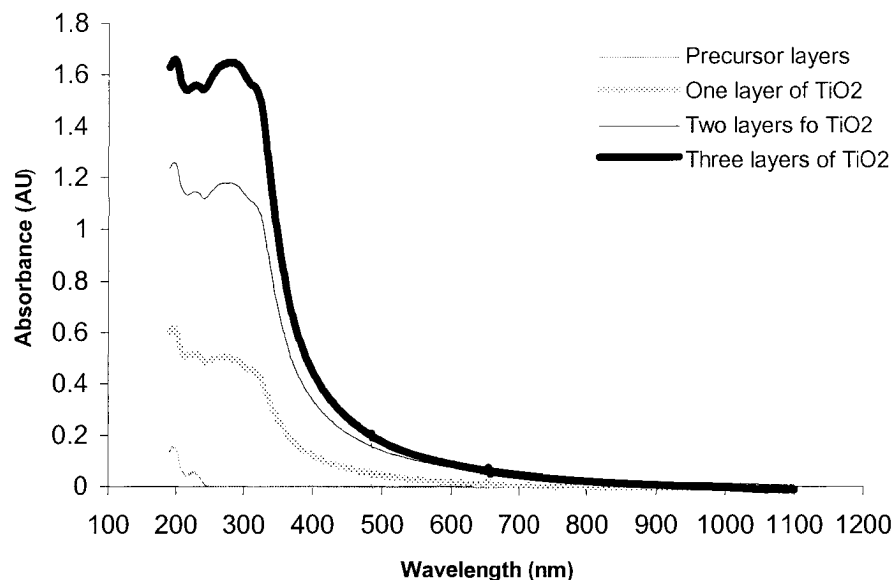


Figure 6.3. UV-vis absorbance with increasing number of layers of TiO<sub>2</sub>.

### **6.3 Wettability of PSS/TiO<sub>2</sub> Multilayer Coatings on Different Substrates**

Figure 6.4 shows the behavior of a water drop while measuring the water contact angle (WCA) values. A continuous decrease in the contact angle with time (in minutes) is observed. The values measured 90s after the drop is placed on the sample surface are used in the discussions that follow. Three substrates (glass, PMMA and PDMS) with different hydrophilic properties were utilized as templates for polyelectrolyte/nanoparticle deposition. Contact angles for bare glass, PMMA and PDMS were measured to be 35°, 75°, 105° respectively. These values closely correspond to these reported properties for the substrates. The deposition of precursor polyelectrolyte layers slightly decreases the WCA of the surfaces, as measured immediately after deposition, but the layers do not retain low WCA during storage. The contact angle changes with the deposition of each TiO<sub>2</sub>/PSS bilayer. It is strongly affected by the

template material used, but finally after deposition of 2 to 20 bilayers we reached a complete wettability:  $WCA = 0^\circ$ . Let us analyze the modification for glass, PMMA, and PDMS surfaces:

Glass: The WCA value after deposition of one layer of  $TiO_2$  on top of (PDDA/PSS)\*3 precursor was found to be  $20^\circ$ , a decrease of  $15^\circ$  as compared with bare glass surfaces, and dropped to  $0^\circ$  after deposition of the second  $TiO_2$  layer (Figure 6.4). Further addition of  $TiO_2$  layers did not change the WCA. Oxygen plasma treatment of glass did not have any effect on the hydrophilicity of the surfaces (WCA remained  $0^\circ$ ).

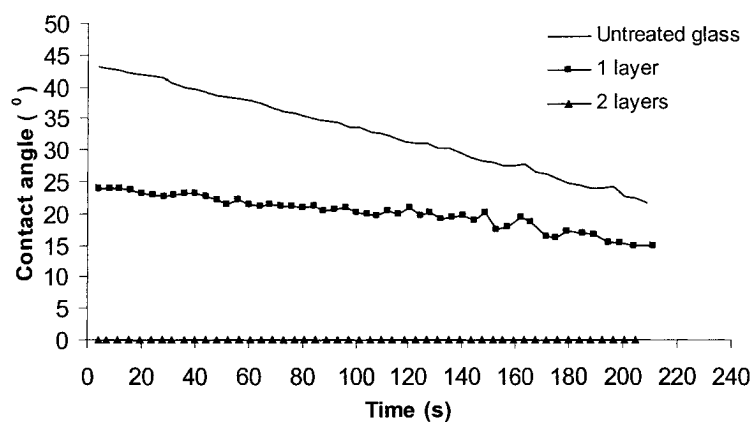


Figure 6.4. Water contact angle measurements on glass with the deposition of different number of layers of  $TiO_2$ .

PMMA: For the case of PMMA, the WCA was observed to be about  $45^\circ$  after the deposition of precursor layers and one  $TiO_2$  layer. It corresponds to a  $30^\circ$  decrease as compared to the bare PMMA. The WCA gradually decreased with increasing number of  $TiO_2$  layers and a value of  $0^\circ$  was achieved after deposition of five  $TiO_2$  layers (Figure 6.5).

This procedure was improved when we made preliminary plasma treatment before the LbL assembly. It is known that oxygen plasma treatment provides charge on the plastic surface which improves adhesion of the first polycation layer<sup>120</sup>. Immediately after treatment with oxygen plasma the contact angle of the PMMA surface reduced to about 30°. This decrease is temporary and the WCA increases with time. The deposition of one layer of TiO<sub>2</sub> on plasma treated PMMA did not change the WCA (the value is about 30°). In this case, zero contact angle was observed after deposition of only two PSS/TiO<sub>2</sub> bilayers.

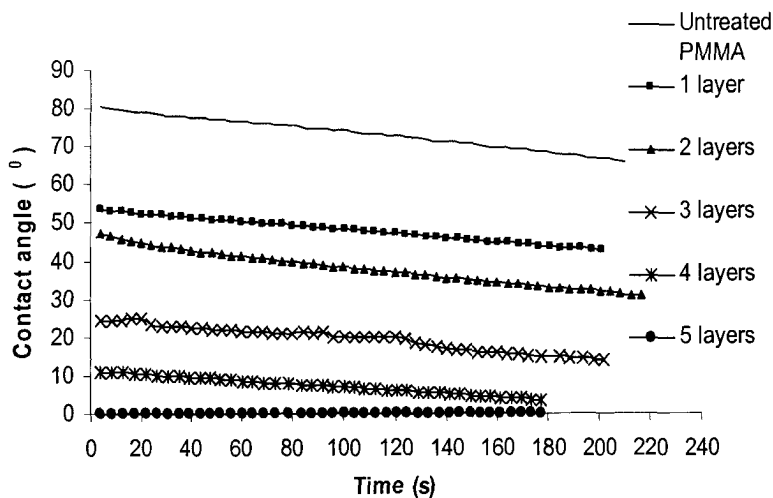


Figure 6.5. Water contact angle measurements on PMMA with the deposition of different number of layers of TiO<sub>2</sub>.

PDMS: The wettability of PSS/TiO<sub>2</sub> nanoparticle coating on PDMS was examined for the surfaces obtained directly after curing and also for those exposed to oxygen plasma. In both cases, the WCA changes more slowly with an increasing number of TiO<sub>2</sub> layers as compared to glass and PMMA templates. After deposition of 5 layers of TiO<sub>2</sub> alternated with PSS on non-treated PDMS, the WCA was only 45° and finally

reaches  $0^\circ$  after 20 alternations of  $\text{TiO}_2$  with PSS (Figure 6.6). Oxygen plasma treatment of the PDMS surface changes the functional groups<sup>121</sup> on the surface and renders it hydrophilic (WCA after plasma treatment is less than  $5^\circ$ ) for a brief period of time<sup>122</sup>. Figure 6.7 shows the contact angles measured on the three substrates after 90 seconds after the water drop was placed. The WCA after deposition of precursor layers and one layer of  $\text{TiO}_2$  on plasma treated PDMS was measured to be  $32^\circ$  and decreased as the number of  $\text{TiO}_2$  layers increased, finally reaching  $0^\circ$  after 5 layers of  $\text{TiO}_2$  (Figure 6.8). Further deposition of PSS/ $\text{TiO}_2$  layers does not change film wettability. Coating PSS on top of  $\text{TiO}_2$  did not change the water contact angle obtained for the previous layer.

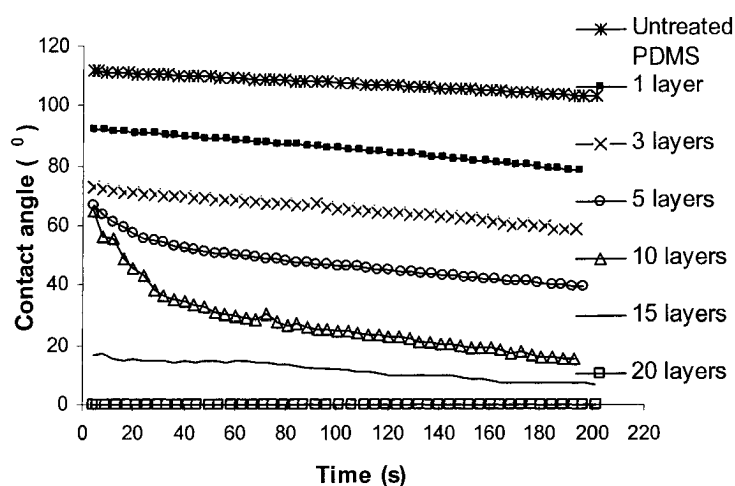


Figure 6.6. Water contact angle measurements on PDMS with the deposition of different number of layers of  $\text{TiO}_2$ .

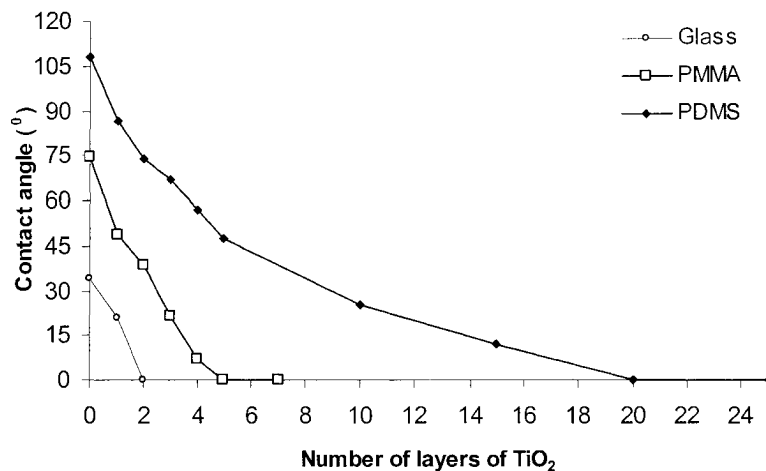


Figure 6.7. Water contact angle of glass, PMMA and PDMS substrates after coating with different number of PSS/TiO<sub>2</sub> bilayers without plasma treatment of the substrates.

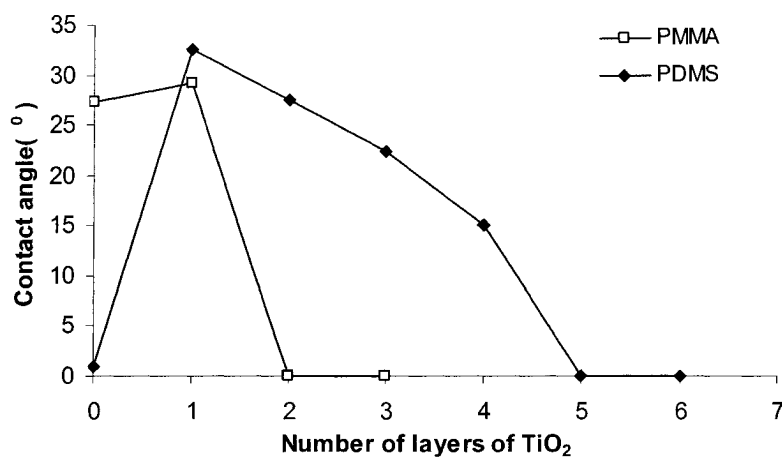


Figure 6.8. Water contact angle of PMMA and PDMS substrates after coating with different number of PSS/TiO<sub>2</sub> bilayers with plasma treatment of the substrates.

Figure 6.9 depicts the variation in contact angle, over time in days, for stored PMMA surfaces that were subjected to different treatments. Oxygen plasma treatment significantly lowers the WCA of the PMMA surface for a brief period, but increases to 40° after 1 day and finally stabilizing at about 50° after several days. Coating PMMA

with different polyelectrolyte combinations alone also shows an initial decrease in the WCA value but eventually increasing to an angle of 60-70° after 6 days. Conversely, PMMA surfaces coated with 5 layers of TiO<sub>2</sub> alternated with PSS show a stable contact angle of 0° from the time of deposition to the 6th day. These results show that PSS/TiO<sub>2</sub> films have longer lasting hydrophilic properties than PSS/PDDA or PSS/PAH films, i.e. we have the ultimate hydrophilic coating (super-hydrophilicity).

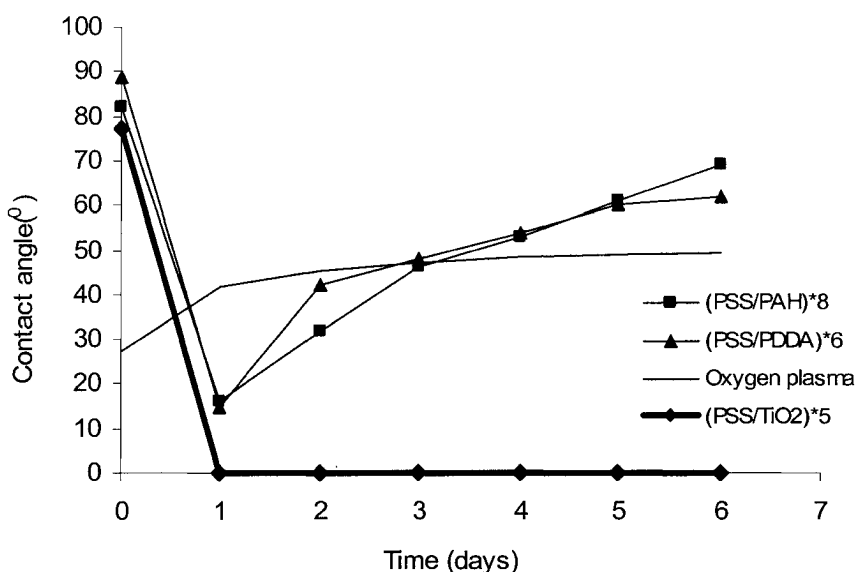


Figure 6.9. Change in water contact angle for various coatings on PMMA during storage; treatment was performed on the first day.

#### **6.4 Effect of Different Types of Nanoparticles on Wettability of LbL Coating**

Wettability of thin films assembled via LbL technique from nanoparticles of different shapes and sizes was investigated to determine if super-hydrophilicity can be introduced into the films by LbL assembly alone and without considering the photosensitive properties of the nanoparticles used. We made multilayer coating of two

types of clays (cylindrical and flat) and  $8 \pm 1$  nm diameter spherical silica multilayer with total thickness from 5 to 200 nm. Table 6.1 illustrates the fact that zero contact angle was not reached for these samples, and super-hydrophilicity is unique for thin films based on TiO<sub>2</sub> nanoparticles. Most likely, it is related to TiO<sub>2</sub> photo-electric properties. The contact angle for LbL assembled PSS/TiO<sub>2</sub> films reaches 0° after deposition of two layers of TiO<sub>2</sub> particles on glass. Contact angles of 14°, 22.5° and 27° were measured for silica, halloysite and montmorillonite coated glass surfaces, respectively.

Table 6.1. Comparison of contact angles of different nanoparticles coated on glass substrates.

Nanoparticles	Polyelectrolyte for alternation	No. of layers	Contact angle, degrees
TiO <sub>2</sub>	PSS	2	0
Halloysite	PDDA	4	22.5
Montmorillonite	PDDA	4	27.0
Silica	PDDA	4	14.0

### **6.5 Biocompatibility of TiO<sub>2</sub> Coated Substrates**

As shown in Figures 6.10 - 6.12, fibroblast cells attached very well to all three substrates that were coated with PSS/TiO<sub>2</sub> films and displayed the typical fibroblast morphology (long spindle shaped cells with pseudopodia). The pattern of cell attachment showed that TiO<sub>2</sub> nanoparticle coated substrates are suitable for cell culture while non coated plastic is not biocompatible. However, further studies are needed for verification of optimal attachment, proliferation, morphology and phenotype determination, which will be discussed in a separate publication. Other research groups, working on

nanoparticle coatings for cell culture, have shown attachment of cells to CdTe nanoparticle films only after coating them with collagen<sup>123</sup>. The authors believe that the cell culture work reported here is the first such instance where successful attachment of cells directly on nanoparticle coated (LbL) substrates was observed.



Figure 6.10. Cell culture of human dermal fibroblasts on glass.



Figure 6.11. Cell culture of human dermal fibroblasts on PMMA.

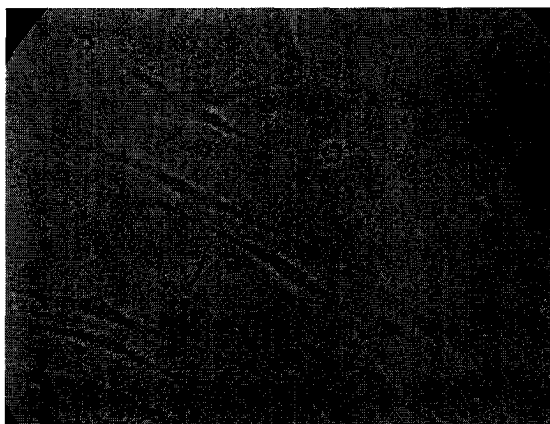


Figure 6.12. Cell culture of human dermal fibroblasts on PDMS.

### **6.6 Conclusion**

It can be concluded from Figure 6.7 that the physical characteristics of the substrate strongly influence development of a hydrophilic  $\text{TiO}_2$  coating. A higher number of  $\text{TiO}_2/\text{PSS}$  alternations are required to obtain a zero water contact angle on as-prepared surfaces of hydrophobic substrates (PMMA and PDMS) independent of the fact that  $(\text{PDDA}/\text{PSS})^*3$  precursor films were pre-deposited on all the templates to prevent the influence of substrate properties on the build-up of the  $\text{TiO}_2/\text{PSS}$  films. It is known that that LbL assembly initially takes place on the substrates only on a few charged surface patches<sup>124</sup> and then  $\text{TiO}_2$  particles, step-by-step, fill the space between them. The treatment of PMMA and PDMS with oxygen plasma, results in the formation of charged functional groups<sup>128,48</sup> on their surfaces, which significantly enhances LbL assembly on these surfaces which results in faster formation of complete  $\text{TiO}_2$ -based films.

Another effect is the appearance of superhydrophilicity of  $\text{TiO}_2/\text{PSS}$  layers in the absence of UV illumination. The adsorption of different dopants can significantly change the properties of  $\text{TiO}_2$ -based photocatalysts<sup>125</sup>. Spectra of  $\text{TiO}_2$  nanoparticle suspensions experience a strong red shift when phosphate, sulfate, carboxylate ions and certain other

additives are present in the mixture<sup>126</sup>. These additives significantly improve sensitivity of TiO<sub>2</sub> catalysts to UV and visible light. Moreover, it has been shown that coatings consisting of smaller nanoparticles (10-30 nm) or having greater roughness show higher photocatalytic activity than bulk films prepared from the same parent material, which is a result of a larger active surface area<sup>127</sup>. Polyelectrolyte/TiO<sub>2</sub> LbL films can be considered to be a network of nanoparticles separated by chains of oppositely charged polyelectrolyte which simultaneously keeps the film from disintegrating. The size-dependant permeability of LbL films makes the high surface area of nanoparticles accessible for substances with molecular weight less than a few thousand<sup>128</sup>. The super-hydrophilicity of TiO<sub>2</sub> is usually ascribed to the chemisorption of water molecules on photoinduced surface defects<sup>129</sup>. We assume that PSS, which has been shown to have hole scavenging properties due to a negatively charged sulfate group and a hydrophobic phenol ring<sup>130</sup>, can provide additional stability to the Ti<sup>3+</sup> sites associated with the highly photoinduced hydrophilicity of TiO<sub>2</sub> surfaces<sup>56</sup>. Moreover, the strong influence of preparation methods on the properties of films with similar composition has been recently reported<sup>131</sup>. The presence of hydroxyl groups (introduced during the preparation) and high photocatalytic activity of Degussa P-25 can cause the absorption of UV and visible light present in room light and forms a hydrophilic layer. It can be seen that the observed hydrophilic properties of PSS/TiO<sub>2</sub> films can be a result of the cooperative action of several different factors including size, structure, component composition and method of preparation.

Stable, long lasting super-hydrophilic coatings with zero contact angle can be obtained on different types of substrates using LbL assembly of TiO<sub>2</sub> nanoparticles. The

complete wettability was shown to be unique to poly(styrenesulfonate) - TiO<sub>2</sub> nanocomposite films. The biocompatibility of the TiO<sub>2</sub> coated surfaces was proven by the successful cell culture of human dermal fibroblast cells on TiO<sub>2</sub> – polyanion multilayers. The super-hydrophilicity and biocompatibility of the TiO<sub>2</sub> nanoparticle coatings provides a new method for surface modification using nanoparticle coatings for applications involving cell and tissue culture on various substrates, including medical implants.

## CHAPTER 7

### INTEGRATION OF LAYER-BY-LAYER ASSEMBLY AND CELL CULTURE

Thin films formed using LbL have been of great interest scientifically for many years and have been used to develop thin films of various polymers for increased or restricted cell attachments on various substrates<sup>87,132</sup>. There has only been one study prior to this, for the formation of cell adhesive nanoparticle thin films<sup>129</sup>, where the investigators have shown that the cells attached to semiconductor films only after coating with a thin layer of collagen on top of the nanoparticles. Nanoparticles have long been studied for the formation of thin films on various substrates<sup>133</sup>. Here we have integrated the formation of thin films of nanoparticles with cell culture to test the viability of cells directly on the nanoparticle thin films.

#### **7.1 Thickness of the Nanoparticle Thin Films**

The change in the thickness with increasing number of layers of nanoparticles is shown in Figure 7.1. The average thickness of the precursor layers was approximately 5 nm. The average growth step per bilayer was found to be 6, 11, 22 and 56 nanometers for silica, TiO<sub>2</sub>, montmorillonite and halloysite, respectively. A linear increase in the thickness of the bilayers was observed for all the nanoparticle films indicating successful deposition of nanoparticles in alternation with the respective polyelectrolytes.

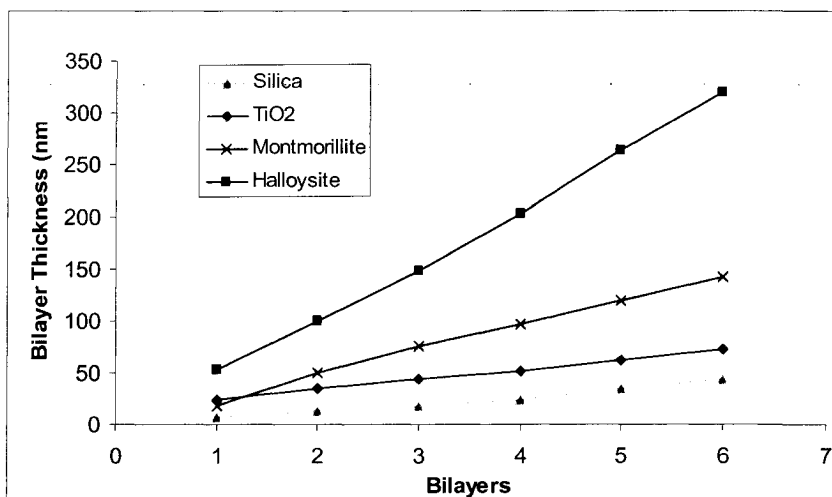


Figure 7.1. Thickness of the nanoparticle thin films measured using quartz resonators.

### **7.2 Cytotoxicity of Nanoparticle Thin Films on Human Dermal Fibroblasts**

A two color fluorescent cell viability assay was performed on cells attached to nanoparticle surfaces which provides simultaneous visualization of both live and dead cells. Live cells show a bright green fluorescence while the dead cells fluoresce red. All four kinds of nanoparticle coated substrates were visualized for cell viability. Cell viability results for a montmorillonite coated substrate is shown in Figure 7.2. The number of cells that are stained with calcein AM (green) is far greater than the number of cells stained with ethidium homodimer-1 (red), which indicates that the nanoparticle thin films offer cell supportive surfaces. Similar kinds of results were obtained with other nanoparticles (data not shown) providing evidence that the selected nanoparticle surfaces do not have any major toxic effect on HDFs and that the cells can survive on the LbL assembled nanoparticle substrates.

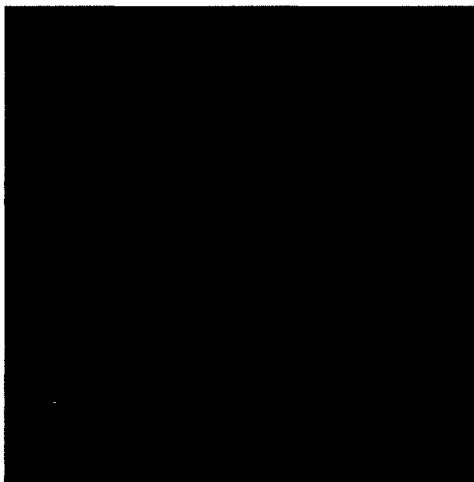


Figure 7.2. Live/dead assay performed on a glass substrate coated with 2 layers of silica.

### **7.3 Proliferation and Phenotype of Human Dermal Fibroblasts on Nanoparticle Thin Films**

Qualitative BrdU cell proliferation assay was performed on the cells attached to the nanoparticle coated substrates. This test shows the incorporation of BrdU during mitosis. Silica, halloysite, montmorillonite and  $\text{TiO}_2$  coatings showed cell proliferation. Figure 7.3 shows the BrdU test results on substrate coated with two layers of  $\text{TiO}_2$  nanoparticles in alternation with PDDA. Similar results were obtained on other nanoparticle coatings also. Quantitative cell proliferation was done using the MTT assay and the results of cell activity on the substrates is depicted in Figure 7.4. One can see that the cells on halloysite, montmorillinoite and  $\text{TiO}_2$  have a higher activity (shown by the absorbance) than the cells on the control and silica surfaces. HDF phenotype was determined by the expression of type I collagen on the nanoparticle coated substrates. Figure 7.5 shows the image of collagen expressed by HDFs on a montmorillinoite coated glass substrate. Collagen can be seen around the nucleus of the cell (elliptical white space in the middle of each cell).



Figure 7.3. Brdu Cell proliferation on a substrate coated with 2 layers of  $\text{TiO}_2$ .

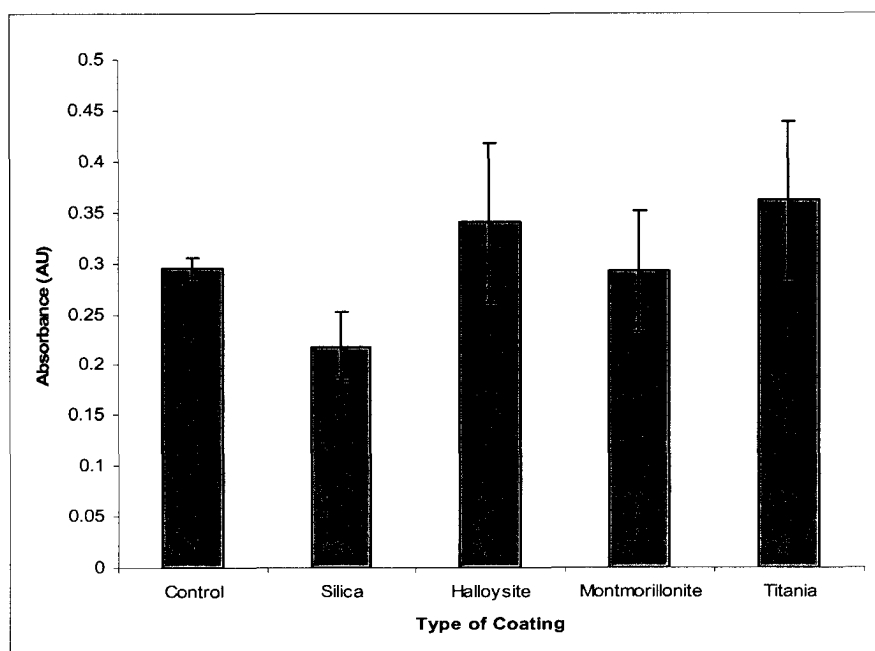


Figure 7.4. MTT based cell activity on LbL assembled nanoparticle thin films.

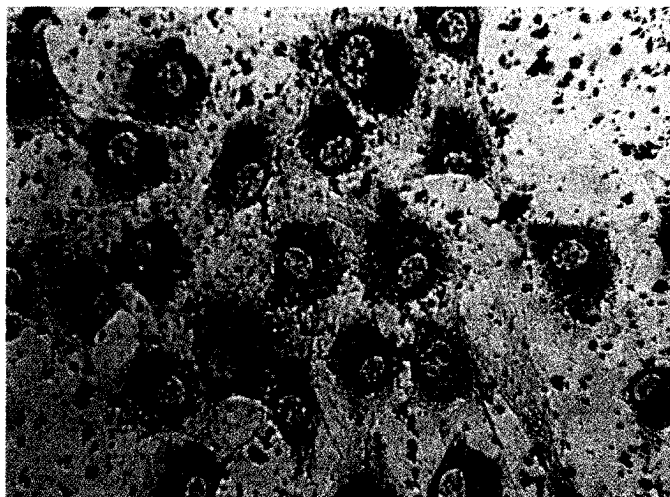


Figure 7.5. Collagen expression by HDFs on a substrate coated with 3 layers of montmorillonite.

#### **7.4 Cell Spreading on Nanoparticle Thin Films**

For visualizing the spreading of the cells on the substrates, HDFs were seeded on the substrates coated with 3 layers of nanoparticles. Scanning electron micrographs of the cells on the substrates after 4 hours of incubation were acquired. The cells on the control (Figure 7.6), halloysite (Figure 7.7), montmorillonite (Figure 7.8) and silica (Figure 7.9) have a rounded morphology, where as some of the HDFs (white arrows in Figure 7.10) on the TiO<sub>2</sub> coated substrates show a morphology that suggests that those cells have partially spread on the substrate. However, most of the cells on TiO<sub>2</sub> still retain their rounded morphology. Figures 7.11 through 7.15 show the morphology of cells on the substrates after 24 hours of seeding. One can clearly see that some cells on montmorillonite (Figure 7.13) and silica (Figure 7.14) substrates still have a rounded morphology suggesting that the cells on these substrates take a longer time for spreading.

The cells on halloysite (Figure 7.12) and  $\text{TiO}_2$  (Figure 7.15) show a spreading morphology.

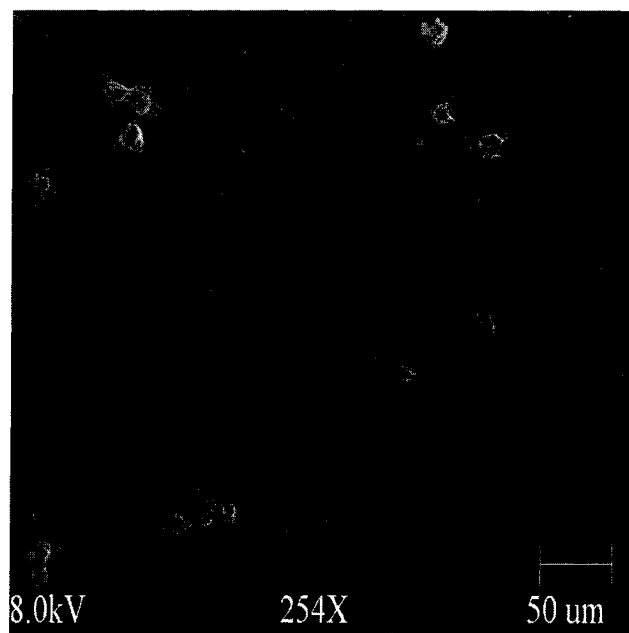


Figure 7.6. Cells attached on control substrate after 4 hours of seeding.

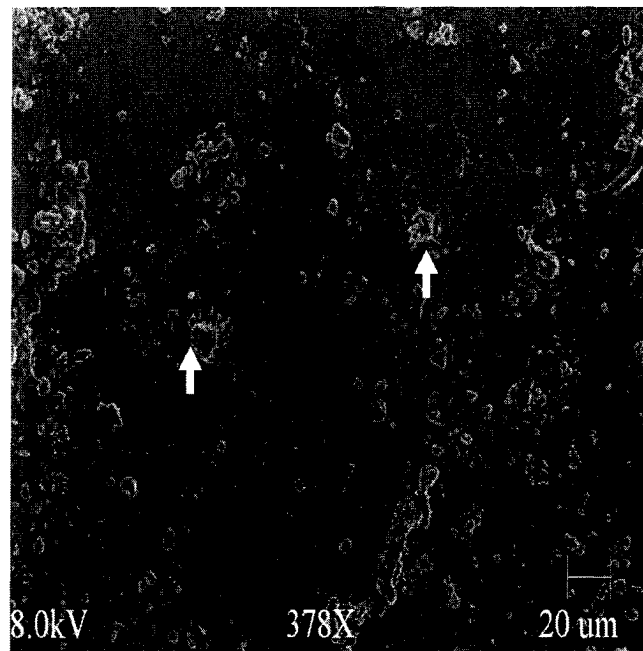


Figure 7.7. Cells attached on a substrate coated with 3 layers of halloysite after 4 hours of seeding.

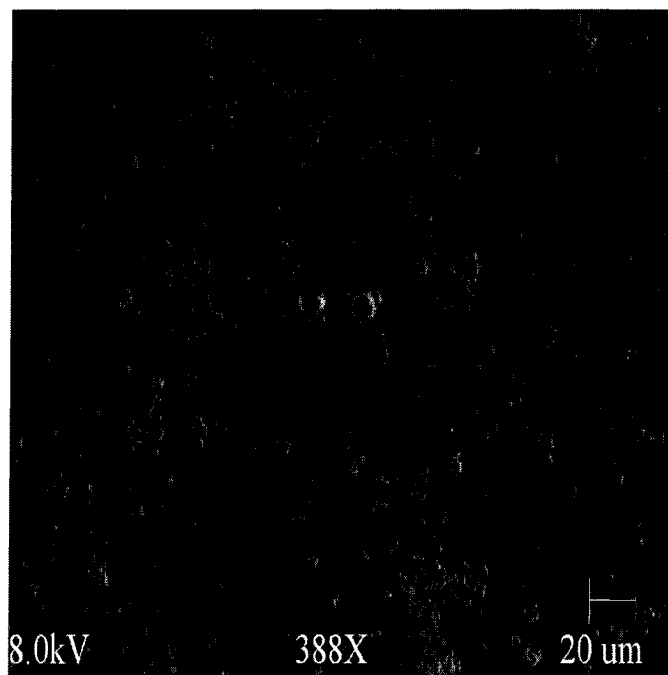


Figure 7.8. Cells attached on a substrate coated with 3 layers of silica after 4 hours of seeding.

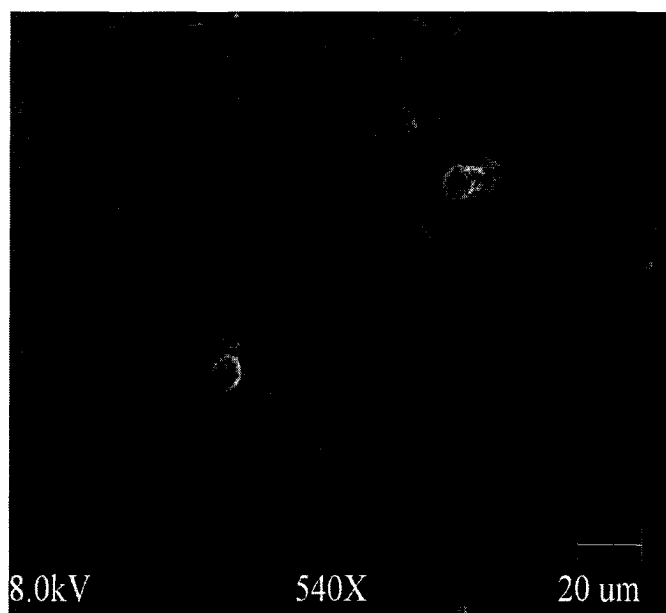


Figure 7.9. Cells attached on a substrate coated with 3 layers of montmorillonite after 4 hours of seeding.

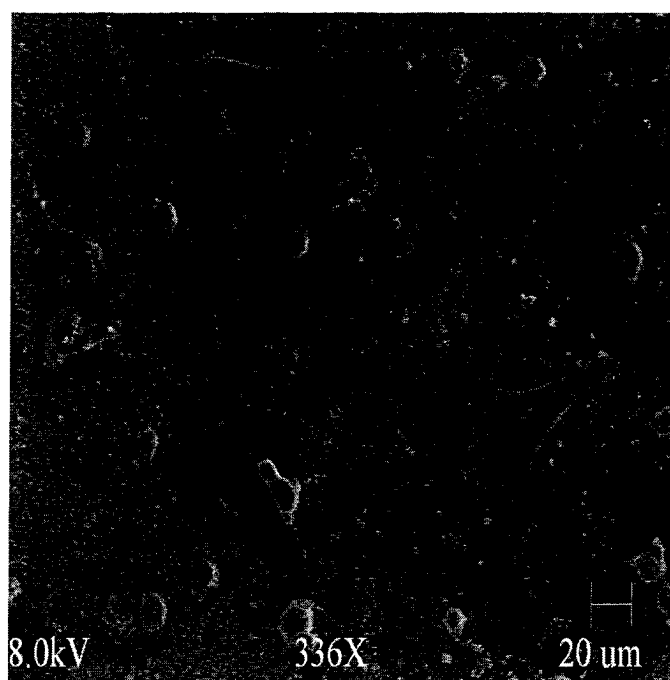


Figure 7.10. Cells attached on a substrate coated with 3 layers of  $\text{TiO}_2$  after 4 hours of seeding.

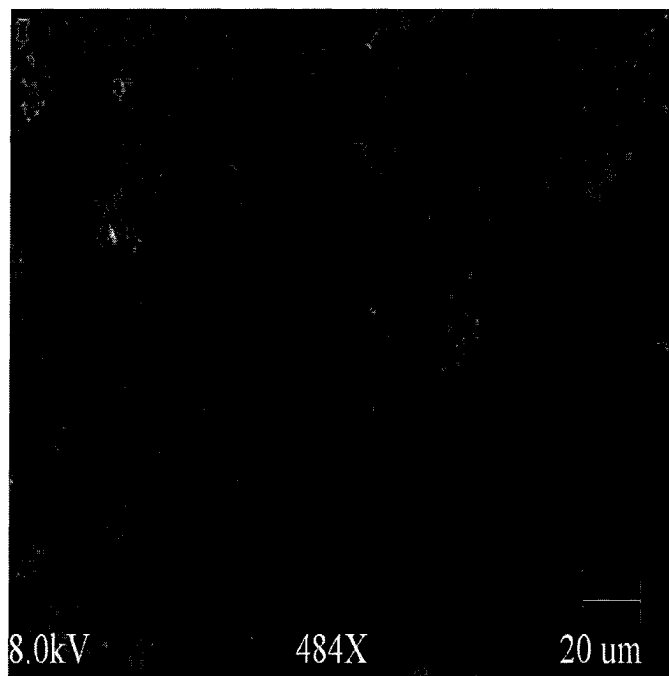


Figure 7.11. Cells attached on control substrate after 24 hours of seeding.

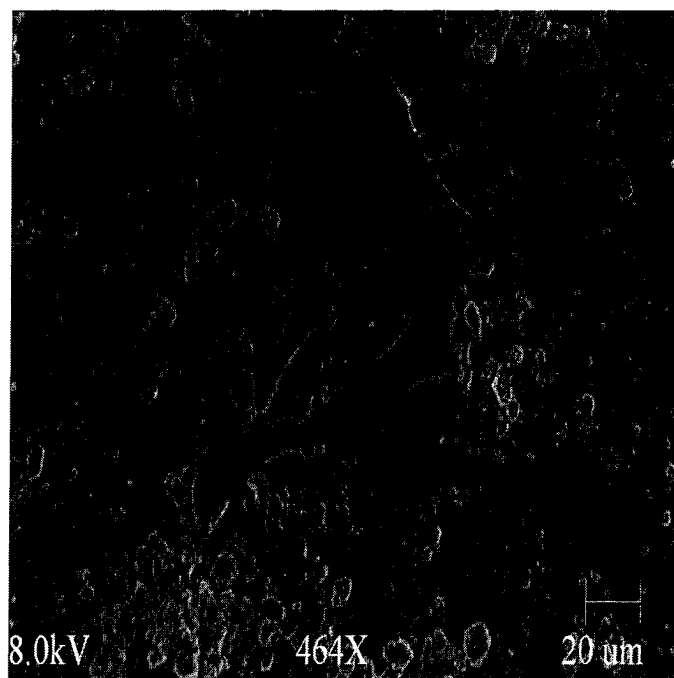


Figure 7.12. Cells attached on a substrate coated with 3 layers of halloysite after 24 hours of seeding.

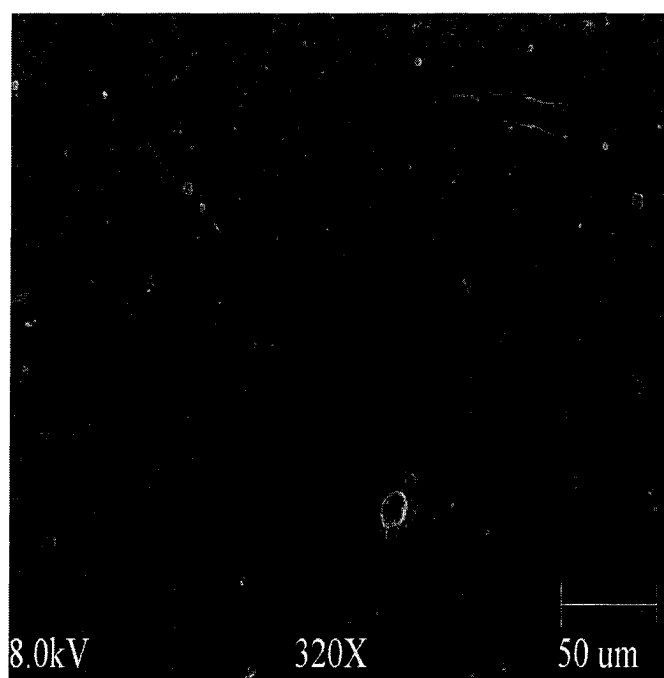


Figure 7.13. Cells attached on a substrate coated with 3 layers of silica after 24 hours of seeding.

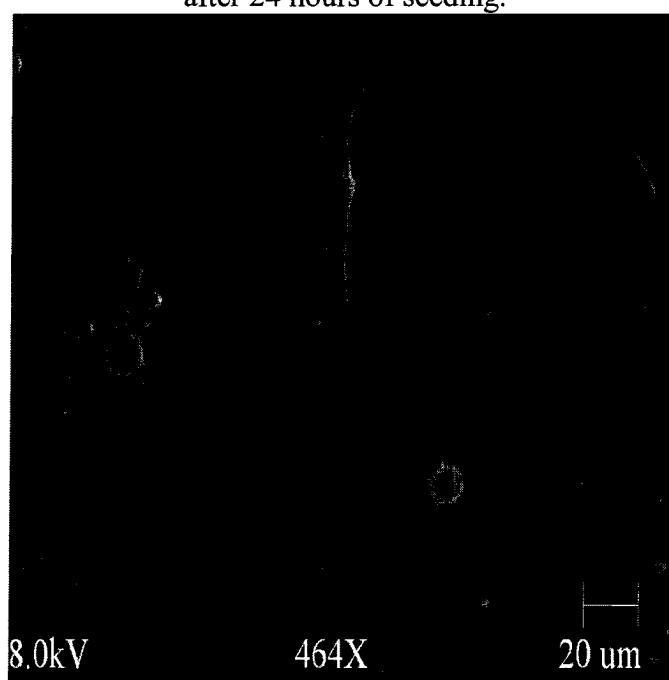


Figure 7.14. Cells attached on a substrate coated with 3 layers of montmorillonite after 24 hours of seeding.

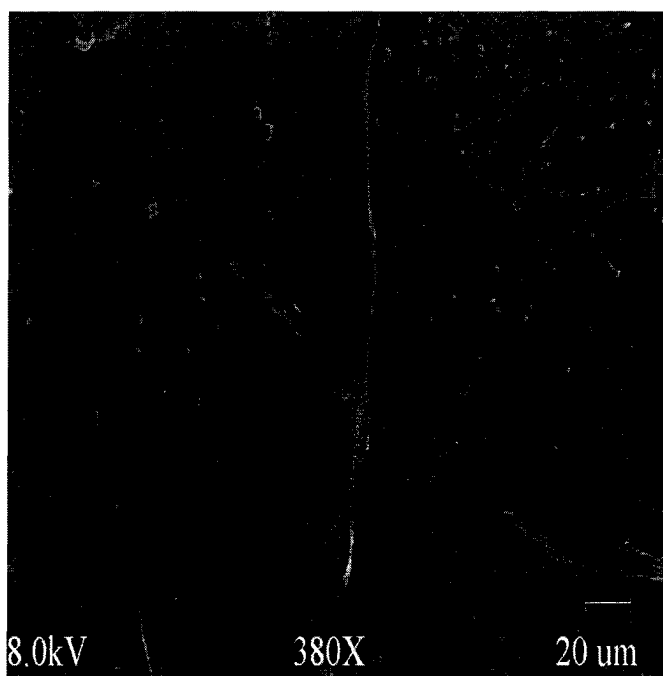


Figure 7.15. Cells attached on a substrate coated with 3 layers of  $\text{TiO}_2$  after 24 hours of seeding.

### **7.5 Conclusion**

The attachment, cytotoxicity and proliferation of cells on novel substrates, *in-vitro*, are the first steps towards the testing the same substrates *in-vivo*. These tests give a basic understanding of the behavior of cells towards the substrates. Toxic, undesirable substrates can be screened by this process, giving us the most suitable substrates for various implantation applications. Nano-phase materials are one such novel substrate surface which has been widely used for testing the behavior of cells *in-vitro*<sup>134</sup>. Research has shown that these materials, when present or coated can positively influence the behavior of cells on substrates<sup>22,25</sup>.

In this chapter, we have discussed the possibility of the surface modification of materials with inorganic nanoparticles, assembled with nanometer precision using LbL

assembly. Our results have shown that inorganic nanoparticle thin films can be assembled with nanometer precision and offer the possibility of including various components (polymers and nanoparticles) for the better functioning of implants. We have shown in this report that the nanoparticles tested, did not have major toxic effects on the cells. Qualitative proliferation of cells on the nanoparticle thin films was shown with the BrdU assays. The cells on these inorganic nanoparticle thin films retained their phenotype by synthesizing type I collagen, the phenotypical marker of HDFs. Partial spreading of the cells on  $\text{TiO}_2$  can be seen 4 hours after incubation and, at 24 hours, the spreading of cells on halloysite and  $\text{TiO}_2$  is complete, where as many cells on montmorillonite and silica still retain a rounded morphology.  $\text{TiO}_2$  and halloysite show faster spreading of cells than the other nanoparticles tested. In conclusion, we have demonstrated the formation of thin films made of inorganic nanoparticles, with the purpose of modifying the surfaces of implantable materials and we have shown the attachment of cells on thus assembled nanoparticle thin films.

## CHAPTER 8

### **LAYER BY LAYER ASSEMBLED TiO<sub>2</sub> THIN FILMS FOR ATTACHMENT AND SPREADING OF STEM CELLS**

The initial study of cell attachment of nanoparticle thin films was verified with the culture of HDFs on 4 different kinds of nanoparticle thin films (previous chapter). The results suggested that TiO<sub>2</sub> and halloysite thin films showed faster attachment of cells. In this chapter, the formation of thin films of nanoparticles and the attachment of stem cells will be discussed. The nanoparticle thin films that offer the best surface for the proliferation of cells will be identified and the attachment, proliferation with different numbers of layers, surface roughness effects and spreading of cells will be discussed.

#### **8.1 Thickness of the Nanoparticle Thin Films**

The thickness of the assembled nanoparticle layers was determined by the deposition of the precursor and nanoparticles on quartz crystal microbalance resonators. The increase in the thickness was plotted against the number of layers of material deposited and is depicted in Figure 8.1. The average bilayer thickness was calculated to be around 11, 6, 22 and 56 nm for titanium dioxide, silica, montmornollite and halloysite, nanoparticles. The bilayer thickness increased linearly with increasing number of bilayers

respectively. Four different resonators were used for the four different types of the material deposited (inset in Figure 8.1). The average thickness of the precursor layers was around 5 nm.

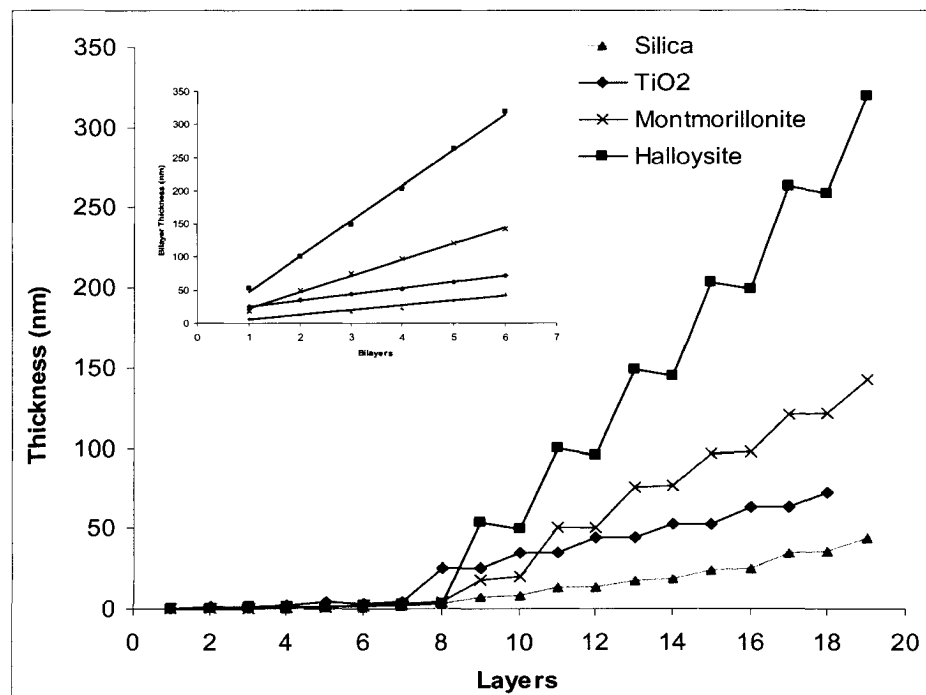


Figure 8.1. Change in thickness of the deposited nanoparticle films, monitored using quartz crystal microbalance. Inset shows the linear increase in thickness of the deposited layers.

## **8.2 Cell Numbers by MTT Assay**

Various nanoparticle coatings were tested for the attachment of MMSC and for cell numbers as a function of different coatings. The results are shown in Figure 8.2. Three bilayers of each type of nanoparticle coating was used to perform this assay. The initial density of seeding on a 2cm\*2cm substrate was 6000 cells/cm<sup>2</sup>. The cells were incubated for 72 hours and the MTT assay performed as previously described in the

materials and methods section. Uncoated glass substrates were used as the control. The data shows that MSC showed a strong preference for the  $\text{TiO}_2$  coated substrates while silica and halloysite showed negative trends in the attachment of the cells. Montmorillonite showed a small increase as compared with silica and halloysite, but is still smaller than the cells attached on the control surface. The cells seeded on the  $\text{TiO}_2$  surface almost tripled in three days (more than the control surface) suggesting that  $\text{TiO}_2$  nanoparticle coatings favor cell attachment and growth. Other nanoparticle coatings show that they may not be suitable for the initial attachment and growth of MMSC (based on Figure 8.2). No long term studies were conducted for the proliferation and attachment of MMSC on silica, halloysite and montmorillonite coated substrates.

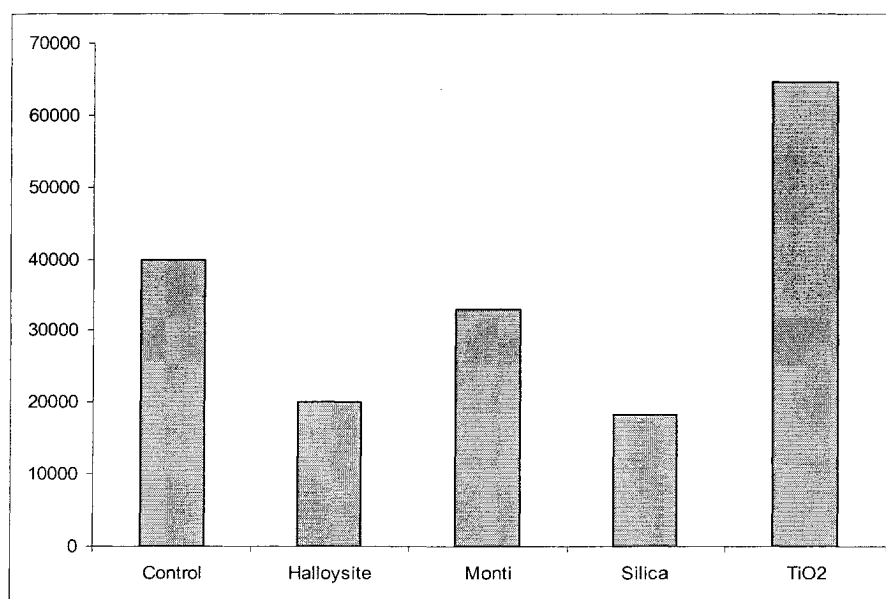


Figure 8.2. Cell numbers on 4 layers of nanoparticles deposited with respective polyelectrolyte layers. The cells were counted using MTT based assay on the third day after seeding the substrates.

### 8.3 Surface Roughness of TiO<sub>2</sub> Thin Films

Surface roughness of the deposited TiO<sub>2</sub> nanoparticle layers was determined using a non contact optical profiler which gives the average roughness of the surfaces. The average roughness in an area of about 0.07 mm<sup>2</sup> was measured for different number of layers of TiO<sub>2</sub> deposited in alternation with PDDA. The R<sub>a</sub> values obtained plotted against the number of layers of TiO<sub>2</sub> deposited shows a linear increase in the roughness with increasing number of layers of TiO<sub>2</sub> (Figure 8.3). Figure 8.4 is the representative data sheet obtained from the optical profiler measurements.

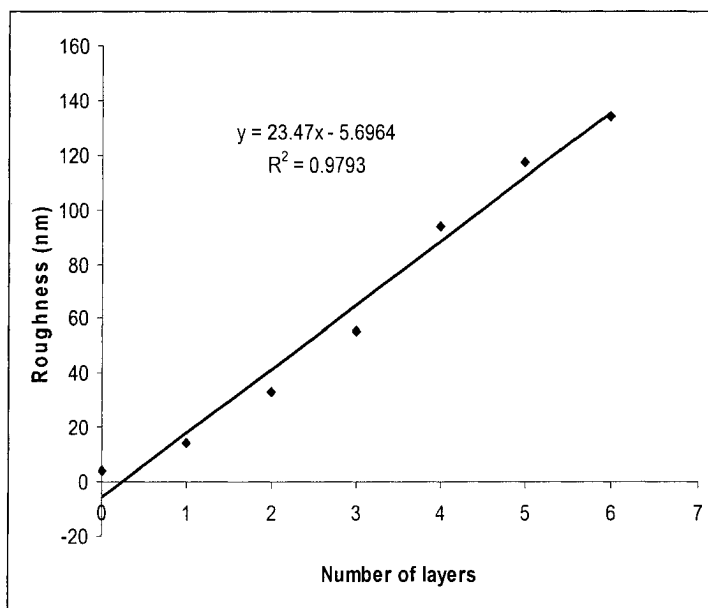


Figure 8.3. Change in surface roughness TiO<sub>2</sub> layers as a function of layer number.

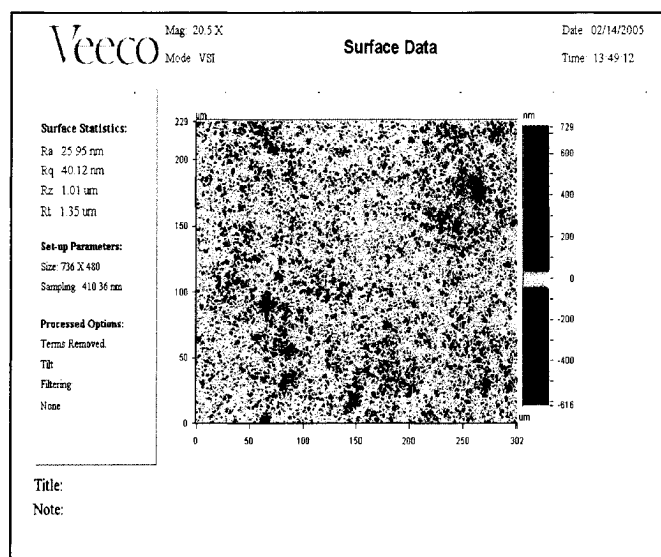


Figure 8.4. Representative data of surface roughness on a substrate coated with 2 layers of  $\text{TiO}_2$ .

#### **8.4 Cytotoxicity of $\text{TiO}_2$ Coated Substrates**

The cytotoxicity of the substrates studied using commercially available fluorescent dyes showed very little cell death on the substrates. Figure 8.5 shows the cytotoxicity test performed on a glass substrate coated with 4 layers of  $\text{TiO}_2$  in alternation with PSS. One can see that all the cells in this image are alive (green). These results show that the  $\text{TiO}_2$  coated substrates support cell culture on them and that these substrates do not have a toxic effect on the attached cells. Quantitative cytotoxicity experiments were not conducted for this report.

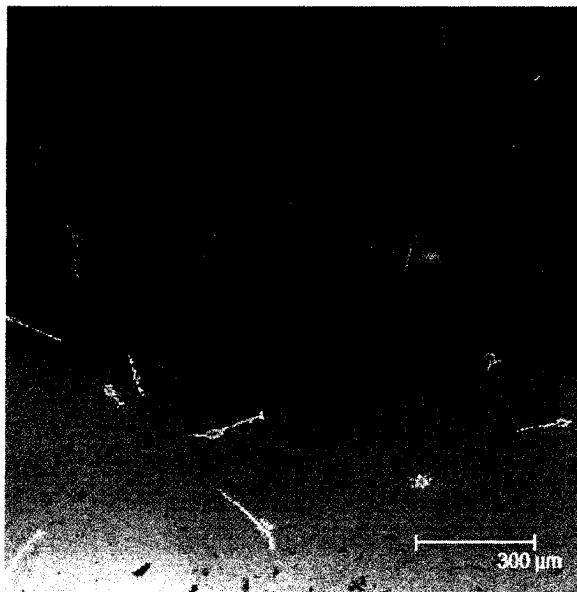


Figure 8.5. Cytotoxicity assay performed on a glass substrate coated with 4 layers of TiO<sub>2</sub>.

### **8.5 Cell Proliferation on TiO<sub>2</sub> Substrates**

Different numbers of TiO<sub>2</sub> layers were coated on glass substrates and MSC were seeded at equal densities (6000 cells/cm<sup>2</sup>) on these substrates. Figure 8.6 shows the results of the MTT assay performed on these substrates 72 hours after seeding. It was observed that coating the substrates with TiO<sub>2</sub> increases the attachment of cells. One layer of TiO<sub>2</sub> increases the number of cells by approximately 20% from the control surface. No obvious trend in the attachment of MSC was observed with increasing number of layers of TiO<sub>2</sub> (increasing surface roughness), but coating the substrates with TiO<sub>2</sub> clearly shows an increase in the number of cells attached after 72 hours. Statistically, significant differences were observed with 1, 2 and 6 layers ( $p < 0.01$ , compared with the control surface) and 4 ( $p < 0.05$ , compared with the control surface) while no significant difference was observed with 3 layers of TiO<sub>2</sub>.

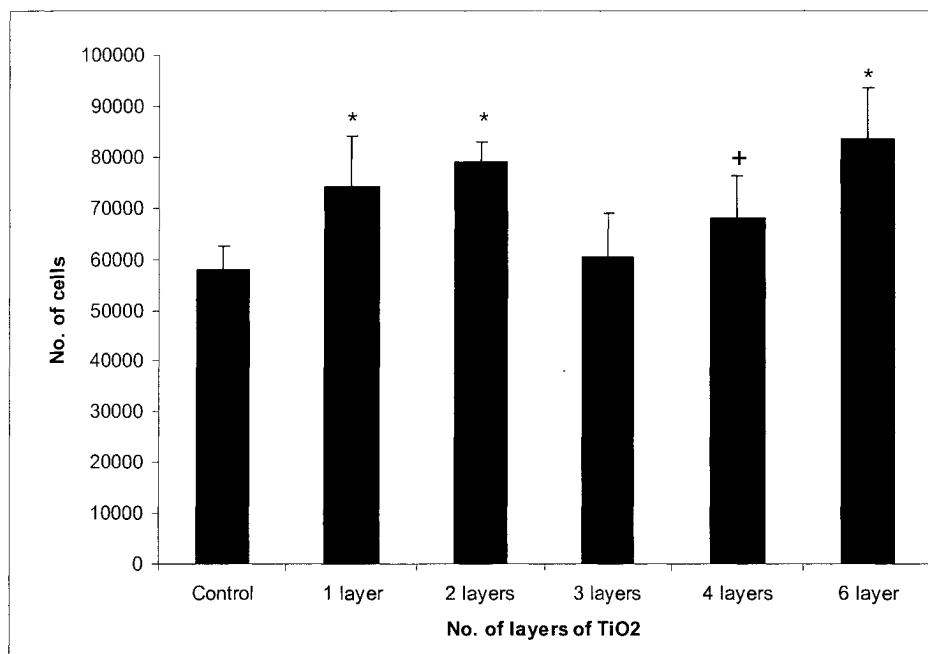


Figure 8.6. Cell numbers on various layers of TiO<sub>2</sub> coated on glass. (\*  $p < 0.01$ , +  $p < 0.05$  compared with the control).

### **8.6 Cell Attachment on TiO<sub>2</sub> Substrates**

The cell attachment studied on the control and for 1 layer and 4 layer substrates is shown in Figure 8.7. The number of cells on the substrate coated with 4 layers of TiO<sub>2</sub> shows a marked increase from the control and also the substrate coated with 1 layer of TiO<sub>2</sub>. The number of attached cells on each substrate increased with increasing time and for all time periods. The number of cells on the substrate coated with 4 layers was found to be more than the control and the substrate coated with 1 layer of TiO<sub>2</sub>. A statistically significant increase in attachment of cells to the substrate coated with 4 layers was found.

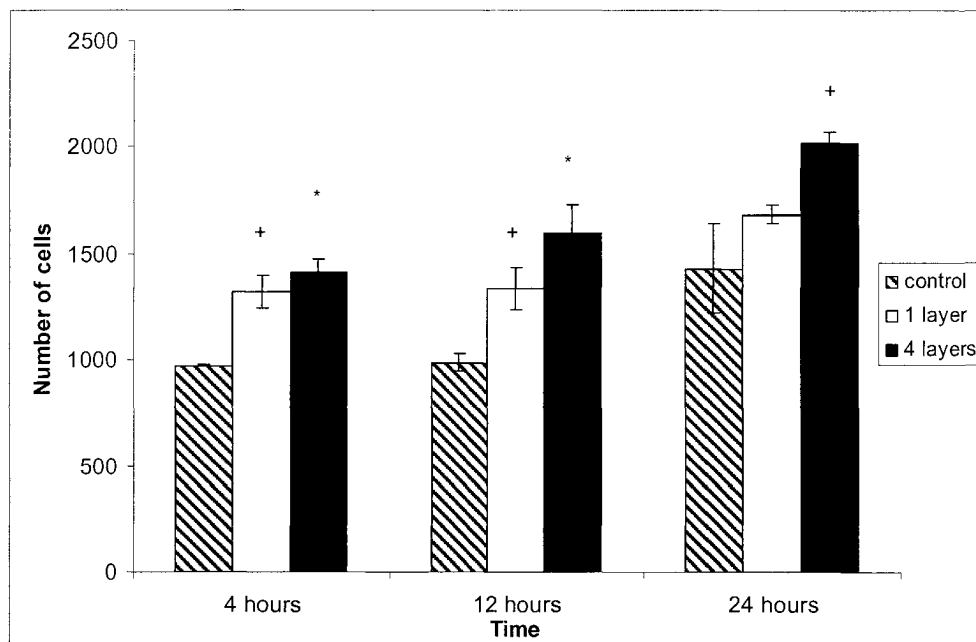


Figure 8.7. Number of cells attached on the control and 1 layer and 4 layer substrates (\*  $p < 0.01$ , +  $p < 0.05$  compared with control).

### **8.7 Cell Spreading Visualized by Scanning Electron Microscopy**

Cell spreading was visualized using scanning electron microscopy. Four different times were chosen for the control (no coating) and for substrates coated with 1 layer and 4 layers of  $\text{TiO}_2$ . The cells on all substrates after 1 hour of seeding had a rounded morphology (data not shown). Figure 8.8 through figure 8.10 show the scanning electron micrographs of the cells on these substrates after 4 hours of seeding. The cells on the control (Figure 8.8) and 1 layer (Figure 8.9) show rounded morphology; where as some cells (white arrows) on 4 layers (Figure 8.10) show a partially spread morphology on the substrate surface. Figure 8.11 through 8.13 show the SEM images of the cells on the substrates after 12 hours of incubation. Most of the cells on the control (Figure 8.11) show rounded morphology of the cells after 12 hours of incubation. On the substrates

coated with 1 layer of  $\text{TiO}_2$ , most of the cells have spread (Figure 8.12). Some cells on 1 layer of  $\text{TiO}_2$  still retain their rounded morphology, however, the number of cells with such morphology is far less than the number of cells that have spread. On the substrate coated with 4 layers of  $\text{TiO}_2$  (Figure 8.13) the cells have long pseudopodia after 12 hours of incubation, suggesting that the cells have already spread on this substrate surface. The morphology of the cells after 24 hours on different substrates is shown in Figures 8.14 through 8.16. The morphology of most of the cells on the control surface (Figure 8.14) suggests that the cells have spread, but many cells remain rounded even after 24 hours of incubation. On the substrate with one layer of  $\text{TiO}_2$  (Figure 8.15), almost all the cells suggest spread morphology, but some of the cells have partially spread (white arrow) suggesting that some of the cells are still spreading. The morphology of the cells on the substrate coated with 4 layers of  $\text{TiO}_2$  (Figure 8.16) after 24 hours shows that the cells have spread and are well adapted to the surface.

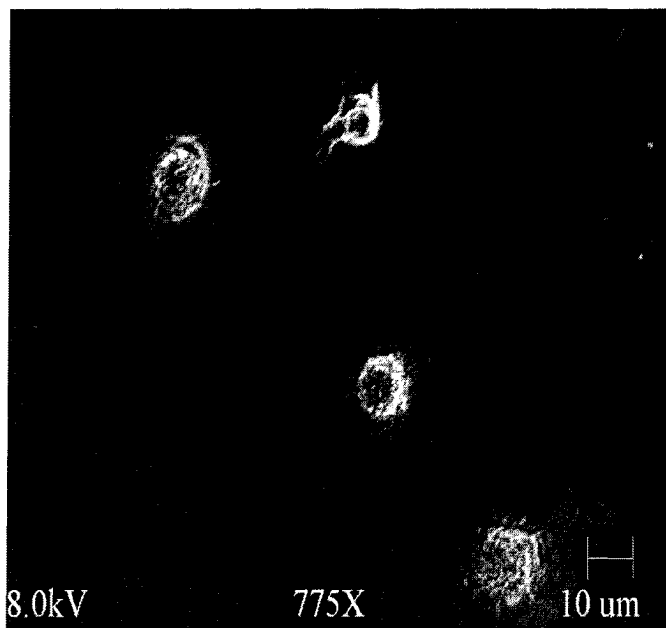


Figure 8.8. Cells attached on control substrate, after 4 hours of seeding.

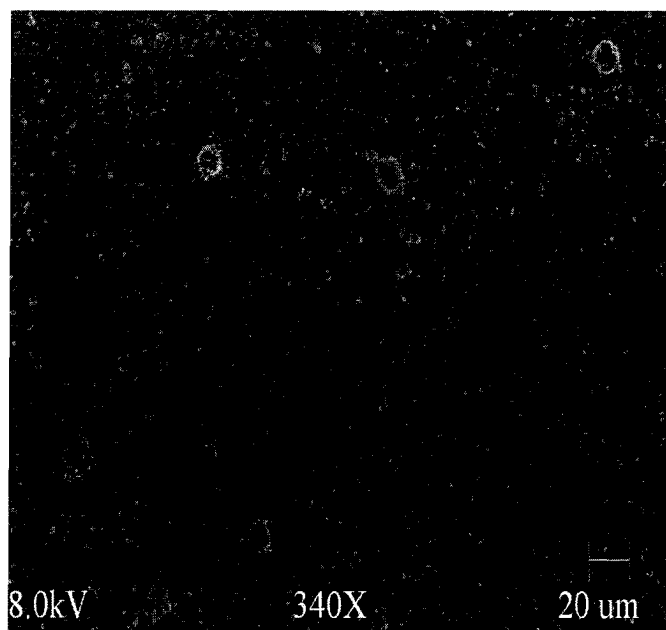


Figure 8.9. Cells attached on a substrate coated with 1 layer of  $\text{TiO}_2$ , after 4 hours of seeding.

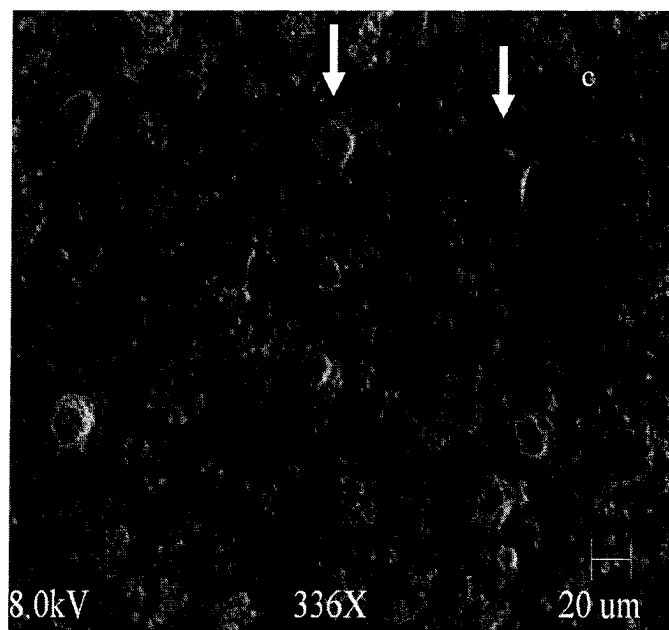


Figure 8.10. Cells attached on a substrate coated with 4 layers of  $\text{TiO}_2$ , after 4 hours of seeding.

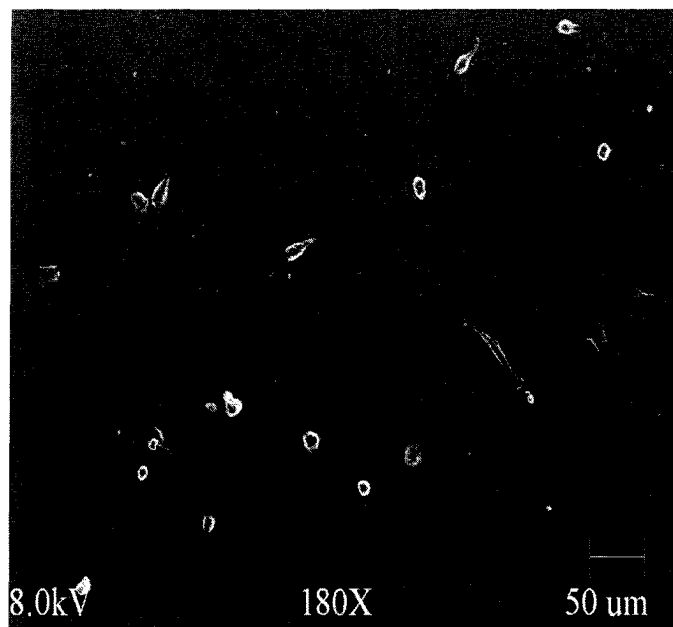


Figure 8.11. Cells attached on control substrate, after 12 hours of seeding.

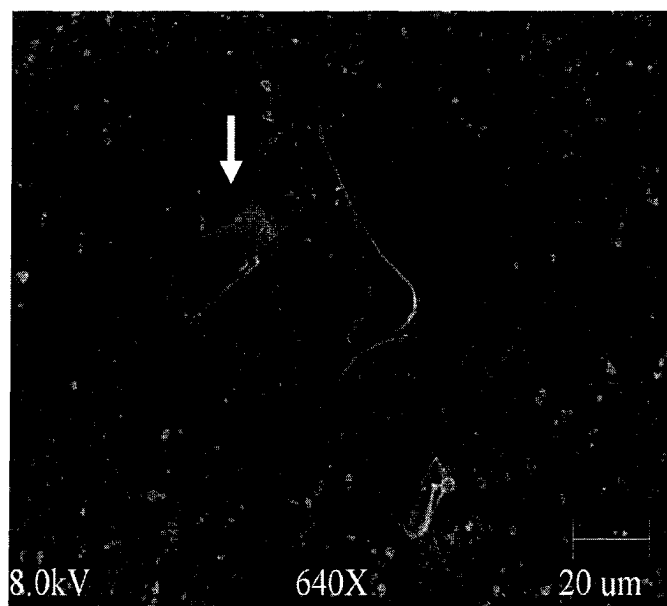


Figure 8.12. Cells attached on a substrate coated with 1 layer of TiO<sub>2</sub>, after 12 hours of seeding.

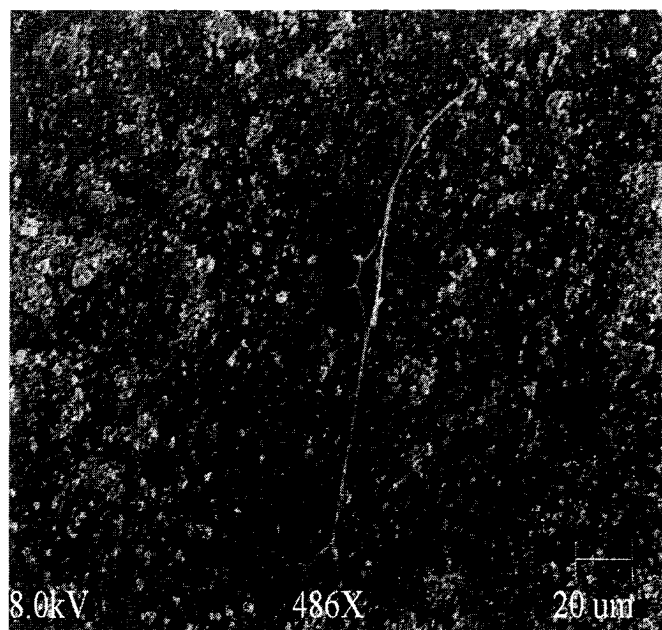


Figure 8.13. Cells attached on a substrate coated with 4 layer of  $\text{TiO}_2$ , after 12 hours of seeding.

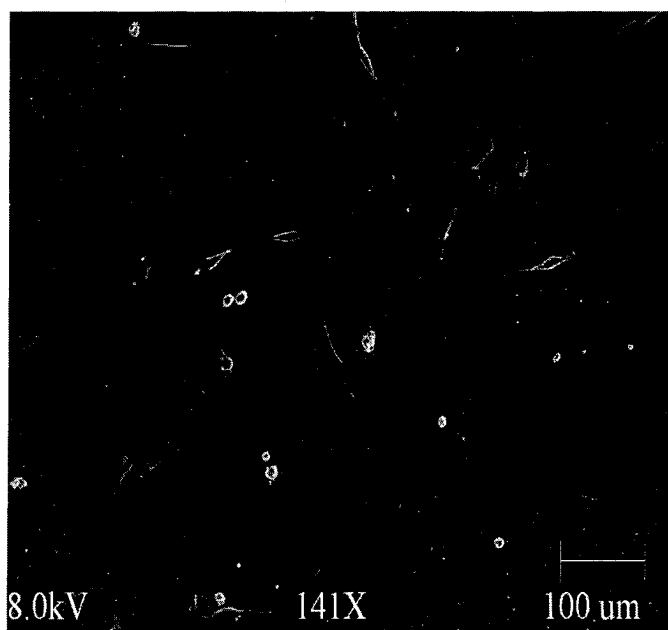


Figure 8.14. Cells attached on control substrate after 24 hours of seeding.

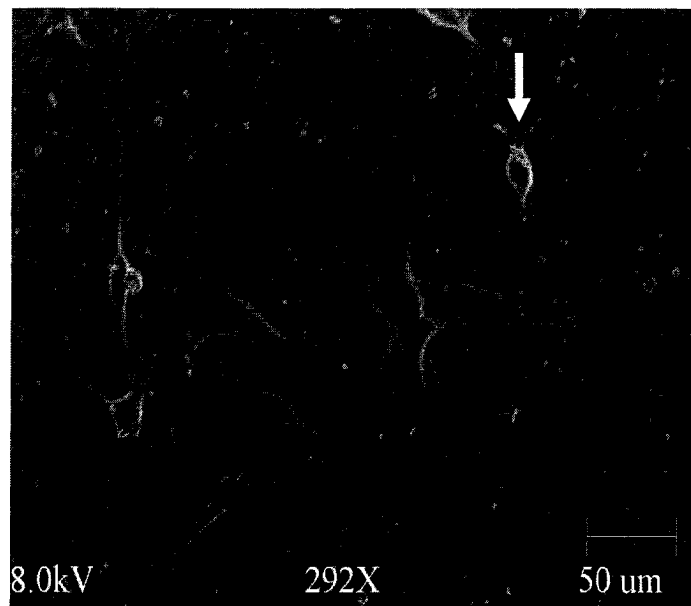


Figure 8.15. Cells attached on a substrate coated with 1 layer of TiO<sub>2</sub> after 24 hours of seeding.

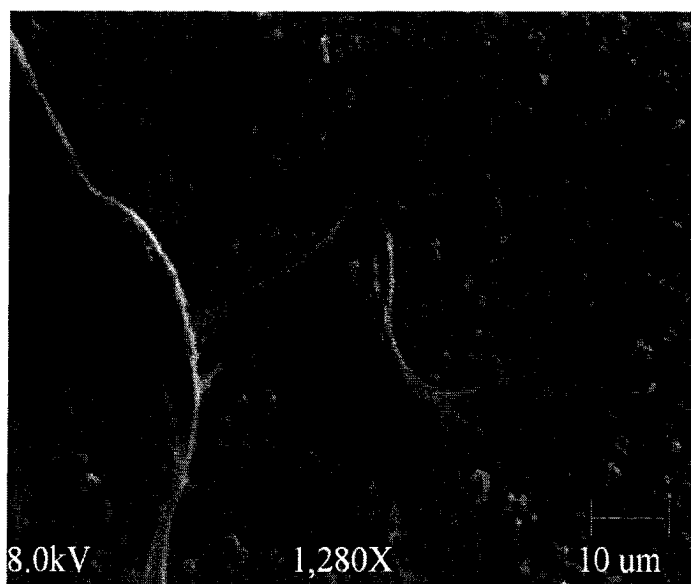


Figure 8.16. Cells attached on a substrate coated with 4 layers of TiO<sub>2</sub>, after 24 hours of seeding.

## **8.8 Conclusion**

Implant modification for cell attachment has been an interesting area of study for many years and various methods have been proposed and implemented. The initial attachment of cells to these surfaces is critical for the functioning and longevity of these materials<sup>135</sup>. Nanostructured materials have been targeted for the purpose of surface modification of implantable materials and these materials have been shown to significantly increase the attachment of cells without compromising the integrity of the implant. Cell cultures for soft and hard tissue replacement have also been shown to increase in the presence of nanomaterials<sup>136</sup>.

LbL has been a method for surface modification with applications in many areas of scientific research and more recently, LbL of macromolecules has been applied to surface treatment and coating for implants<sup>137</sup>. LbL offers the possibility to include multiple components (drugs, enzymes) in the nanophase coatings, offering the possibility of unique compositions for increasing the attachment of cells. Sanin et al<sup>129</sup> were the first to show the attachment of cells to nanoparticles thin films, by coating collagen on these thin films. To the best of our knowledge, there has been only two previous studies on the attachment of cells directly on nanoparticle thin films, which were accomplished by our group<sup>22,23</sup>. In the previous study of attachment of human dermal fibroblasts on nanoparticle thin films, we observed higher and faster attachment of cells on TiO<sub>2</sub> nanoparticle thin films among 4 different kinds of nanoparticles tested. In this study, we have selected TiO<sub>2</sub> nanoparticle thin films for surface modification and various studies have been performed.

Mesenchymal stem cells are a versatile cell line since their numbers can be expanded significantly and differentiated into multiple cell types with various applications for tissue engineering. Our studies with MSC on nanoparticle thin films showed that more cells attached to TiO<sub>2</sub> coated substrates (compared to the control). One explanation may be that an initial adsorption of a thin layer of negatively charged extracellular matrix proteins<sup>138</sup> from the cell culture media on the positively charged TiO<sub>2</sub> surface encouraged initial cell attachment and may explain the increased attachment of MSC on the TiO<sub>2</sub> nanoparticle thin film. Moreover, TiO<sub>2</sub> is a known biocompatible material and the chemistry of cell adhesion on TiO<sub>2</sub> promotes this increased attachment. Cell attachment studies showed an increased attachment of MSC on a rougher TiO<sub>2</sub> surface (higher number of layers, 4 layers of TiO<sub>2</sub>) than a smoother TiO<sub>2</sub> surface or the control surface. This is probably due to the increased surface area available for the cells to interact with the material<sup>105</sup> on a rougher surface as opposed to lower surface area available on a lower surface roughness material of the same composition and chemistry of cell attachment behavior. The results from the attachment studies are corroborated by the scanning electron micrographs of the cells. It can be deduced from the electron micrographs that the cells attached and spread faster and had good adaptation on surfaces with a higher number of TiO<sub>2</sub> layers (greater surface roughness/surface area) than a surface with a lower number of TiO<sub>2</sub> layers (lower surface roughness/surface area). After 24 hours, cells retained rounded morphology on the control surface (Figure 8.14), whereas at 4 hours on a 4 layer surface (Figure 8.10), the cells show signs of spreading across the substrate and at 12 hours (Figure 8.13), they have spread and have long pseudopodia, a sign of good adaptation to a rougher surface. A one layer TiO<sub>2</sub> surface shows a trend

that is intermediate between the control and 4 layer surfaces. We conclude that a combination of chemistry of cell adhesion and the surface properties make TiO<sub>2</sub> a good candidate for further studies with MSC.

In conclusion, LbL assembly of TiO<sub>2</sub> nanoparticles offers a promising tool for the modification of implantable surfaces for increased attachment of cells. This method can be cost effectively utilized for such purposes without compromising the integrity of the implant strength. Our future work is directed towards promoting chondrogenesis and osteogenesis of MSC on TiO<sub>2</sub> surfaces for possible applications for soft and hard tissue repair and reconstruction using the LbL technique.

## CHAPTER 9

### SUMMARY AND FUTURE WORK

The formation of thin films by LbL nanoassembly has been one of the main techniques to produce ordered nanometer featured multilayer surfaces over the past decade and half. The applications of this novel technique have been in the fields that include tissue engineering, protective coatings, drug delivery, encapsulation, lithographic applications, devices like solar cells, nano and micro-reactors etc. Many of these applications have used LbL in conjunction with other techniques to form functional thin film coatings and surfaces. In this dissertation, we have discussed two such integrations: 1) LbL and microfabrication and 2) LbL and tissue engineering. In section one, the formation of microstrip complexes consisting of polyelectrolytes in combination with other polyelectrolytes, polyelectrolyte/protein and polyelectrolyte/ion were formed inside a multiphase laminar flow microfluidic channel. The width and the relative positions of these microstrips inside the channel were altered with concentration, diffusion coefficient and flow rate of the individual inlet reactant species. The main theory used in this work was that multiple reactant entities flowing parallel to each other interact only by molecular diffusion. This diffusion of species into the interface of the liquids (reactant species) produces the reaction product as a thin strip. The effects of the flow rate of the individual species and the diffusion coefficient was studied with the software simulation

of the experimental conditions and the experimental results corroborated with the simulated conditions. Other work in this integration were the formation of pH sensitive channels by coating the surface of the channels with a pH sensitive dye, the selective coating of micro particles inside the channel and electric field effects on the formation of the complex. Atomic force microscopy and confocal microscopy were used to study the formation of these complexes in the channels. The integration of cell culture techniques with microfluidics and LbL is one such project that can be undertaken to form cell culture platforms to test various stimuli affecting the behavior of cells. Moreover, the formation of these cell culture test beds offers an easy to use, disposable, cheap and well controlled platform for these kinds of tests. As a subsection of the integration of microfabrication and LbL, quasi 2-D nanomembranes were fabricated using a variation of LbL known as the spin assisted LbL process and these nanomembranes were fixed on an array of micrometer holes fabricated using standard microfabrication techniques. The collective deflection data from these membranes was collected to speed up the process of optimization of the nanomembranes. One of the many applications of such membranes is a miniature pressure sensor in a gas flow environment. This is an application that is being pursued with collaborators at Iowa State University. Other possible work includes the formation of functional bioactive membranes and chemical sensors.

The formation of thin films on planar substrates is an area in which LbL assembly has been used extensively. There have been more than one thousand publications since the year 2000 alone. Many of these publications have been for the formation of functional bioactive thin films on substrates like glass, plastic and metals. Other applications of these thin films have been the formation of coatings as protective layers and the

fabrication of functional devices useful in the physical sciences. In the second part of this dissertation, the formation of thin films consisting mainly of nanoparticles is discussed. These thin films were used as coatings for superhydrophilic, biocompatible layers. The first subsection of this work focuses on the formation of superhydrophilic coatings consisting of  $\text{TiO}_2$  nanoparticles. Previous research has been on the formation of the thin films of  $\text{TiO}_2$  using sputtering, evaporation, SAMs etc. which produced films with superhydrophilic properties only under illumination from either under a UV lamp or sunlight. In our work, we have assembled thin films of  $\text{TiO}_2$  nanoparticles with overall film thickness ranging from a few nanometers to about 300 nm. These thin films, assembled on substrates with varying initial wettability, showed superhydrophilic characteristics on all substrates without the need for an external illumination source. Depending on the type of substrate used, complete wettability was achieved after a number of alternations of the nanoparticles with oppositely charged polyelectrolytes. It was shown that the number of such alternations was reduced after treating the substrates with oxygen plasma, which accelerated the assembly process, such that 5 alternations were required instead of 20, after plasma treatment. These superhydrophilic coatings were shown to be long lasting, which are not possible by coating with other kinds of materials on these substrates. The superhydrophilicity of the coating was shown to be unique to  $\text{TiO}_2$ , by coating the substrates with other kinds of nanoparticles (to eliminate the hydrophilicity due to surface roughness). Finally, in this work, for the first time we have shown the attachment of cells directly on nanoparticle thin films.

In the second subsection, the formation of cell adhesive nanoparticle thin films was elaborated. Two different cell types were studied on the nanoparticle thin films. First

a preliminary study of human dermal fibroblasts was done to prove the actual attachment, proliferation and spreading of cells on the thin films. Four different nanoparticles were assembled as thin films on glass substrates with oppositely charged polyelectrolytes and the effects of these nanoparticles on the cells were analyzed. The nanoparticles did not offer a toxic environment to the cells and the cells thrived on the thin films. Active cell proliferation was found on these thin films and the cells retained their phenotype. This pilot study with the nanoparticles opened a new method of surface modification to impart nanostructured surface features for the cells. Many research groups have shown that cells attached and proliferated faster on surfaces with nanometer surface features. Using this as a motivation for our work with the second cell type (stem cells), we have shown that the surface roughness increases with an increasing number of layers of LbL assembled nanoparticles. With increasing surface roughness, increased cell attachment and proliferation was observed. Cell attachment and spreading was faster on the rougher surfaces compared with the same surface with lower surface roughness. An extension of this work is the inclusion of drug loaded nanoparticles to differentiate the stem cells into various other kinds of cells. A sustained release system is another possible method to control and regulate the differentiation of the stem cells.

In conclusion, we have accomplished the integration of LbL nanoassembly with microfabrication techniques and tissue engineering. These two integrations are of great importance in the biological and physical sciences. Functional, engineered, multi-component, nanometer thick films that perform as well as or better than their thicker counterparts is a unique aspect of LbL nanoassembly which was used as a tool in this dissertation for the formation various surface coatings.

## REFERENCES

- 1 Y. Lvov, G. Decher and Helmuth Mohwald, Assembly, structural characterization, and thermal behavior of layer-by-layer deposited ultrathin films of poly(vinyl sulfate) and poly(allylamine), *Langmuir* 1993, 9, 481-486.
- 2 R.K. Iler, Multilayers of colloidal particles, *Journal of Colloids and Interface Science* 1966, 21, 569-594.
- 3 F. Brand and H. Dautzenberg, Structural analysis in interpolyelectrolyte complex formation of sodium poly(styrenesulfonate) and diallyldimethylammonium chloride- acrylamide copolymers by viscometry, *Langmuir* 1997, 13, 2905-2910.
- 4 S. Gavryushov and P. Zielenkiewicz, Electrostatics of a DNA-like polyelectrolyte: effects of solvent dielectric saturation and polarization of ion hydration shells, *J. Phys. Chem. B* 1999, 103, 5860-5868.
- 5 E. Seyrek, P. Dubin, C. Tribet, E. Gamble, Ionic strength dependence of protein-polyelectrolyte interactions, *Biomacromolecules* 2003, 4, 273.
- 6 M. Antonietti, Nanostructured materials: Self-organization of functional polymers, *Nature Materials* 2003, 2, 9-10.
- 7 A. Diaspro, D. Silvano, S. Krol, O. Cavalleri, A. Gliozzi, Single living cell encapsulation in nano-organized polyelectrolyte shells *Langmuir* 2002, 18, 5047-5050.
- 8 S. Quake, A. Scherer, From micro- to nanofabrication with soft materials, *Science* 2000, 290, 1536-1540.
- 9 P. Kenis, R. Ismagilov, G. Whitesides, Microfabrication inside capillaries using multiphase laminar flow patterning, *Science* 1999, 285, 83-85.
- 10 P. Kenis, R. Ismagilov, S. Takayama, G. Whitesides, S. Li, H. White, Fabrication inside microchannels using fluid flow, *Acc. Chem. Res.* 2000, 33, 841-847.
- 11 R. Ferrigno, A. Stroock, T. Clark, M. Mayer, G. Whitesides, Membraneless vanadium redox fuel cell using laminar flow, *J. Am. Chem. Soc.* 2002, 124, 12930-12931.

- 12 S. Takayama, J. McDonald, E. Ostuni, M. N. Liang, P. Kenis, R. Ismagilov, G. Whitesides, Patterning cell and their environments using multiple laminar fluid flows in capillary networks, *Proc. Natl. Acad. Sci. USA* 1999, 96, 5545.
- 13 L. Kam, S. Boxer, Spatially selective manipulation of supported lipid bilayers by laminar flow: steps toward biomembrane microfluidics, *Langmuir* 2003, 19, 1624-1631.
- 14 J. Oakey, J. Allely, D. Marr, Laminar-flow-based separations at the microscale, *Biotechnol. Prog.* 2002, 18, 1439-1442.
- 15 A. Hatch, A. Kamholz, K. Hawkins, M. Munson, E. Shilling, B. Weigl, P. Yager, A rapid diffusion immunoassay in a T-sensor, *Nature Biotechnology* 2001, 19, 461-465.
- 16 E. Delamarche, A. Bernard, H. Schmid, A. Bietsch, B. Michel, H. Biebuyck, Microfluidic networks for chemical patterning of substrates: design and application to bioassays, *J. Am. Chem. Soc.* 1998, 120, 500-504.
- 17 J. C. McDonald and G. M. Whitesides, Poly(dimethylsiloxane) as a material for fabricating microfluidic devices, *Accounts of Chemical Research* 35, 7, 2002
- 18 D. G. Shchukin, D. S. Kommireddy, Y. Zhao, T. Cui, G. B. Sukhorukov, Y. M. Lvov, Polyelectrolyte micropatterning using a laminar flow microfluidic device, *Advanced Materials*, 16, 389-393, 2004.
- 19 C. Jiang, S. Markutsya, V. V. Tsukruk, Compliant, robust, and truly nanoscale free-standing multilayer films fabricated using spin-assisted layer-by-layer assembly, *Adv. Mater.* 2004, 16, 157-161.
- 20 D. Yoo, S. S. Shiratori, and M. F. Rubner, Controlling bilayer composition and surface wettability of sequentially adsorbed multilayers of wear polyelectrolytes, *Macromolecules* 1998, 31, 4309-4318.
- 21 Y. Gao, Y. Masuda, and K. Koumoto, Light-excited superhydrophilicity of amorphous TiO<sub>2</sub> thin films deposited in an aqueous peroxotitanate solution, *Langmuir* 2004, 20, 3188-3194.
- 22 D. S. Kommireddy, A. A. Patel, T. G. Shutava, D. K. Mills, and Y. M. Lvov, Layer-by-layer assembly of tio<sub>2</sub> nanoparticles for stable hydrophilic biocompatible coatings, *Journal of Nanoscience and Nanotechnology*, 5, 1081-1087, 2005.
- 23 D. S. Kommireddy, I. Ichinose, Y. M. Lvov and D. K. Mills, Nanoparticle multilayer: Surface modification for cell attachment, Submitted in *Journal of Biomedical Nanotechnology*, 2005.

- 24 M. C. Berg, S. Y. Yang, P. T. Hammond, and M. F. Rubner, Controlling Mammalian Cell Interactions on Patterned Polyelectrolyte Multilayer Surfaces, *Langmuir* 2004, 20, 1362-1368.
- 25 Luke G. Gutwein, and Thomas J. Webster, Increased viable osteoblast density in the presence of nanophase compared to conventional alumina and titania particles, *Biomaterials* 25, 4175-4183 (2004)
- 26 D. S. Kommireddy, S. M. Sriram, Y. M. Lvov and D. K. Mills, Layer-by-layer assembled TiO<sub>2</sub> nanoparticle thin films – a new surface modification approach for stem cell attachment, Submitted in *Biomaterial*, 2005
- 27 M. A. Unger, H. P. Chou, T. Thorsen, A. Scherer, S. R. Quake, Monolithic microfabricated valves and pumps by multilayer soft lithography, *Science* 2000, 288, 113-116.
- 28 S. Li, C. W. Macosko, H. S. White, Electrochemical processing of conducting polymer fibers, *Science* 1993, 259, 957-960
- 29 Y. Xia, E. Kim, G. M. Whitesides, Micromolding on capillaries: applications in materials science, *J. Am. Chem. Soc.* 1996, 118, 5722-5731.
- 30 A. Y. Fu, C. Spence, A. Scherer, F. H. Arnold, S. R. Quake, A microfabricated fluorescence-activated cell sorter, *Nature Biotechnology* 1999, 17, 1109-1111.
- 31 R. S. Kane, S. Takayama, E. Ostuni, D. E. Ingber, G. M. Whitesides, Patterning proteins and cells using soft lithography, *Biomaterials* 1999, 20, 2363-2376.
- 32 S. L. R. Barker, D. Ross, M. J. Tarlov, M. Gaitan, L. E. Lacascio, Control of flow direction in microfluidic devices with polyelectrolyte multilayers, *Anal. Chem.* 2000, 72, 5925-5929.
- 33 S. Takayama, E. Ostuni, P. LeDuc, K. Naruse, D. E. Ingber, G. M. Whitesides, Subcellular positioning of small molecules, *Nature* 2001, 411, 1016-1016.
- 34 K. Macounova, C. R. Cabrera, M. R. Holl and P. Yager, Generation of natural pH gradients in microfluidic channels for use in isoelectric focusing, *Analytical Chemistry* 2000, 72, 3745-3751.
- 35 E. A. Schilling, A. E. Kamholz and P. Yager, Cell lysis and protein extraction in a microfluidic device with detection by a fluorogenic enzyme assay, *Analytical Chemistry* 2002, 72, 1798-1804.

- 36 S. Takayama, E. Ostuni, P. Leduc, K. Naruse, D. E. Ingber and G. M. Whitesides, Selective chemical treatment of cellular microdomains using multiple laminar streams, *Chemistry and Biology* 2003, 10, 123-130.
- 37 P. S. Dittrich and P. Schuille, An integrated Microfluidic system for reaction, high sensitivity detection and sorting of fluorescent cells and particles, *analytical Chemistry* 2003, 75, 5767-5774.
- 38 J. Kruger, K. Singh, A. O'Neill, C. Jackson, A. Morrison, P. O'Brien, Development of a microfluidic device for fluorescence activated cell sorting, *Journal of Micromechanics and Microengineering* 2002, 12, 486-494.
- 39 H. Mao, T. Yang and P. Cremer, Design and characterization of immobilized enzymes in microfluidic systems, *Analytical Chemistry* 2002, 74, 379-385.
- 40 H. Mao, P. S Cremer and M. D. Mason, A sensitive, versatile microfluidic assay for Bacterial Chemotaxis, *PANS* 2003, 100, 5449-5454.
- 41 K. Landfester, Polyreactions in miniemulsions, *Macromol. Rapid Comm.* 2001, 22, 896-936.
- 42 V. A. Kabanov, Physicochemical basis and the prospects of using soluble interpolyelectrolyte complexes, *Polymer Sci.* 1994, 36, 143-156.
- 43 H. M. Buchhammer, G. Petzold and K. Lunkwitz, Salt effect on formation and properties of interpolyelectrolyte complexes and their interactions with silica particles, *Langmuir* 1999, 15, 4306-4310.
- 44 D.V. Volodkin, N. G. Balabushevitch, G. B. Sukhorukov and N. I. Larionova, Inclusion of proteins into polyelectrolyte microparticles by alternative adsorption of polyelectrolytes on protein aggregates, *Biochemistry* 2003, 68, 236-241.
- 45 J. M. Gonzalez-Saiz and C. Pizarro, Polyacrylamide gels as support for enzyme immobilization by entrapment, effect of polyelectrolyte carrier, pH and temperature on enzyme action and kinetics parameters, *European Polymer Journal*, 2001, 37, 435-444.
- 46 E. V. Kudryashova, A. K. Gladilin and V.V. Mozhaev, Enzyme-polyelectrolyte complexes in water-ethanol mixtures: Negatively charged groups artificially introduced into  $\alpha$ -chymotrypsin provide additional activation and stabilization effects, *Biotechnology and Bioengineering*, 1997, 55, 267-273.
- 47 A. Rogalski, Infrared detectors: status and trends, *Progr. Quant. Electron.* 27, 59-210 (2003).

- 48 E. Defay, C. Millon, C. Malhaire and D. Barbier, PZT thin films integration for the realization of a high sensitivity pressure microsensor based on a vibrating membrane. *Sens.Actuat.A* 2002, 99, 64–67.
- 49 F. Hedrich, S. Billat and W. Lang, Structuring of membrane sensors using sacrificial porous silicon. *Sens.Actuat.A* 2000, 84, 315–323.
- 50 J. L. Davidson, D. R. Wur, W. P. Kang, D. L. Kinser and D.Kerns,D. V. Polycrystalline diamond pressure microsensor, *Diam. Related Mater.* 1996, 5, 86–92.
- 51 D. R Lee, X-ray scattering from freestanding polymer films with geometrically curved surfaces, *Phys. Rev. Lett.* 2003, 90, 185503-185509.
- 52 N. Cuvillier, V. Petkova, M. Nedyalkov, F. Millet and J. J. Benattar, Protein insertion within a biological freestanding film, *Physica B* 2000, 283, 1–5.
- 53 S. V. Yablonskii, K. Nakano, A. S. Mikhailov, M. Ozaki and K. Yoshino, Thermal photodetector using freely suspended liquid-crystal films, *Jpn J.Appl. Phys.* 2003, 42, 198–201.
- 54 G. Decher and J. B. Schlenoff, *Multilayer Thin Films*, Wiley-VCH, Weinheim, 2003.
- 55 A. S. Zahr, M. de Villiers and M. V. Pishko, Encapsulation of drug nanoparticles in self-assembled macromolecular nanoshells, *Langmuir* 2005, 21, 403.
- 56 D. M. DeLongchamp and P. T. Hammond, Side-by-side directed Multilayer patterning using surface templates, *Adv. Mater.* 2001, 13, 1455.
- 57 X. Shi, M. Shen, H. Möhwald, Polyelectrolyte multilayer nanoreactors toward the synthesis of diverse nanostructured materials, *Prog. Polym. Sci.* 2004, 29, 987-994.
- 58 T. R. Farhat and P. T. Hammond, Designing a new generation of proton-exchange membranes using layer-by-layer deposition of polyelectrolytes, *Adv. Funct. Mater.* 2005, 15, 945-954
- 59 A. A. Mamedov, N. A. Kotov, M. Prato, D. M. Guldi, J. P. Wicksted and A. Hirsch, Molecular design of strong single-wall carbon nanotube/polyelectrolyte multilayer composites, *Nat. Mater.* 2002, 1, 190-194.
- 60 C. Jiang, S. Markutsya and V. V. Tsukruk, Collective and individual plasmon resonances in nanoparticle films obtained by spin-assisted layer-by-layer assembly, *Langmuir* 2004, 20, 882.

- 61 H. Ko, C. Jiang, H. Shulha and V. V. Tsukruk, Carbon nanotube arrays encapsulated into freely suspended flexible films *Chem. Mater.* 2005, 17, 2490-2493.
- 62 Z. Tang, N. A. Kotov, S. Magonov and B. Ozturk Nanostructured artificial nacre *Nat. Mater.* 2003, 2, 413.
- 63 D. Zhou, A. Bruckbauer, C. Abell, D. Klenerman and D-J. Kang, Fabrication of three-dimensional surface structures with highly fluorescent quantum dots by surface-templated layer-by-layer assembly, *Advanced Materials* 2005, 17, 1243-1248.
- 64 D. G. Shchukin, G. B. Sukhorukov and H. Möhwald, Biomimetic fabrication of nanoengineered hydroxyapatite/polyelectrolyte composite shell, *Chem. Mater.* 2003, 15, 3947.
- 65 J. Cho, K. Char, J.-D. Hong and K.-B. Lee, Fabrication of highly ordered multilayer films using a spin self-assembly method, *Adv. Mater.* 2001, 13, 1076.
- 66 C. Jiang, S. Markutsya, Y. Pikus and V. V. Tsukruk, Freely suspended nanocomposite membranes as highly-sensitive sensors *Nat. Mater.* 2004, 3, 721.
- 67 A. A. Mamedov and N. A. Kotov, Free-standing layer-by-layer assembled films of magnetite nanoparticles, *Langmuir* 2000, 16, 5530-5533.
- 68 C. Jiang, B. M. Rybak, S. Markutsya, P. E. Kladitis and V. V. Tsukruk, Self-recovery of stressed nanomembranes *Appl. Phys. Lett.* 2005, 86, 121912.
- 69 S. Markutsya, C. Jiang, Y. Pikus and V. V. Tsukruk, Free-suspended layer-by-layer nanomembranes: testing micromechanical properties. *Adv. Funct. Mater.*, 2005, 15, 771-780
- 70 C. Jiang, S. Markutsya, H. Shulha and V. V. Tsukruk, Freely suspended gold nanoparticles arrays, *Adv. Mater.* 2005, 17, in press.
- 71 A. D. Stroock, R. S. Kane, M. Weck, S. J. Metallo and G. M. Whitesides, Synthesis of free-standing quasi-two-dimensional polymers, *Langmuir* 2003, 19, 2466-2471.
- 72 F. Hua, T. Cui and Y. Lvov, Ultrathin cantilevers based on polymer-ceramic nanocomposite assembled through layer-by-layer adsorption, *Nano Lett.* 2004, 4, 823-827.
- 73 M. Miyauchi, A. Nakajima, K. Hashimoto and T. Watanabe, A highly hydrophilic thin film under  $1 \mu\text{w}/\text{cm}^2$  uv illumination *Adv. Mater.* 2000, 12, 1923.

- 74 A. Fujishima, and K. Honda, Electrochemical photolysis of water at a semiconductor electrode, *Nature* 1972, 238, 37.
- 75 H. Tada, Y. Konishi, A. Kokubu and S. Ito, Patterned TiO<sub>2</sub>/SnO<sub>2</sub> bilayer type photocatalyst. 3. preferential deposition of pt particles on the SnO<sub>2</sub> underlayer and its effect on photocatalytic activity, *Langmuir* 2004, 20, 3816-3189.
- 76 A. Nakajima, K. Hashimoto, T. Watanabe, K. Takai, G. Yamauchi and A. Fujishima, Transparent superhydrophobic thin films with self-cleaning properties, *Langmuir* 2000, 16, 7044-7047.
- 77 M. Miyauchi, A. Nakajima, A. Fujishima, K. Hashimoto and T. Watanabe, Photoinduced surface reactions on TiO<sub>2</sub> and SrTiO<sub>3</sub> films: photocatalytic oxidation and photoinduced hydrophilicity, *Chemistry of Materials* 2000, 12, 3-5.
- 78 H. Y. Lee, Y. H. Park and K. H. Ko, Correlation between Surface Morphology and Hydrophilic/Hydrophobic Conversion of MOCVD-TiO<sub>2</sub> Films, *Langmuir* 2000, 16, 7289-7293.
- 79 H. Irie, H. Mori and K. Hashimoto, Interfacial structure dependence of layered TiO<sub>2</sub>/WO<sub>3</sub> thin films on the photoinduced hydrophilic property, *Vacuum* 2004, 74, 625.
- 80 T. R. Farhat and J. B. Schlenoff, Corrosion control using polyelectrolyte multilayers *Electrochem. Solid-State Lett.* 2002, 5, B13-B15.
- 81 M. C. Berg, S. Y. Yang, P. T. Hammond and M. F. Rubner, Controlling mammalian cell interactions on patterned polyelectrolyte multilayer surfaces, *Langmuir* 2004, 20, 1362-1367.
- 82 D. Yoo, S. S. Shiratori and M. F. Rubner, Controlling bilayer composition and surface wettability of sequentially adsorbed multilayers of wear polyelectrolytes, *Macromolecules* 1998, 31, 4309-4317.
- 83 L. Zhai, F. C. Cebeci, R. E. Cohen and M. F. Rubner, Stable superhydrophobic coatings from polyelectrolyte multilayers, *Nano Lett.* 2004, 4, 1349-1353.
- 84 D. A. Chang-Yen and B. K. Gale, A monolithic PDMS waveguide system fabricated using soft-lithography techniques, *Lab on a Chip* 2003, 3, 297-303.
- 85 Y. Lvov, K. Ariga, M. Onda, I. Ichinose and T. Kunitake, Alternate assembly of ordered multilayers of SiO<sub>2</sub> and other nanoparticles and polyions, *Langmuir* 1997, 13, 6195-6203.

- 86 J. A. He, R. Mosurkal, L. A. Samuelson, L. Li and J. Kumar, Dye-sensitized solar cell fabricated by electrostatic layer-by-layer assembly of amphoteric TiO<sub>2</sub> nanoparticles Langmuir 2003, 19, 2169-2174.
- 87 N. I. Kovtyukhova, B. R. Martin, J. K. N. Mbindyo, P. A. Smith, B. Razavi, T. S. Mayer and T. E. Mallouk, Layer-by-layer assembly of rectifying junctions in and on metal nanowires J. Phys. Chem. 2001, B 105, 8762-8769.
- 88 L. H. Li, Y. M. Kong, H. W. Kim, Y. W. Kim, H. E. Kim, S. J. Heo and J. Y. Koak, Improved biological performance of Ti implants due to surface modification by micro-arc oxidation, Biomaterials 2004, 25, 2867-2875.
- 89 K. Mustafa, A. Odlen, A. Wennerberg, K. Hultenby and K. Arvidson, The influence of surface topography of ceramic abutments on the attachment and proliferation of human oral fibroblasts, Biomaterials 2004, 26, 373-381
- 90 D. D. Deligianni, N. Katsala, S. Ladas, D. Sotiropoulou, J. Amedee, Y. F. Missirlis, Effect of surface roughness of the titanium alloy Ti6Al4V on human bone marrow cell response and on protein adsorption, Biomaterials 2001, 22, 1241-1251.
- 91 X. Zhua, J. Chen, L. Scheideler, R. Reichl and J. Geis-Gerstorfer, Effects of topography and composition of titanium surface oxides on osteoblast responses Biomaterials 2004, 25, 4087-4103.
- 92 R. L. Price, M. C. Waid, K. M. Haberstroh and T. J. Webster, Selective bone cell adhesion on formulations containing carbon nanofibers, Biomaterials 2003, 24, 1877-1887.
- 93 T. J. Webster, R. W. Siegel and R. Bizios, Nanoceramic surface roughness enhances osteoblast and osteoclast functions for improved orthopaedic/dental implant efficacy Scripta mater. 2001, 44, 1639-1642.
- 94 X. Zhu, J. Chen, L. Scheideler, R. Reichl and J. Geis-Gerstorfer, Effects of topography and composition of titanium surface oxides on osteoblast responses, Biomaterials 2004, 25, 4087-4103.
- 95 A. Okumura, M. Goto, T. Goto, M. Yoshinari, S. Masuko, T. Katsuki and T. Tanaka, Substrate affects the initial attachment and subsequent behavior of human osteoblastic cells (Saos-2). Biomaterials 2001, 22, 2263-2271.
- 96 Y. Wan, Y. Wang, Z. Liu, X. Qu, B. Han, J. Bei and S. Wang, Adhesion and proliferation of OCT-1 osteoblast-like cells on micro and nano scale topography structured poly(L-lactide), Biomaterials 2005 26, 4453-4459.

- 97 T. J. Webster, E. L. Hellenmeyer and R. L. Price, Increased osteoblast functions on theta+delta nanofiber alumina, *Biomaterials* 2005, 26, 953-960.
- 98 L. G. Gutwein and T. J. Webster, Increased viable osteoblast density in the presence of nanophase compared to conventional alumina and titania particles, *Biomaterials* 2004, 25, 4175-4183.
- 99 T. J. Webster and J. U. Ejiofor, Increased osteoblast adhesion on nanophase metals: Ti, Ti6Al4V, and CoCrMo, *Biomaterials* 2004, 25, 4731-4739.
- 100 L. Ponsoynet, K. Reybier, N. Jaffrezic, V. Comte, C. Lagneau, M. Lissac and C. Martelet, Relationship between surface properties (roughness, wettability) of titanium and titanium alloys and cell behaviour, *Materials Science and Engineering C* 2003, 23, 551-560.
- 101 X. Zhua, J. Chena, L. Scheidlera, R. Reichlb, R. G. Gerstorfer, Effects of topography and composition of titanium surface oxides on osteoblast responses, *Biomaterials* 2004, 25, 4087-4103.
- 102 M. Ahmad, D. Gawronski, J. Blum, J. Goldberg, G. Gronowicz, Differential response of human osteoblast-like cells to commercially pure (cp) titanium grades 1 and 4, *J. Biomed. Mater. Res.* 1999, 46, 121-131.
- 103 T. J. Webster, C. Ergun, R. H. Doremus, R. W. Siegel, R. Bizios, Enhanced osteoclast-like cell functions on nanophase ceramics, *Biomaterials* 2001, 22, 1327-1333.
- 104 L. G. Gutwein, T. J. Webster, Increased viable osteoblast density in the presence of Nanophase compared to conventional alumina and titania particles, *Biomaterials* 2004, 25, 4175-4183.
- 105 A. Thapa, D. C. Miller and T. J. Webster and K. M. Haberstroh, Nano-structured polymers enhance bladder smooth muscle cell function, *Biomaterials* 2003, 24, 2915-2926.
- 106 A. Tourovskaia, T. Barber, B. T. Wickes, D. Hirdes, B. Grin, D. G. Castner, K. E. Healy and A. Folch, Micropatterns of chemisorbed cell adhesion-repellent films using oxygen plasma etching and elastomeric masks, *Langmuir* 2003, 19, 4754-4764.
- 107 S. A. Catledge, M. Fries and Y. K. Vohra, Nanostructured surface modifications for biomedical implants, *Encyclopedia of Nanoscience and Nanotechnology*, vol. 7, iss. 1, pp. 741-762(22) American Scientific Publishers
- 108 D. Terala, Masters Thesis, Louisiana Tech University, 2004.

- 109 G. Ibarz, L. Dahne, E. Donath and H. Mohwald, Smart micro- and nanocontainers for storage, transport, and release *Advanced Materials* 2001, 14, 1324-1327.
- 110 R. Bird, W. Stewart and E. Lightfoot, *Transport Phenomena*, John Wiley and Sons, New York, 1960.
- 111 J. Georges, Investigation of the diffusion coefficient of polymers and micells in aqueous solutions using the Soret effect in cw-laster thermal lens spectrometry, *Spectrochim. Acta Part A* 2003, 59, 519-524.
- 112 J. Brody, T. Osborn, F. Forster and P. Yager, A planar microfabricated fluid filter, *Sensors and Actuators A* 1996, A54, 704-708.
- 113 T. J. Su, J. R. Lu and J. Penfold, The conformational structure of bovine serum albumin layers adsorbed at the silica-water interface, *J. Phys. Chem. B* 1998, 102, 8100-8108.
- 114 G. Sukhorukov, in book: "Novel Methods to Study Interfacial Layers", Ed. D. Möbius and R. Miller, 2001, Elsevier, p.384-415.
- 115 K. Ashley, J. C. Meredith, D. Raghavan, E. J. Amis and A. Karim, Combinatorial investigation of dewetting polystyrene thin films on gradient hydrophobic surfaces, *Polymer* 2003, 44, 769-772.
- 116 R. Song, M. Y. M. Chiang, A. J. Crosby, A. Karim, E. J. Amis and N. Eidelman, Combinatorial peel tests for the characterization of adhesion behavior of polymeric films, *Polymer* 2005, 46, 1643-1652.
- 117 C. Poilane, P. Delobelle, C. Lexcelent, S. Hayashi and H. Tobushi, Analysis of the mechanical behavior of shape memory polymer membranes by nanoindentation, bulging, and point membrane deflection tests, *Thin Solid Films* 2000, 379, 156-165.
- 118 N. Tang, R. L. Engelstad and E. G. Lovell, Point-deflection method for in-situ stress determination of advanced lithographic masks, *Microelectronic Eng.* 2002, 61-62, 271-276.
- 119 K. L. Johnson, *Contact Mechanics*, Cambridge University Press, 1985.
- 120 Y. Lvov, H. Haas, G. Decher, H. Möhwald and A. Kalachev, Assembly of polymeric molecular films onto the plasma treated glass, *J. Phys. Chemistry*, 1993, 97, 12835-12840.

- 121 D. C. Duffy, J. C. McDonald, O. J. A. Schueller and G. M. Whitesides, Rapid prototyping of microfluidic systems in poly(dimethylsiloxane), *Anal. Chem.* 1998 70, 4974-4983.
- 122 B. T. Ginn and O. Steinbock, Polymer surface modification using microwave oven generated plasma, *Langmuir* 2003 19, 8117-8118.
- 123 V. A. Sinani, D. S. Koktysh, B. G. Yun, R. L. Matts, T. C. Pappas, M. Motamedi, S. N. Thomas and N. A. Kotov, Collagen coating promotes biocompatibility of semiconductor nanoparticles in stratified LBL films, *Nano Lett.* 2003, 3, 1177.
- 124 V. Tsukruk, V. Bliznyuk, D. Visser, A. Campbell, T. Bunnig and W. Adams, Electrostatic deposition of polyionic monolayers on charged surfaces, *Macromolecules* 1997, 30, 6615-6621.
- 125 Y. Liu, J.I. Dadap, D. Zimdars and K.B. Eisenthal, Study of interfacial charge-transfer complex on TiO<sub>2</sub> particles in aqueous suspension by second-harmonic generation, *J. Phys. Chem.B* 1999, 103, 2480-2487.
- 126 T. Rajh, M.C. Thurnauer, P. Thiyagarajan and D.M. Tiede, Structural characterization of self-organized TiO<sub>2</sub> nanoclusters studied by small angle neutron scattering, *J.Phys.Chem.B* 1999, 103, 2172-2177.
- 127 Y. Masuda, T. Sugiyama, W.S. Seo and K.Koumoto, Deposition mechanism of anatase TiO<sub>2</sub> on self-assembled monolayers from an aqueous solution, *Chem. Mater.* 2003 15, 2469-2476.
- 128 A. Antipov, G. Sukhorukov, S. Leporatti, I. Radchenko, E. Donath and H. Mohwald, Electrolyte multilayer capsule permeability control, *Colloids and Surfaces A* 2002, 198, 535-541.
- 129 Kataoka, M. C. Gurau, F. Albertorio, M. A. Holden, S. M. Lim, R. D. Yang and P. S. Cremer, Investigation of water structure at the TiO<sub>2</sub>/aqueous interface, *Langmuir* 2004, 20,1662-1668.
- 130 T. Rajh and J. Rabani, Effects of charge polymers on interfacial electron transfer processes in CdS colloidal systems, *Langmuir* 1999,7, 2054-2059.
- 131 B. H. Sohn, T. H. Kim and K. Char, Process-dependent photocatalytic properties of polymer thin films containingTiO<sub>2</sub> nanoparticles: Dip vs spin self-assembly methods, *Langmuir*, 18, 7770 (2002).
- 132 H. P. Zheng, M. C. Berg, M. F. Rubner and P. T. Hammond, Controlling cell attachment selectively onto biological polymer-colloid templates using polymer-on-polymer stamping, *Langmuir* 2004, 20, 7215-7222.

- 133 Y. Lvov, R. Price, B. Gaber and I. Ichinose, Thin film nanofabrication via layer-by-layer adsorption of tubule halloysite, spherical silica, proteins and polycations *Colloids and Surfaces: Engineering* 2002, 198-200, 375-382.
- 134 J. U. Ejiogor and T. J. Webster, Biomedical implants from nanostructured materials, *Dekker Encyclopedia of Nanoscience and Nanotechnology*, 2004, 263-275.
- 135 A. Okumura, M. Goto, T. Goto, M. Yoshinari, S. Masuko, T. Katsuki and T. Tanaka. Substrate affects the initial attachment and subsequent behavior of human osteoblastic cells (Saos-2), *Biomaterials* 2001, 22, 2263-2271.
- 136 T. J. Webster, M. C. Waid, J. L. McKenzie, R. L. Price and J. U. Ejiogor, Nanobiotechnology: carbon nanofibres as improved neural and orthopaedic implants, *Nanotechnology* 2004, 15, 48-54.
- 137 P. Tryoen-Toth, D. Vautier, Y. Haikel, J. C. Voegel, P. Schaaf, J. Chluba and J. Ogier, Viability, adhesion, and bone phenotype of osteoblast-like cells on polyelectrolyte multilayer films. *J Biomedical Materials Research* 2002, 60, 657-667.
- 138 E. Brynda, J. Pachernik, M. Houska, Z. Pientka and P. Dvorak, Surface Immobilized Protein Multilayers for Cell Seeding, *Langmuir* 2005 released on the web.

## VITA

Mr. Dinesh Kommireddy was born in Madanapelli, AP, India and was brought up in the Tirupathi, AP, India. After completion of primary education in his home town, he did his bachelors in Mechanical Engineering at Vellore Engineering College (1995-99). After finishing his bachelors, he was admitted at Louisiana Tech University for masters in Industrial Engineering (1999-2001). He enrolled in Ph.D (2001-2005) in engineering at Louisiana Tech University after the completion of masters.

### Reports of Invention

- Titanium Dioxide Layer-by-Layer Assembly for Stable Super Hydrophilic Coatings, **Dinesh S. Kommireddy**, Amish A. Patel, Tatsiana G. Shutava and Yuri M. Lvov.
- Layer-by-Layer Assembled Nanoparticle thin films for Cell Culture, **Dinesh S. Kommireddy**, Yuri M. Lvov and David K. Mills.

### Journal Publications

- “Layer-by-Layer Assembled TiO<sub>2</sub> Nanoparticle Thin Films – A New Surface Modification Approach for Stem Cell Attachment” **Dinesh S. Kommireddy**, Shashikanth M. Sriram, Yuri M. Lvov and David K. Mills, submitted in *Biomaterials*.
- “Inhibitory Effect of Catalase on Hydrogen Peroxide Induced Oxidation of Hemoglobin in Layer-by-Layer Films” Tatsiana G. Shutava, **Dinesh S. Kommireddy**, Yuri M. Lvov, submitted in *JACS*.
- “Nanoparticle Multilayers: Surface Modification for Cell Attachment and Growth” **Dinesh S. Kommireddy**, Izumi Ichinose Yuri M. Lvov and David K. Mills, 2005, 3, 286-290.
- “Gradient Array of Freely Suspended Nanomembranes”, Chaoyang Jiang, **Dinesh S. Kommireddy**, Vladimir V. Tsukruk, 2005, Accepted in *Advanced Functional Materials*.

- “Layer-by-Layer Assembly of TiO<sub>2</sub> Nanoparticles for Stable Hydrophilic Biocompatible Coatings” **Dinesh S. Kommireddy**, Amish A. Patel, Tatsiana G. Shutava, David K. Mills, Yuri M. Lvov. *Journal of Nanoscience and Nanotechnology*, 2005, 5, 1081-1087.
- “Process-Structure Map for Diamond-Like Carbon Fibers from Ethene at Hyperbaric Pressures” J. L. Maxwell, M. Boman, R. W. Springer, A. Nobile, K. DeFriend, L. Espada, M. Sandstrom, **D. Kommireddy**, J. Pegna, D. Goodin. *Advanced Functional Materials* 2005, 15 (7), 1077-1087.
- “Ph Responsive Decomposable Layer-by-Layer Nanofilms and Capsules on the Basis of Tannic Acid”, Tatsiana G. Shutava, Malcolm Prouty, **Dinesh S. Kommireddy** and Yuri M. Lvov. *Macromolecules*, 2005, 38, 2850-2858.
- “Polyelectrolyte Micropatterning Using a Laminar Flow Microfluidic Device” Dmitry G. Shchukin, **Dinesh S. Kommireddy**, Yongjun Zhao, Tianhong Cui, Gleb B. Sukhorukov, Yuri M. Lvov. *Advanced Materials*, 2004, 16, 5, 389-393.
- “Electrostatic Layer-by-Layer Nano-Assembly: Films, Cantilevers, Micropatterns and Nanocapsules” **Dinesh Kommireddy**, Jingshi Shi, Xiaodong Yan, Haifeng Ji, Yuri M Lvov. *Nanofabrication: Technologies, Devices, and Applications, SPIE conference proceedings*, 2004, 5592, 120-131.

### Conferences and Meetings

- “Layer-by-Layer Nanomembrane on Patterned Surfaces” Michael E. McConney, Chaoyang Jiang, **Dinesh Kommireddy**, and Vladimir V. Tsukruk, presented at the *2005 Fall ACS meeting*, Washington D.C.
- “Multilayered Polyelectrolyte/Natural Polyphenol Nanofilms and Microcapsules for Protein Encapsulation and Protection Against Free Radical Oxidation” Tatsiana Shutava, Malcolm Prouty, **Dinesh Kommireddy**, Yuri Lvov, presented at the *2005 Fall ACS meeting*, Washington D.C.
- “Stem Cells Attachment and Viability on Nanoparticle Scaffolds” Shashikanth, M. Sriram, **Dinesh, S. Kommireddy**, Yuri M. Lvov, and David K. Mills, presented at the *Regenerate 2005 conference*, Atlanta, June 2005.
- “Layer-by-Layer Engineered Thin Films and Microcapsules with Antioxidant Properties Based on Polyelectrolytes and Natural Polyphenols” Tatsiana G. Shutava, Malcolm Prouty, **Dinesh S. Kommireddy**, Anna Shutova, Yuri M. Lvov, *Society for Biomaterials*, Memphis, April, 2005.
- “Layer-by-Layer Assembled Nanoparticle Thin Films for Cell Culture” **Dinesh S. Kommireddy**, Yuri M. Lvov, David K. Mills, *Society for Biomaterials*, Memphis, April, 2005.
- “Stem Cell Vability and Proliferation on Nanoparticle Thin Films” Shashikanth M Sriram, **Dinesh S. Kommireddy**, Yuri M. Lvov and David K. Mills, *The Institute for Biological Engineering conference*, Athens, GA, March, 2005.
- “Nanoparticle Thin Films for Cell Culture” **Dinesh S. Kommireddy**, Yuri M. Lvov and David K. Mills, *Houston Society for Engineering in Medicine and Biology*, Houston, February 2005.

- “Nano-Organized Thin Films for Surface Modification” **Dinesh S. Kommireddy**, Amish A. Patel, Tatsiana G. Shutava, David K. Mills, Yuri M. Lvov. *South West Regional Meeting*, Dallas, 2004.
- “Polyelectrolyte Micro-Capsules as Reactors for Synthesis of Bio-Polymers”, Rohit Ghan, Tatsiana G. Shutava, **Dinesh S. Kommireddy**, Yuri M. Lvov. *South West Regional Meeting*, Dallas, 2004.
- “Electrostatic Layer-by-Layer Nano-Assembly: Films, Cantilevers, Micropatterns and Nanocapsules” **Dinesh S. Kommireddy**, Jingshi Shi, Yuri M. Lvov. *SPIE Optics East*, Philadelphia, 2004, Presented by Yuri M. Lvov.
- “Layer-by-Layer Assembly and Polyion/Protein Complex Formation Inside PDMS Microchannels”, **Dinesh S. Kommireddy**, Yuri M. Lvov. *HSEMB*, Houston, 2004.
- “Laminar Flow Microfluidic Devices for Layer-by-Layer Nanoassembly” **Dinesh S. Kommireddy** and Yuri M. Lvov. *NSF Grantees Confernece*, Dallas, 2004.
- “Laminar flow Nano-assembly of Polyion Complexes Inside Y-shaped Microchannels”, **Dinesh S. Kommireddy**, Dmitry G. Shchukin and Yuri M Lvov. *Tex-MEMS V*, Dallas, 2003.
- “Laser Assisted Chemical MicroSculpturing of 3-D Materials” **Dinesh S. Kommireddy**, James L. Maxwell and Mats E. Boman. *The 2<sup>nd</sup> Louisiana Conference on Microfabrication and Materials Science*, Baton Rouge, 2001.